Prediction of Structures and Properties for Organic Superconductors

Thesis by

Ersan Demiralp

In Partial Fulfillment of the Requirements
for the Degree of
Doctor of Philosophy

California Institute of Technology
Pasadena, California

1996
(Submitted 12 December 1995)

To my parents

Acknowledgements

I am indebted to many generous people for their help and support during my stay at Caltech. My deepest debt of gratitude is to my advisor, Bill Goddard. His intellectual influence is evident throughout this thesis. Of all the members of the Goddard group, I would especially like to thank Siddharth Dasgupta, Tahir Çağın, Naoki Karasawa, Guanhua Chen, Francesco Faglioni, Xinlei Hua, Jean-Marc Langlois, Jim Gerdy, Charles Musgrave, Xiaojie Chen, Ken Brameld for their friendship and support. I thank Terumasa Yamasaki of Asahi Chemical, a friend and a colleague for his enjoyable friendship. My thanks also go to Kürşad Kızıloğlu for his "eski dostluğu."

Mine'm has been a constant inspiration for me: "So oft have I invoked thee for my Muse." Finally, I would like to thank my family, in particular my parents who have been my deepest source of support.

Abstract

The main contributions of this thesis to the field of organic superconductors are basically (a) the band structure calculations for the investigations of the conduction properties of $\kappa-(BEDT-TTF)_2Cu(NCS)_2$ using 2-D Hubbard Model with Unrestricted Hartree-Fock (UHF) theory, (b) *ab initio* quantum mechanical calculations for the structural characterizations and the properties of the donors of the organic superconductors, (c) electron-transfer boat-vibration (ET-BV) mechanism for the superconductivity of these materials, (d) developing force fields for BEDT-TTF and BEDT-TTF$^+$.

To provide a basis for understanding the puzzling electronic properties of the organic superconductor $\kappa-(BEDT-TTF)_2Cu(NCS)_2$ (with $T_c = 10.4$ K), we carried out band calculations using the 2-D Hubbard Model with Unrestricted Hartree-Fock (UHF) theory. The electron transfer hopping interactions are from *ab initio* calculations and the Hubbard parameter ($U_{opt} = 0.678950$ eV) is adjusted to fit Shubnikov-de Haas and magnetic breakdown experiments. The calculations lead to a two-band semi-metal with a momentum gap separating the electron and the hole bands. The anomalous experimental observations are explained in terms of BEDT-TTF related phonons coupling these two bands (lower temperature) and by anion related phonons (higher temperature). These results also provide a framework for describing the conduction properties of other such complexes.

The donors of all known one- or two-dimensional organic superconductors, X, are based on a core organic molecule that is either tetrathiafulvalene (denoted as TTF) or tetraselenafulvalene (denoted as TSeF) or some mixture of these two molecules. Coupling X, with appropriate acceptors, Y, leads to superconductivity. The oxidized form of X may be X^+ or X_2^+ species in the crystal. Using *ab initio* Hartree-Fock (HF) calculations (6-31G** basis set), we show that BEDT-TTF deforms to a boat structure (C_2 symmetry) with an energy 28 meV (0.65 kcal/mol) lower than

planar BEDT-TTF (D_2 symmetry). On the other hand BEDT-TTF$^+$ is planar. Performing *ab initio* quantum mechanical calculations (HF/6-31G**) also on the other donors of organic superconductors, we find that all known organic superconductors involve an X that deforms to a boat structure while X^+ is planar. This leads to a coupling between charge transfer and the boat deformation phonon modes. We propose that this electron-phonon coupling is responsible for the superconductivity and predict the isotope shifts (δT_c) for experimental tests of the electron-transfer boat-vibration (ET-BV) mechanism. We suggest that new higher temperature organic donors can be sought by finding modifications that change the frequency and stability of this boat distortion mode. Based on this idea we have developed similar organic donors having the same properties and have suggested that with appropriate electron acceptors they will also lead to superconductivity.

The highest transition temperature T_c organic superconductors all involve molecule BEDT-TTF coupled with an appropriate acceptor. The experimental structures exhibit considerable disorder in the outer rings and concomitant uncertainty in the structures of BEDT-TTF. We find that Hartree-Fock (6-31G** basis set) calculations leads to results within 0.01Å and 1° of experiment for the ordered regions allowing us to predict to composite structures expected to have this accuracy. We report optimized geometries and atomic charges for BEDT-TTF, BEDT-TTF$^+$, and BEDT-TTF$^{+\frac{1}{2}}$ that should be useful for atomistic simulations.

The vibrational levels of BEDT-TTF and BEDT-TTF$^+$ have been only partially observed and assigned. In order to provide a complete consistent description of all levels, we carried out HF calculations for all fundamental vibrational frequencies of BEDT-TTF and BEDT-TTF$^+$ and obtained the Hessians for these structures. With these Hessians and available experimental frequencies, we developed the force fields for the neutral and cation BEDT-TTF molecules by using Hessian-biased method.

Contents

Chapter 1 Introduction

Organic molecular solids are commonly regarded as insulators. They usually have few charged species and poor overlap between orbitals of neighboring molecules. In the last fifteen years, new organic solids were found to exhibit metallic and even superconducting behavior. These organic metals (also called synthetic metals) contain only non-metallic elements such as carbon, hydrogen, sulfur, etc. in their conduction frameworks. They also show interesting low dimensional behaviors. In this thesis, we study the structures and the properties of the organic superconductors, except C_{60} systems. Development of new organic materials is still in progress and very promising for making higher transition temperature superconductors. Organic materials are one of the best candidates for new superconductors since organic species can be systemically modified.

In 1979, Bechgaard made $(TMTSF)_2Y$ (now known as Bechgaard salts) which consist of chains of TMTSF cations alternating with chains of inorganics anions, Y (See Figure 1 in Section 3.3 for the nomenclature of organic donors).[1] For the first Bechgaard salts, Y was PF_6, AsF_6, SbF_6, etc. In 1980, $(TMTSF)_2PF_6$ was shown to become superconductor at 1.4 K under an applied pressure of 6.5 kbar.[2] Other Bechgaard salts were also shown to be superconducting under similar pressures. Later, Bechgaard synthesized an ambient pressure organic superconductor $(TMTSF)_2ClO_4$ (T_c = 1.4 K) with smaller spacing along chain of TMTSF stack.[3] These successes opened the field of quasi one- or two-dimensional organic superconductors. The superconducting temperatures of Bechgaard salts are very low (1 to 3 K). However, several new donors of organic superconductors, such as BEDT-TTF, BEDO-TTF, MDT-TTF, were synthesized to increase T_c during the last fifteen years. The highest transition temperature organic superconductors all involve molecule BEDT-TTF (also denoted as ET) coupled with an appropriate acceptor. In 1983, first ET superconductor, $(ET)_2ReO_4$ was shown to be superconducting at

2 K under 4 kbar.[4] Since that time, more than twenty ET salts were found to be superconducting.[5] The highest T_c of these materials is 11.6 K at ambient pressure for $\kappa-(ET)_2Cu[N(CN)_2]Br$ (12.8 K at 0.3 kbar for $\kappa-(ET)_2Cu[N(CN)_2]Cl$. See Figure 1 for $\kappa-(ET)_2Cu[N(CN)_2]Br$). The number of organic superconductors is growing by synthesizing both new electron-donor molecules as well as new species. There could be many substitutions to obtain higher T_c, but it is not totally clear which system would be best. The mechanism of the superconductivity in these materials should be clarified for rational design of higher T_c organic superconductors.

Most of the organic superconductors are of the form $D_2^+A^-$ with two donor molecules sharing one charge. Different ways of stacking of the donor molecules lead to many polymorphic phases. ET sometimes give many phases with one anion. For example, $(ET)_2I_3$ have nine phases denoted by α, β, γ, δ, ξ, η, ϵ, κ, θ.[5] Four of these phases, α, κ, θ, β show superconductivity with T_c between 1.5 K to 8.1 K. These materials show a variety of electronic behaviors, i.e. semiconducting, metallic, superconducting, etc.

The isotopic shift experiments [6,7,8,9,10,11] show that the mechanism of superconductivity involves the electron-phonon coupling and Bardeen-Cooper-Schrieffer (BCS) theory. The electron-phonon matrix elements should be calculated to estimate T_c for a BCS system. To this end, one should obtain the electronic and the vibrational structures of these materials. Full quantum mechanical calculations are not practical for these systems which contain on the order of hundred atoms in their unit cells. Thus, one can employ the model Hamiltonians for the electronic structure calculations and the force field methods for the phonon calculations. In Chapter 2, we performed electronic band structure calculations using the 2-D Hubbard Model with Unrestricted Hartree-Fock (UHF) theory for the organic superconductor $\kappa-(ET)_2Cu(NCS)_2$ (with $T_c = 10.4$K) to provide a basis for understanding the conduction properties of this material (See Figure 2 and 3). The problem of electron-electron interactions and their effects on the properties of physical systems are very important in solid state physics. Hubbard proposed a model for the problem of electron correlations in the d-electrons of the transition metals.[12,13] In recent years, there have been many studies

on high T_c superconducting materials using Hubbard Model. The Hubbard Model has a simple Hamiltonian:

$$H^H = \sum_{<ij>,\sigma} \left(t_{ij} a^\dagger_{i\sigma} a_{j\sigma} + t_{ij} a^\dagger_{j\sigma} a_{i\sigma} \right) + U \sum_i n_{i\sigma} n_{i-\sigma} \quad , \tag{1}$$

where $a^\dagger_{i\sigma}, a_{i\sigma}$, and $n_{i\sigma}$ are the creation, annihilation, and number operators, respectively, for the electron with spin σ at site i and t_{ij} are the hopping matrix elements and U is the on-site Coulomb interaction. Here, $< ij >$ indicates that the sum is taken over nearest neighbor atoms. Despite the simplicity of this Hamiltonian, Hubbard Model could not be solved exactly except in one dimension.[14] The organic superconductor $\kappa-(ET)_2Cu(NCS)_2$ possesses a number of puzzling electronic properties, including the temperature dependence of resistivity, magnetic susceptibility, and Hall coefficient. Each unit cell of κ-$(ET)_2Cu(NCS)_2$ has two $Cu(NCS)_2^-$ units and two $(ET)_2^+$ dimers packed perpendicular to each other in a parallel planar layer. Since a plane of $(ET)_2^+$ dimers is sandwiched between the insulating $Cu(NCS)_2^-$ planes and two-dimensional electronic conduction behavior is observed, we describe the electronic structure with a two-dimensional (2-D) Hamiltonian. There is no exact solution for the 2-D Hubbard Model, hence we use Unrestricted Hartree-Fock (UHF) approximation to describe electron-electron interaction terms,

$$n_{i\sigma} n_{i-\sigma} \approx n_{i\sigma} < n_{i-\sigma} > + < n_{i\sigma} > n_{i-\sigma} - < n_{i\sigma} >< n_{i-\sigma} > . \tag{2}$$

The UHF wavefunction is a Slater determinant of spin orbitals,

$$\Psi = \prod_{\mathbf{k}b\sigma}^{N_{occ}} a^\dagger_{\mathbf{k}b\sigma} |vac> \quad , \tag{3}$$

where the spatial orbitals for up-spin are allowed to be different from those with down-spin. Here, b, $\mathbf{k}$ denote the band index and k-point in the Brillouin Zone (BZ) respectively. The variational equations have the form

$$H^{HUHF} \psi_{\mathbf{k}b\sigma} = \epsilon_{\mathbf{k}b\sigma} \psi_{\mathbf{k}b\sigma} \quad , \tag{4}$$

which must be solved self-consistently. Each UHF orbital is expanded in terms of the basis set $\{\chi_\varrho\}$ consisting of the Highest Occupied Molecular Orbital (HOMO) on each ET

$$\psi_{\mathbf{k}b\sigma} = \sum_{\varrho} \chi_\varrho c_{\mathbf{k}b\sigma}(\varrho) \quad . \tag{5}$$

The results of our band structure calculations are encouraging for the understanding of several different electronic behaviors of ET salts.

The conducting molecular solid are charge-transfer (CT) salts with donor (D) and acceptor (A) molecules. The charge transfer between donor and acceptor molecules of the solid can be written as:

$$A_n + D_m \rightarrow A_n^{-\rho} + D_m^{+\rho} \quad ,$$

where ρ is the amount of charge transferred. Several important issues related to the molecular and the crystal properties should be considered to create a conducting molecular solid. First, the solid should be stable with the charged building blocks. Then, these charges should overcome Coulomb repulsions and delocalize to form metallic bands. The electronic structure and the properties of the molecule (such as ionization potential, electron affinity, polarizability, etc.) affect the nature and the magnitude of the molecular interaction forces. The shape of the molecule is crucial for the crystal packing due to van der Waals interactions. This leads to the interrelations between the molecular arrangement and the molecular interactions. The stability and the conduction properties of the molecular solid depend on these relations. In Chapter 3, we present *ab initio* quantum chemical Hartree-Fock (HF) calculations for the structures and the properties of the donors of the organic superconductors. These organic materials show anisotropic conduction with high conductivity in the plane (mostly for ET salts) or along chain (mostly for TMTSF salts) of the donors. Thus, the changes in the properties of these molecules upon chemical modification (structure, ionization potential, shape and energy of the molecular orbitals) are important for understanding the electronic and crystal structures of materials containing these organic donors. We have performed *ab initio* quantum mechanical geometry op-

timizations for a number of donors in both the oxidized (X^+) and neutral (X) states. We find that *all known donors for superconductors lead to a distorted boat conformation and a planar conformation* X^+. As an electron hops from X to X^+, the original X distorts from boat to planar. This leads to a coupling between conduction electrons and vibration (phonons) that is, we believe, the salient coupling for superconductivity. With this insight, we have modeled electron-transfer boat-vibration (ET-BV) mechanism for the superconductivity of these materials. Using this model, we estimated the isotope effects and found that our estimations are consistent with the available experimental results.

In principle, one can perform quantum chemical calculations to obtain any property for an isolated molecule. Recent developments of the computer hardware and the software make it possible to do *ab initio* quantum mechanical calculations for the donors of the organic superconductors. Despite this progress, *ab initio* quantum mechanical calculations are still not practical for large systems such as molecules with more than 100 atoms and crystals. Molecular mechanics or force field method is suitable for calculations on large systems. In general, the electrons are much faster than nuclei, thus the electronic and nuclear motions are treated separately in the Born-Oppenheimer approximation. Starting from the Born-Oppenheimer approximation, the electronic states are averaged out to obtain atomic interaction potentials. In molecular mechanics or force field method, each atom is a classical particle interacting with atomic interaction potentials. Force fields are usually described in terms of the sum of short-range valence interactions and long-range nonbond interactions:

$$E = E_{val} + E_{nb} \quad . \tag{6}$$

The valence interactions are typically written as

$$E_{val} = E_{bond} + E_{angle} + E_x + E_{torsion} + E_{inversion} \tag{7}$$

to include bond stretch E_{bond}, angle bend E_{angle}, angle-bond and bond-bond cross E_x,

dihedral torsion $E_{torsion}$, inversion $E_{inversion}$ terms. The nonbond interactions are typically written as

$$E_{nb} = E_{vdW} + E_Q \tag{8}$$

to include van der Waals E_{vdW} and electrostatic E_Q terms. The main advantage of the force field approach is the reduction of the computational cost for large systems. The amount of computer memory and time is drastically reduced by using the molecular mechanics. For example, the quantum chemical frequency calculation (HF 6-31G** basis set) took 14 hours 10 minutes 65 seconds on JPL Cray and molecular mechanical frequency calculation took $\sim$ 3.5 seconds on SGI Indigo workstation for neutral ET. On the other hand, the force field approach can not be applied to the problems where quantum effects are important. Another important point about the force fields is the development of the reliable force field which will lead to reliable results. Hence, it is very important to use some experimental or accurate quantum mechanical information when one develops a force field. The Biased Hessian method uses the experimental or accurate quantum mechanical frequencies to develop a force field. However, this is an involved optimization process and can be very time consuming. But once a reliable force field is obtained for a system, all kinds of molecular mechanical or molecular dynamical calculations can be performed. In Chapter 4, we present the calculated vibrational spectra for the equilibrium structures of ET (boat) and ET^+ (planar). Using calculated structures, Hessians and available experimental frequencies we have developed the force fields for the neutral and cation ET molecules. These results should be helpful for the assignments of the modes and for the calculations of the phonon structures of the crystals containing ET molecules.

Although most of our calculations are performed on ET systems, the applications of the models that are presented in this thesis on the other donors of organic superconductors are straightforward.

References

1. Bechgaard K., Jacobsen C. S., Mortensen K., Pedersen H. J., Thorup N., *Solid State Commun. 33*, (1980) 1119.

2. Jerome D., Mazaud A., Ribault M., Bechgaard K., *J. Phys. Lett. 41*, (1980) L95.

3. Bechgaard K., Carneiro K., Olsen M., Rasmussen F. B., Jacobsen C. S., *Phys. Rev. Lett., 46*, (1981) 852.

4. Parkin S. S., Engler E. M., Schumaker R. R., Lagier R., Lee V. Y., Scott J. C., Greene R. L., *Phys. Rev. Lett., 50*, (1983) 270.

5. Mori H., *Int. J. of Modern Physics B, 8* (1994) 1-45.

6. Tokumoto M., Konishito N., Tanaka Y., Anzai H., *Journal of the Physical Society of Japan, 60*, (1991) 1426.

7. Oshima K., Urayama H., Yamochi H., Saito G., *Synthetic Metals, 27* (1988) A473.

8. Schirber J. E., Overmyer D. L., Carlson K. D., Williams J.M., Kini A. M., Wang H. H., Charlier H. A., Love B. J., Watkins D. M., Yaconi G. A., *Phys Rev B 44*, (1991), 4666.

9. Mori H., Hirabayashi I., Tanaka S., Mori T., Maruyama Y., Inokuchi H., *Synthetic Metals, 55-57* (1993)2437.

10. Heidmann C. P., Andres K., Schweitzer D., *Physica 143B*, (1986), 357.

11. Saito G., Yamochi H., Nakamura T., Komatsu T., Matsukawa N., Inoue T., Ito H.,Ishiguro T., Kusunoki M., Sakaguchi K., Mori T., *Synthetic Metals, 55-57* (1991) 2883.

12. Hubbard J., *Proc. Roy. Soc., A276* (1963) 238-257

13. Hubbard J., *Proc. Roy. Soc., A277* (1964) 237-259

14. Lieb E.H., Wu F.Y., *Phys. Rev. Lett., 20*, (1968) 1445-1448

Figure Captions

Figure 1. The crystal structure of $\kappa - ET_2Cu[N(CN)_2]Br$

Figure 2. The crystal structure of $\kappa - (ET)_2Cu(NCS)_2$

Figure 3. Top view of the crystal structure of $\kappa - (ET)_2Cu(NCS)_2$

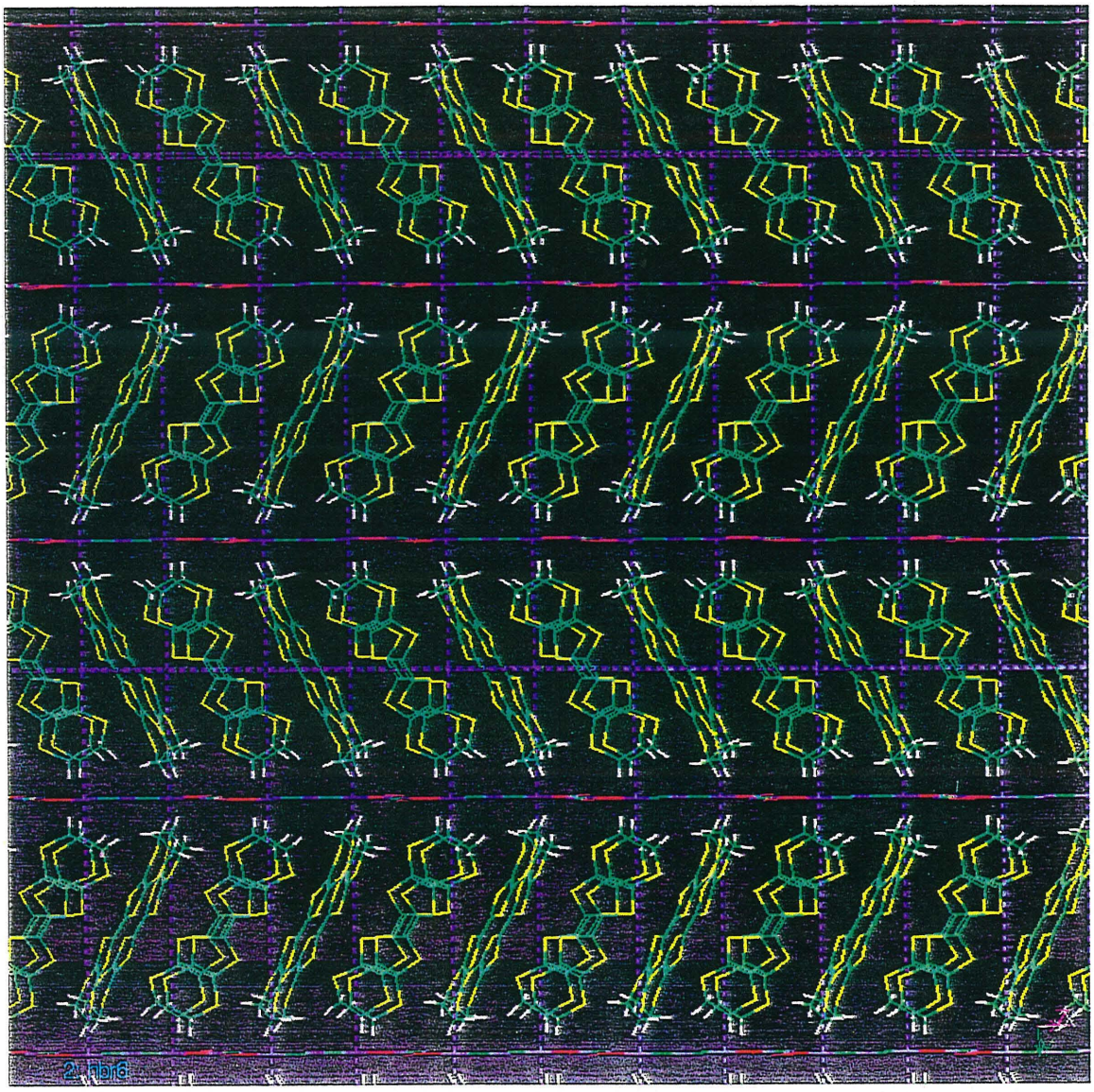

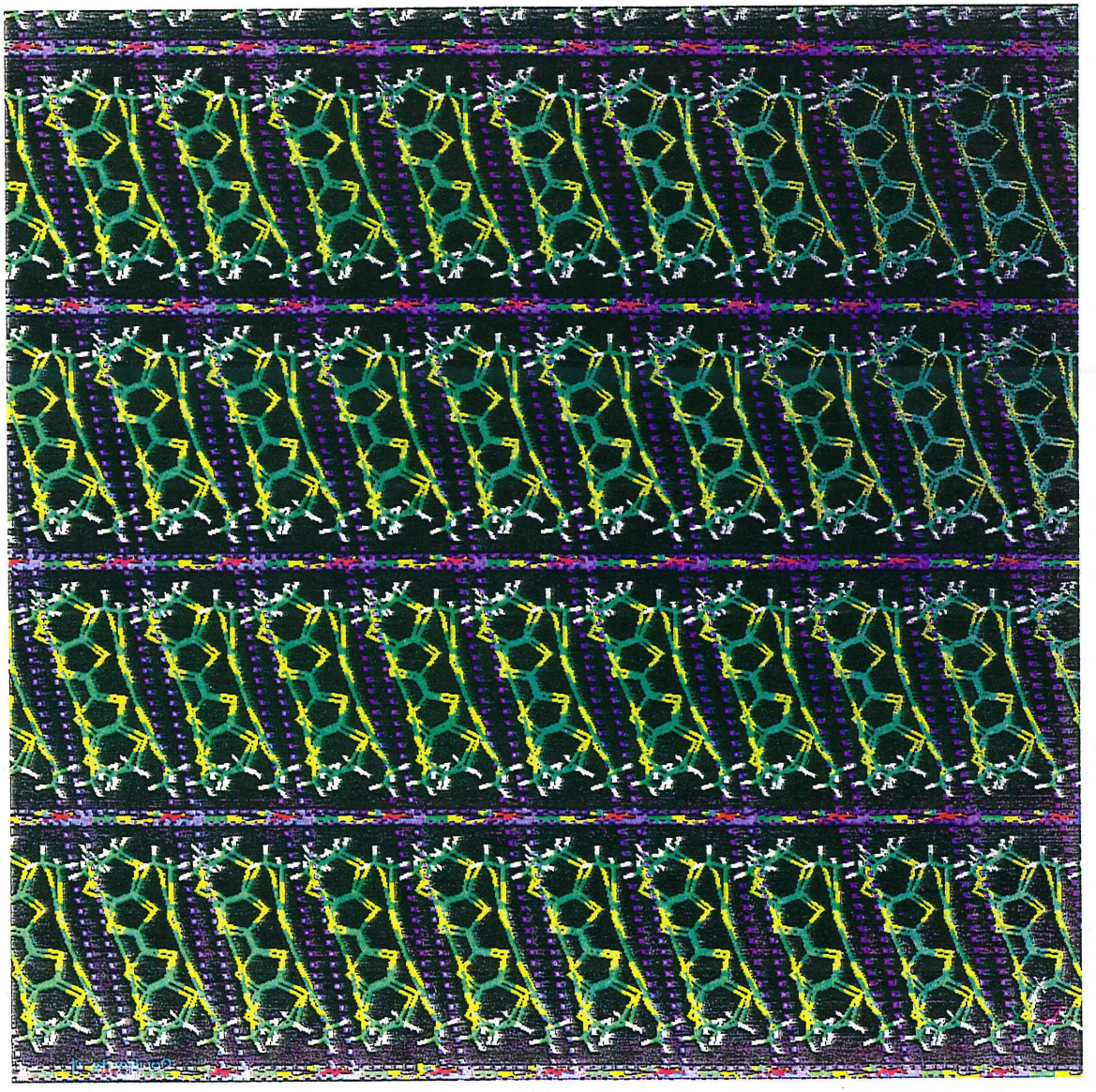

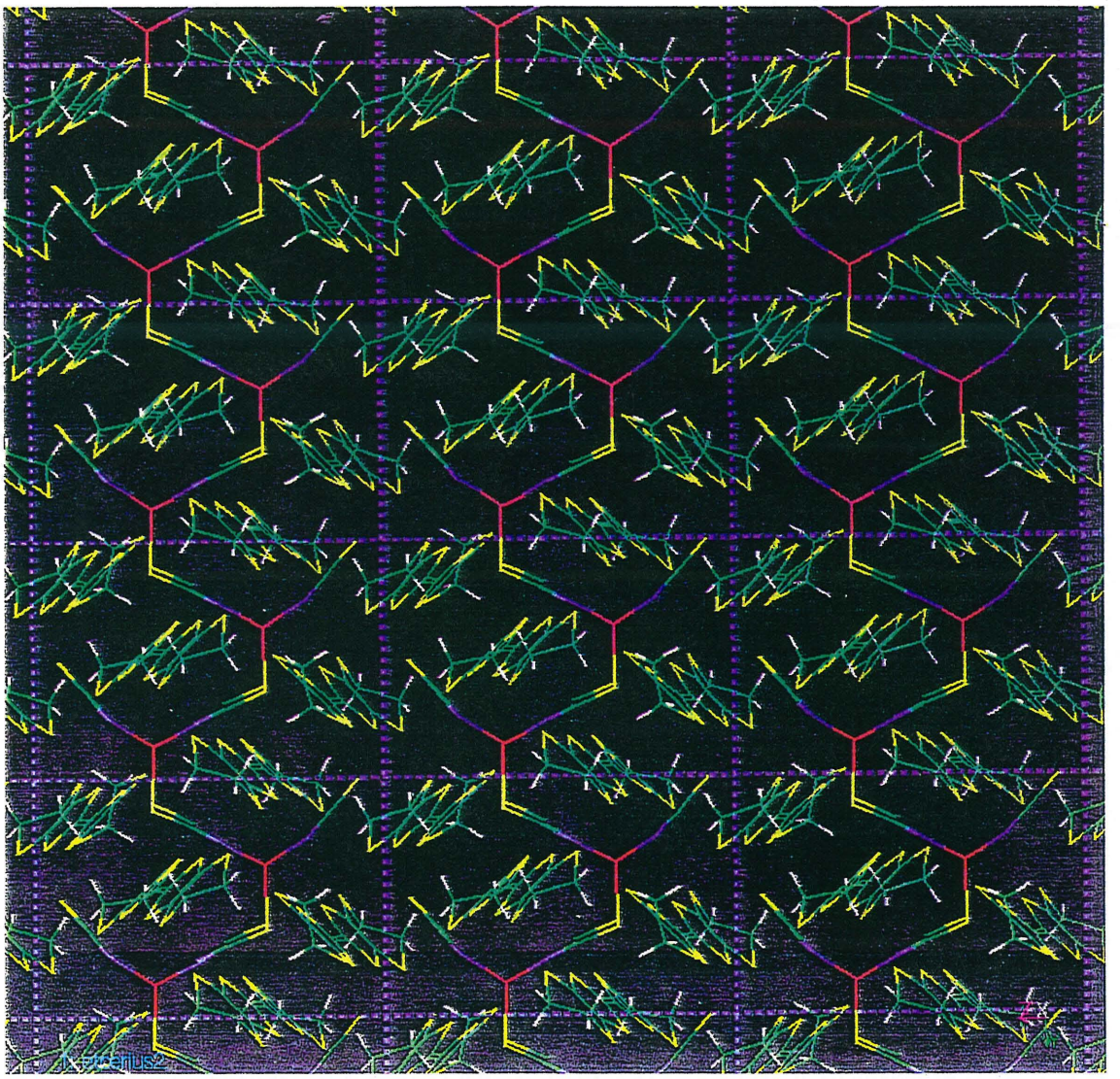

Chapter 2 Band Structure Calculations for $\kappa - (BEDT - TTF)_2Cu(NCS)_2$

The Conduction Properties of the Organic Superconductor, $\kappa-(BEDT-TTF)_2Cu(NCS)_2$, Based on the Hubbard Unrestricted Hartree-Fock Band Model

Abstract

The organic superconductor $\kappa-(BEDT-TTF)_2Cu(NCS)_2$ (with $T_c = 10.4$K) possesses a number of puzzling electronic properties, including the temperature dependence of resistivity, magnetic susceptibility, and Hall coefficient. To provide a basis for understanding these properties, we carried out band structure calculations using the 2-D Hubbard Model with Unrestricted Hartree-Fock (UHF) theory. The electron transfer hopping interactions are from *ab initio* calculations and the Hubbard parameter ($U_{opt} = 0.678950$ eV) is adjusted to fit Shubnikov-de Haas and magnetic breakdown experiments. The calculations lead to a two-band semi-metal with a momentum gap separating the electron and hole bands. The anomalous experimental observations are explained in terms of ET related phonons coupling these two bands (lower temperature) and by anion related phonons (higher temperature). These results also provide a framework for describing the conduction properties of other such complexes.

1.0 Introduction

Since 1980 the superconducting transition temperature, T_c, of quasi one- and two-dimensional organic superconductors has improved from 1.4 K[1] to 12.8 K.[2] The best systems involve bis(ethylenedithio)tetrathiafulvalene (denoted as BEDT-TTF or ET, shown in the Figure 1). Depending upon the acceptor and the packing, these systems exhibit a variety of electronic behaviors, including semiconducting, metallic, and superconducting.

One of the most interesting systems is $\kappa-(ET)_2Cu(NCS)_2$, which exhibits $T_c =$ 10.4 K at ambient pressure (See Figure 2 and 3 in Chapter 1). In κ-$(ET)_2Cu(NCS)_2$, a layer of ET molecules paired into $(ET)_2^+$ dimers is sandwiched between insulating $Cu(NCS)_2^-$ planes. [The oxidation states are based on the ESR results[3] for Cu plus charge neutrality.] This leads to conduction anisotropy along a, b and c directions of[27] $\sigma_{a^*} : \sigma_b : \sigma_c = \frac{1}{600} : 1 : 1.2$. These systems can be considered as 2-D electronic conductors (bc plane). Each unit cell of κ-$(ET)_2Cu(NCS)_2$ has two $Cu(NCS)_2^-$ units and two $(ET)_2^+$ dimers packed perpendicular to each other in a parallel planar layer.

The electronic behavior of this salt is complex. As indicated in Figure 2a, the resistivity, ρ, is a maximum around 100 K. ρ increases as T^2 below 100 K but decreases as $e^{a/T}$ for above 100 K. As indicated in Figure 2b, the Hall coefficient, R_H, is positive (hole-like) and both decreases rapidly and linearly as temperature increases to $T =$ 60K; above 60 K R_H decreases very slowly with T. As indicated in Figure 2c, the magnetic susceptibility, χ, is positive and almost constant (Pauli paramagnetism) between 100 K and 300 K. Below 100 K, χ decreases monotonically about 15% until $T = T_c$ where it plummets to near zero. The superconducting T_c is *higher* by 0.5 to 0.6 K when the hydrogens in ET are replaced by deuteriums (an inverse isotope effect).

Shubnikov-de Haas[5] (SdH) (Figure 2d), magnetic breakdown[16] (Figure 2e) and thermopower[14] (Figure 2f) experiments on $\kappa-(ET)_2Cu(NCS)_2$ have been explained qualitatively in terms of a two-band model derived from tight-binding band structure calculations reported by Oshima et al.[5] and by LeBlanc et al.[6] However explana-

tions for the puzzling anomalies in the resistivity, susceptibility, and Hall effect have not been provided. Several different mechanisms, (e.g. band gap opening,[8] polaron formation[9]) have been offered to explain the anomaly of the resistivity around 100K. However, no consistent explanation has been given for all these phenomena.

In this paper we develop a model for explaining these electronic properties. It is based on the band structure (Section 2) of $\kappa - (ET)_2Cu(NCS)_2$ calculated using a Hubbard model combined with Unrestricted Hartree-Fock (H-UHF) theory. The predictions are compared with experiment in Section 3.

2.0 UHF Calculations Using the 2-D Hubbard Model

Since a plane of $(ET)_2^+$ dimers is sandwiched between the insulating $Cu(NCS)_2^-$ planes and since two-dimensional electronic conduction behavior is observed, we will describe the electronic structure with a two-dimensional (2-D) Hamiltonian. The highest two occupied molecular orbitals (MO) of ET are separated by 1.068 eV (HF calculations with the 6-31G** basis set); hence we will consider only the Highest Occupied Molecular Orbital (HOMO) on each ET molecule. The hopping matrix elements (t_{ij}) for HOMO's on neighboring ET molecules are small compared to the Coulomb interaction between two electrons in the same MO. Thus, electron correlation effects are important, requiring a Hubbard model.

2.1 The Hubbard-UHF Calculations

We describe the electronic structure in terms of a 2-D Hubbard model with the Hamiltonian (1):

$$H^H = \sum_{<ij>,\sigma} \left(t_{ij} a_{i\sigma}^\dagger a_{j\sigma} + t_{ij} a_{j\sigma}^\dagger a_{i\sigma} \right) + U \sum_i n_{i\sigma} n_{i-\sigma} \quad , \tag{1}$$

where $a_{i\sigma}^\dagger$, $a_{i\sigma}$, and $n_{i\sigma}$ are the creation, annihilation, and number operators, respectively, for the electron with spin σ at site i. Here, $< ij >$ indicates that the sum is taken over the six nearest neighbors of each molecule. For the electron transfer integrals t_{ij}, we use the values (Table 1) of LeBlanc et al.[6] obtained from *ab initio* generalized valence bond (GVB) calculations (on dimers corresponding to nearest-

neighbor ET molecules, using a minimal basis set). For the Hubbard parameter U we estimate in Section 2.2 that $U \sim 0.80$ eV. Consequently, we calculated the band structure using values of U in the range of 0 to 1.0 eV.

We find the following results:

i. $U \leq U_a = 0.6780$ eV leads to metallic behavior, with a nearly filled third band (17% hole states) and a partially filled fourth band (17% electron states).

ii. $U \leq U_a$ leads to an equal probability of up-spin and down-spin at each site[10] while $U > U_a$ leads to antiferromagnetic behavior.

iii. $U_a < U < U_i = 0.698960$ eV leads to semi-metallic behavior (nonoverlapping third and fourth bands)

iv. $U < U_{closed} = 0.685195$ eV leads to open orbits for electrons and closed orbits for holes, but $U > U_{closed}$ leads to closed orbits for both

v. $U \geq U_i$ leads to semiconducting or insulating behavior (a gap between the third and the fourth bands).

vi. $U_{opt} = 0.678950$ eV leads to results in agreement with current experiments on $\kappa - ET_2Cu(NCS)_2$.

There is no exact solution for the 2-D Hubbard model, and hence we use the UHF approximation to describe electron-electron interaction terms,

$$n_{i\sigma}n_{i-\sigma} \approx n_{i\sigma} < n_{i-\sigma} > + < n_{i\sigma} > n_{i-\sigma} - < n_{i\sigma} >< n_{i-\sigma} > \quad . \tag{2}$$

The average $< n_{i\sigma} >$ for finite temperature is defined as the sum over all four bands

$$\langle n_{i\sigma} \rangle = \sum_{b=1}^{4} n_{b\sigma}(i)$$

of the occupation number

$$n_{b\sigma}(i) = \frac{1}{\Omega} \sum_{k} \frac{n_{\mathbf{k}b\sigma}(i)}{[1 + e^{\beta(E_k - \mu)}]} \quad , \tag{3}$$

where k is summed over the Brillouin Zone for all four bands. Here $\beta = \frac{1}{k_B T}$, Ω is a normalization factor, and μ is the chemical potential.

The UHF wavefunction is a Slater determinant of spin orbitals,

$$\Psi = \prod_{\mathbf{k}b\sigma}^{N_{occ}} a^{\dagger}_{kb\sigma}|vac> \quad , \tag{4}$$

where the spatial orbitals for up-spin are allowed to be different from those with down-spin. The variational equations have the form

$$H^{HUHF}\psi_{\mathbf{k}b\sigma} = \epsilon_{\mathbf{k}b\sigma}\psi_{\mathbf{k}b\sigma} \quad ,$$

which must be solved self-consistently. Each UHF orbital is expanded in terms of the basis set $\{\chi_\varrho\}$ consisting of the HOMO orbital on each ET

$$\psi_{\mathbf{k}b\sigma} = \sum_{\varrho} \chi_\varrho c_{\mathbf{k}b\sigma}(\varrho) \quad .$$

This leads to the multiband equation (5) for each spin

$$\sum_{\eta} \left[U < n_{\varrho,-\sigma} > \delta_{\eta\varrho} + t_{\eta\varrho} e^{i\mathbf{k}\cdot\mathbf{R}_{\eta\varrho}}\right] c_{\mathbf{k}b\sigma}(\eta) = \epsilon_{\mathbf{k}b\sigma} c_{\mathbf{k}b\sigma}(\varrho) \quad , \tag{5}$$

where $\delta_{\eta\varrho}$ is the Kronecker delta function and $\mathbf{R}_{\eta\varrho}$ is the distance vector between neighboring sites. For $t_{\eta\varrho}$ we use the values obtained by Leblanc et al.[6] from GVB calculations.

2.2 The Value of U

To estimate the value of U we carried out Hartree-Fock (6-31G** basis set) calculations[11] on the successive ionization potentials of isolated ET and ET^+ molecules. This leads to

$$IP_1 = E_{ET^+} - E_{ET} = 5.80eV$$

and

$$IP_2 = E_{ET^{+2}} - E_{ET^+} = 9.93eV \quad .$$

Thus for a vacuum we obtain

$$U_{vac} = IP_2 - IP_1 = 4.13eV \quad . \tag{6}$$

In the crystal, U_{vac} is reduced by screening. ET is nearly planar with a length of ~13.5Å (from the hydrogen of one end to the hydrogen of the other end) and 6 nearest neighbors at an average distance of 3.80Å from the middle.[12] Adding 1.0 Å for the radius of the hydrogen atoms, we take $a \approx 15.5$Å as the effective length of ET.

Taking each ET as a charged conducting ellipsoid with semiaxes $a = \frac{15.5}{2}$Å and $> b = c = \frac{3.8}{2}$Å, leads the potential

$$\Phi(q) = \frac{q}{\sqrt{a^2 - b^2}} tanh^{-1} \sqrt{\frac{a^2 - b^2}{a^2}} = q\ 3.993\ \ eV \tag{7}$$

on the surface of the ellipsoid, where q is the electric charge (in units of absolute electron charge) on the ellipsoid. By bringing the charge from infinity, the IP's in the crystal are estimated as

$$(IP_1)_{sc} = IP_1 - \Phi(1) + \frac{\Phi(1)}{\epsilon}$$

and

$$(IP_2)_{sc} = IP_2 - \Phi(2) + \frac{\Phi(2)}{\epsilon} \quad .$$

This leads to

$$U_{sc} = (IP_2 - IP_1)_{sc} = U_{vac} - \frac{\epsilon - 1}{\epsilon}\Phi(1) \quad . \tag{8}$$

We use $\epsilon = 6$ based on the estimate by Vlasova et al.[13] for the static dielectric constant of $(ET)_2Cu(NCS)_2$ in the b direction (in the plane of ET molecules). Using Φ from (7) in (8) leads to $(IP_1)_{sc} = 2.47$ eV, $(IP_2)_{sc} = 3.27$ eV and $U_{sc} = 0.80$ eV. Thus we considered the range $0 < U < 1.0$ eV for the band calculations. Comparing to experiment (vide infra) we conclude that $U_{opt} = 0.678950$ eV.

2.3 The Band Structure

Since the unit cell of $\kappa-(ET)_2Cu(NCS)_2$ has four ET molecules, there are four bands based on the HOMO orbitals. With two electrons transferred to the $Cu(NCS)_2^-$ units, there are six electrons (two holes) to be shared by the HOMO's of the four ET molecules. Thus, 3/4 of all states are occupied.

Figure 3 shows the band structures for various values of U from 0 eV to 1.0 eV and Figure 4 shows the corresponding Fermi surfaces. The Fermi energy is taken as the energy reference, leading to negative energies for occupied levels and positive energies for empty levels.

With UHF the energies and eigenstates of up-spin and down-spin are allowed to be different at the same k-point. However, we find that for $U \leq U_a = 0.6780$ eV the band structures for spin-up and spin-down electrons are the same.[10] This leads to calculated spin densities that are nearly the same ($< n_{i\alpha} > \approx < n_{i\beta} > \approx 0.75$) for all sites. Our calculations (Table 2) lead to slight deviations from the expected spin density of 0.75. Thus with $U = 0$ two sites have 0.7511 while the other two have 0.7489. This indicates that the four ET molecules have slightly different environments. Very slight differences between $< n_{i\alpha} >$ and $< n_{i\beta} >$ occur for $U < U_a = 0.678$ eV. Thus we find a net spin density of $S_{net} = 0.0003$ at $U = 0.670$, 0.0007 at $U = 0.674$ and $S_{net} = 0.0050$ at $U = 0.678$. Above $U_a = 0.6780$ eV the net spin density rises rapidly as shown in Figure 5b. The numerical calculations are carried to a point where $< n_{i\sigma} >$ is converged to better than 0.001 so that these small differences are part of the H-UHF model.

For $U > U_a$, the on-site Coulomb repulsion causes a significant difference between the up-spin and down-spin densities at the same site ($< n_{\alpha i} > \neq < n_{\beta i} >$), leading to antiferromagnetic character. Thus the down-spin bands differ increasingly from the up-spin bands. The band structures are almost identical except for small differences in the second and third bands, especially along $M - \Gamma$. This is shown in Figures 3i (up-spin) and 3j (down-spin) for $U = 1.0$ eV. We conclude below that the value of $U_{opt} = 0.678950$ eV (Figure 3c) explains the electronic behavior of those systems.

Table 2 shows up-spin and down-spin densities for various values of U. A good

measure of spin unpairing is

$$S_{net} = \frac{1}{4}\sum_i | < n_{i,\sigma} - n_{i,-\sigma} > | \quad , \tag{9}$$

which is tabulated in Table 3 and shown in Figure 5b. We see that

i. $S_{net} \approx 0.0$ for $U \leq U_a = 0.6780$ eV.

ii. for $U > U_a$, S_{net} equals to 0.018 at $U_{opt} = 0.678950$ eV. Then, S_{net} increases rapidly to $S_{net} = 0.123$ at $U = 0.679$ eV, $S_{net} = 0.322$ at $U = 0.690$ eV, and $S_{net} = 0.362$ at $U_i = 0.698960$ eV. Above U_i it increases more slowly, finally reaching $S_{net} \rightarrow 0.500$ as $U \rightarrow \infty$.

iii. $S_{net} = 0.5$ for a perfect antiferromagnetic ($U = \infty$); thus S_{net} can be considered as the average spin density on each ET.

The *conduction band occupancy* (see Table 3, and Figure 5a) is constant, $N_c = 0.1697$, for $U \leq U_a = 0.6780$ eV. It decreases rapidly to $N_c = 0$ at $U_i = 0.698960$ eV.

Figures 6(a), 6(b), 6(c) and 6(d) show the density of states per spin at $U = 0$, $U_a = 0.678$ eV $U = 0.678950$ eV and $U = 0.679$ eV. The effective mass is defined as

$$m* = m_e \frac{N_b(E_F)}{N_0} \quad , \tag{10}$$

where N_b is the band density of states, N_0 is the density of states for free electrons and E_F is the Fermi energy. This leads to $m_v^* = 0.90$, $m_c^* = 1.14$ for $U = 0$ eV and $m_v^* = 0.99$, $m_c^* = 1.08$ for $U_{opt} = 0.678950$ eV, where v and c denote the third (valence) and fourth (conduction) bands.

Applying Fermi-Dirac statistics to the calculated band structure leads to the temperature dependence for the conduction band occupation (N_c) shown in Figure 7. The valence band occupation is given by $N_v = 1 - N_c$. For both $U = 0$ eV and $U_{opt} = 0.678950$ eV, N_c increases monotonically with temperature.

Table 4 lists various characteristic energies of the band structure (measured relative to the bottom of the lowest band).

The band picture is strongly affected by the splitting of the bands. For $U \leq$

$U_a = 0.6780$ eV the third and fourth bands overlap along the $M - Y$ and $M - Z$ directions in reciprocal space, leading to metallic character. For $U \leq U_i = 0.698960$ eV, this leads to holes in the third band and electrons in the fourth. For $U \geq U_i$ the fourth (conduction) band and third (valence) band are totally separated, leading to a semiconductor or an insulator. For $U_a < U < U_i$ the third and fourth bands do not overlap at the same k points. Thus orbitals at the Fermi surface in the conduction bands no longer connect to orbitals in the valence band, leading to semi-metallic behavior.

2.4 Calculational Details

The $\kappa - ET_2Cu(NCS)_2$ crystal is monoclinic with space group $P2_1$, Z=2, and lattice parameters $a = 16.256$Å, $b = 8.4564$Å, $c = 13.143$Å and $\beta = 110.276°$ at $T = 298$K.[12]

This leads to reciprocal lattice vectors (1/Å units) of

$$\vec{A} = 2\pi \frac{\vec{b} \times \vec{c}}{V} = 2\pi \left(\frac{1}{a\ sin\beta}, 0, 0 \right) \quad , \tag{11a}$$

$$\vec{B} = 2\pi \frac{\vec{c} \times \vec{a}}{V} = 2\pi \left(0, \frac{1}{b}, 0 \right) \quad , \tag{11b}$$

$$\vec{C} = 2\pi \frac{\vec{b} \times \vec{c}}{V} = 2\pi \left(\frac{-1}{c\ tan\beta}, 0, \frac{1}{c} \right) \quad , \tag{11c}$$

where V is the volume of the unit cell.

Leblanc et al.[6] performed GVB calculations on ET dimers to obtain the transfer integrals, t_{ij}, between ET molecules [using the experimental room temperature structure[12] of $\kappa - ET_2Cu(NCS)_2$]. These t_{ij} values are given in Table 1 using the notation in Figure 8. We used these transfer integrals and corresponding experimental room temperature crystal structure in our calculations.

Every conduction layer (bc-plane) of ET molecules is sandwiched by the insulating layers of anion $Cu(NCS)_2$ along the a-axis. Since the nonzero t_{ij} are in the bc-plane, the relevant 2-D Brillouin zone is for the BC-plane. $\vec{B}$ and $\vec{C}$ are perpendicular to each other with lengths $B = 0.74300947$Å^{-1} and $C = 0.50971229$Å^{-1}, leading to

a rectangular Brillouin zone. The point Y lies along $\vec{B}$, Z lies along $\vec{C}$, and M is at the corner of the Brillouin zone (see Figure 4). Hence, $Y = \pi\ (0, 0.11825363, 0)$, $Z = \pi\ (0.02810889, 0, 0.07608613)$, $M = \pi\ (0.02810889, 0.11825363, 0.07608613)$. The distances between these points are $d(\Gamma Z) = 0.25485614\text{Å}^{-1}$, $d(\Gamma Y) = 0.37150473\text{Å}^{-1}$, and the ratio is $\frac{d(\Gamma Z)}{d(\Gamma Y)} = 0.68601048$. We used 150 points along B and 102 points along C.

For each U, the eigenvalues and eigenvectors were solved at each k-point leading to $4 \times (150 \times 102) = 61200$ energies for up-spin electrons and 61200 energies for down-spin electrons for the four bands of $\kappa - ET_2Cu(NCS)_2$. Since there are 3 up-spin electrons and 3 down-spin electrons for each 4 ET molecules, the 45900 states with lowest energies were occupied for each spin. The average densities were calculated using (3) for both up-spin and down-spin electrons. This process was continued iteratively by using the new densities in (5) to obtain new energies and eigenvectors at each k-point for both up- and down-spins. The up and down energies at each k-point were saved and compared with energies of previous iteration at the same k-point for all k-points of the Brillouin zone. The process was considered converged when the RMS error of the energies was less than 10^{-9} eV. This took ~15 iterations for $U = 0.3$ eV, ~400 iterations for $U = 0.678$ eV, ~15 iterations for $U = 1.0$ eV. For the converged wavefunctions, we calculated band occupancies, density of states, and the Fermi surface.

3.0 Comparison with Experiment

3.1 Magnetic Experiments

Using the band structures from Section 2, we will examine the various experimental results. In making the comparisons we should emphasize that the t_{ij} values are based on minimum basis GVB calculations using the room temperature crystal structure. Thus exact quantitative agreement cannot be expected.

Thermopower[3,7] and Hall effect measurements (vide infra) indicate that hole conduction dominates,[14] that electronic conduction is parallel to the b axis and that hole conduction is parallel to the c axis. This is consistent with U values between 0 and

$U_{closed} = 0.685195$ eV, which give band structures with a Fermi surface that is closed for holes and open sheets for electrons. As U increases above $U_a = 0.6780$ eV the closed hole orbits shrink toward Z while the open electrons orbits move toward Y. The open electron orbits touch the BZ boundary at Y for $U_{closed} \approx 0.685195$ eV, and above this value[15] lead to closed orbits around the M point (this would disagree with the SdH experiments discussed below). As U approaches U_i the hole orbits shrink to zero at Z while the electron orbits shrink to zero at M. At $U_i = 0.698960$ eV the 3rd and 4th band separate leading to a semiconductor for $U > U_i$.

At a temperature of 1 K and for magnetic fields above 8 T, Oshima et al.[5] observed magnetoresistance [Shubnikov-de Haas (SdH)] oscillations related to the extremal area A of the Fermi surface normal to the field direction. The relation is

$$\Delta\left(\frac{1}{H}\right) = \frac{2\pi e}{\hbar c A} \quad , \tag{12}$$

where H is the magnitude of magnetic field. They concluded that the observed oscillations correspond to a cylindrical Fermi surface containing 18% of the Brillouin zone. Sasaki et al.[16] observed the SdH effect at 0.5 K and above 8 T (see Figure 2d) and found that the observed oscillations correspond to 16.3% occupation of the Brillouin zone. From a band structure based on the extended Hückel (EH) approximation (with the room temperature crystal structure), Oshima et al.[5] found a "closed region of about 18%." These results can be compared to our result of 16.9% for $U = 0.678950$ eV. The antiferromagnetic transition reduces the area of the closed part of the BZ. This closed portion totally disappears for $U \geq U_i$. Thus SdH experiments are in reasonable agreement with our results for $U = 0.678950$ eV.

The occurrence of magnetic breakdown (jumping of electrons between the open and closed orbits under the magnetic field) supports the topology of Fermi surface found by us and others,[5,6] namely a closed valence band orbit and an open conduction band orbit (see Figure 2e).[16] These jumps correspond to the interband (between the third and the fourth bands) transitions. This suggests that $U > U_a = 0.6780$ eV but $U < U_{closed} = 0.685195$ eV.

For large gaps, the probability of magnetic breakdown electronic transitions is very small. The estimate is that magnetic breakdown transitions do not occur if

$$\hbar\omega_c << \frac{E_g^2}{E_F} \quad , \tag{13}$$

where ω_c is the cyclotron frequency and E_g is the direct gap between the third and the fourth band. Sasaki et al.[16] observed magnetic breakdown at 0.5K for fields above $H = 22T$, obtaining a value of $\frac{E_g^2}{E_F} = 0.3417$ meV. We find $\frac{E_g^2}{E_F} = 0.1291$ meV, 0.3197 meV and 8.4913 meV for $U = 0.678$ eV, 0.678950 eV and 0.679 eV respectively. Thus $\frac{E_g^2}{E_F}$ is very sensitive to U for $U \geq 0.678$ eV.

These comparisons with experiment suggest that the band structure for $U_{opt} \sim$ 0.678950 eV in Figures 3 and 4 best describes the $\kappa - ET_2Cu(NCS)_2$ salt. Both Oshima et al.[5], and LeBlanc et al.[6] also obtained overlapping bands and hence metallic conductivity, leading to a similar qualitative picture of the band structure. However, Extended Hückel (EH) calculations do not describe[5,6] the antiferromagnetic states, and hence EH calculations cannot provide a quantitative explanation of the magnetic breakdown experiments.

Our results ($U_{opt} = 0.678950$ eV) suggest a very small antiferromagnetic coupling with a net spin density of about 0.018 spins on each ET. Such antiferromagnetic behavior has not yet been detected for $\kappa - ET_2Cu(NCS)_2$. However, for the related (nonsuperconducting) compound $\kappa - (ET)_2Cu[N(CN)_2]Cl$, Miyagawa et al.[17] and Welp et al.[18] found such an antiferromagnetic state (it becomes superconducting with $T_c = 12.8$ K under pressure of 0.3 kbar). Miyagawa et al.[17] observed a moment of (0.4-1.0)μ_b/dimer for $\kappa-(ET)_2Cu[N(CN)_2]Cl$. We believe that these results support our conclusion that the normal state of $\kappa - ET_2Cu(NCS)_2$ is a weakly antiferromagnetic conductor. These $\kappa-(ET)_2CuX$ salts are similar and expected to have similar band structures. The dramatic differences in the conduction properties of these two crystals could likely arise from small differences in t_{ij} and U values due to the slight differences in packing. Thus changing U to $U_i = 0.698960$ eV for $\kappa-ET_2Cu(NCS)_2$, would lead to an insulating antiferromagnetic ground state with a moment of 1.4 μ_b/dimer (taking

g=2.0). The temperature dependence of the susceptibility χ of $\kappa - ET_2Cu(NCS)_2$ shown in Figure 2c could be due to this very weak antiferromagnetism with a net spin density 0.04 per dimer for $U_{opt} = 0.678950$ eV. χ decreases as temperature decreases for T $\leq$100 K (antiferromagnetic behavior) and shows little temperature dependence between 100 K and 300 K (Pauli paramagnetic behavior). The spin unpairing could be reduced by small changes in the t_{ij} and U values due to slight changes in the packing (e.g., the observed change in the interlayer spacing, which has a maximum around 100 K). In this case, the weak antiferromagnetic contribution may decrease as temperature increases above 100 K, allowing Pauli paramagnetism to become dominant. Thus, Hubbard model is able to describe the puzzling magnetic properties of these κ salts.

3.2 Resistivity Experiments

The lattice spacing $d_{100} = a \cdot sin\beta$ shows a maximum around 100 K. This maximum has been attributed[19] to structural changes in the hydrogen bonding between the terminal $-CH_2CH_2-$ group of ET and the anion layer -SCN-Cu-NCS-. The bond length of Cu-N also shows an anomaly around 100 K.[20]

The resistivity increase in Figure 2a is proportional to T^2 until it peaks at $T = 100$ K, and then decreases exponentially with $1/T$ like a semiconductor. The ratio of resistivities $\frac{R(100K)}{R(300K)}$ increases when tensile stress is applied along b axis.[21] Where electron-electron scattering dominates, we expect the temperature dependence of the conductivity to be proportional to $\frac{1}{T^2}$ while if electron-phonon scattering dominates we expect it to be proportional to $\frac{1}{T}$ (for large T). Thus experiment implies that electron-electron scattering dominates for low T.

One might attempt to explain the semiconducting behavior of the resistivity in terms of polarons. Polaron formation is plausible for this salt, especially around the central (TTF) part of ET molecule. Indeed, quantum chemistry calculations show that the central part of ET molecule changes most upon ionization.[22,23,24] However, the temperature dependence of the thermopower for $T \geq 100K$ (see Figure 2f) argues against polaron formation. For polarons in metallic systems, the thermopower should

be constant, i.e.

$$S \sim \frac{k_b}{q} log\rho \quad , \tag{14a}$$

where ρ is the electron density. For polarons in semiconductor systems, the thermopower (see Figure 2f) behaves as[25]

$$S \sim \frac{1}{T} \quad . \tag{14b}$$

This second type temperature behavior is exhibited by κ-$(ET)_2Cu(NCS)_2$ for $T \geq 100K$, suggesting that the system is semiconductor-like. However, such semiconducting behavior is not consistent with the constant Pauli susceptibility observed for $T \geq 100K$, see Figure 2c.

Electron-phonon scattering has the same effect on both spins and hence does not affect the magnetic susceptibility even though it may dramatically affect conductivity. Hence, we conclude that electron-phonon scattering must be involved in the anomalous resistivity. This can explain the semiconductor-like conductivity since the relaxation time for electron-phonon scattering is proportional to $\frac{1}{T}$. Thus only electron-phonon scattering would avoid a thermally activated region.

Based on the UHF calculations and using these experimental results as a guide, we propose the following model for this system:

a. Below 100K, this system is semi-metallic. This happens when $U > U_a = 0.6780$ eV and $U < U_i = 0.698960$ eV. At low temperatures, the phonon densities are low, hence there are no transitions between valence and conduction bands. As the temperature increases the electron-phonon couplings promote electronic transitions between these bands.

b. Around 100K, the electrons begin coupling to phonons of the anion layer. Due to this coupling, the resistivity has a peak.

The phonons of the anion layers may scatter the electrons between different ET molecules. The anion layer is insulating, but electrons can be scattered from one ET to a nearest-neighbor ET (on the same side of anion layer) by coupling to a phonon of the anion layer. Hence, this interaction will depend on the vibrations of ET and

of the anion, the distance of ET molecules from the anion layer, and the electronic structure. Changes in the ET-anion layer interaction will modify the electron-phonon coupling. Thus this mechanism involving scattering of ET electrons by anion phonons can also explain the interlayer spacing anomaly[19] and the tensile stress effects on the resistance.[21] Consequently this model suggests that the conductivity has the form

$$S_c \approx \frac{\alpha}{T^2} \tag{15a}$$

for $T < 100K$ (where α is a constant). For $T > 100$K the electrons begin to scatter with the phonons of anion layer, leading to the form

$$S_c \approx \frac{\gamma e^{-\epsilon_g/k_b T}}{T} \quad , \tag{15b}$$

where γ is a constant and ϵ_g is the gap between Fermi surface and the bottom of the anion band. Thus we can understand the behavior of the resistivity in Figure 2a.

3.3 Hall Measurements

The Hall coefficient R_H is observed (see Figure 2b) to be positive, decreasing with temperature as

$$R_H = -aT + b \quad , \tag{16}$$

but with a dramatic break in the slope at 60K. The magnitude of the slope is 33 times larger below 60K than above! There is no discontinuity in R_H around 100K where the resistivity exhibits a hump.[26]

Figure 7 shows that the change in carrier density is negligible between $T = 0$ K and 300 K for both $U = 0$ eV and $U_{opt} = 0.678950$ eV.

For the parabolic two-band model, the Hall coefficient is given as

$$R_H = \frac{1}{|e|c} \frac{p\mu_p^2 - n\mu_n^2}{(p\mu_p + n\mu_n)^2} \quad , \tag{17a}$$

where n, p are the electron, hole carrier densities and μ_n, μ_p are the corresponding

mobilities. Since $n = p$, this leads to

$$R_H = \frac{1}{p|e|c}\frac{\mu_p^2 - \mu_n^2}{(\mu_p + \mu_n)^2} = \frac{1}{p|e|c}\frac{\mu_p - \mu_n}{\mu_p + \mu_n} \quad . \tag{17b}$$

Similarly, for the parabolic two-band model, the conductivity is given as:

$$S_c = S_n + S_p = n|e|\mu_n + p|e|\mu_p = p|e|(\mu_n + \mu_p) \quad . \tag{17c}$$

The relaxation times for electron-phonon and electron-electron scattering are proportional to $\frac{1}{T}$ and $\frac{1}{T^2}$ respectively. Thus we take the temperature dependence of the mobilities, μ_n and μ_p, to be

$$\mu_n = \frac{\mu_0}{T} + \frac{\mu_1}{T^2} \quad , \tag{18a}$$

$$\mu_p = -\frac{\mu_0}{T} + \frac{\mu_2}{T^2} \quad . \tag{18b}$$

This leads to

$$S_c = p|e|(\frac{\mu_1 + \mu_2}{T^2}) \quad , \tag{19}$$

and

$$R_H = \frac{1}{p|e|c}(\frac{\mu_2 - \mu_1}{\mu_2 + \mu_1} - \frac{2\mu_0}{\mu_2 + \mu_1}T) \quad . \tag{20}$$

Comparing with (16) leads to

$$a = (\frac{1}{p|e|c})\frac{2\mu_0}{\mu_2 + \mu_1} \tag{21a}$$

and

$$b = (\frac{1}{p|e|c})\frac{\mu_2 - \mu_1}{\mu_2 + \mu_1} \quad . \tag{22a}$$

The dramatic change in the slope of R_H at $T = 60$K must arise from a large change in μ_0. This could arise from transitions between the third and fourth bands caused by the increased electron-phonon scattering with increased T.

4.0 Discussion and Conclusions

We should emphasize that the band calculations presented here include significant

approximations. The Hubbard model is a crude model of the many-body electron correlations and UHF is a simple mean field approximation to this model. We have used first principles calculations[5] to obtain the t_{ij} matrix elements; however, these calculations used a minimal basis set and the room temperature crystal structure. In addition, we ignored the role of the anion layer and of deeper bands. Even so there is only one adjustable parameter (U) in our theory and the optimum value is close to a first principles estimate. Thus given the good agreement of the final band properties with experiment, we believe that the resulting model is useful for describing the electronic structure of this class of organic superconductors.

The Hubbard UHF calculations lead to the following conclusions for $\kappa - (ET)_2Cu(NCS)_2$. We find that the system is semi-metallic and weakly antiferromagnetic with a momentum gap between the third and fourth bands. As the temperature is increased, the ET phonons couple the electrons in these two bands. We believe that this explains the anomalous Hall effect and susceptibility. Above 100K, we believe that electron-phonon scattering by phonons of the anion layer scatter the conduction electrons, leading to the anomalous temperature dependence in the resistivity.

The calculated band structure is very sensitive to U. This may be partly an artifact of the Hubbard-UHF approximation. However, it may also signify the frustration between antiferromagnetic coupling, vibrations of the ET and electronic coupling that is at the heart of the superconducting in these systems.[22]

References

1. Jerome D., Mazaud A., Ribault M., Bechgaard K., *J. Phys. Lett. 41*, (1980) L95.

2. Wang HH, Carlson KD, Geiser U, Kini AM, Schultz AJ, Williams JM, Montgomery LK, Kwok WK, Welp U, Vandervoort, Schirber J.E., Overmyer D.L., Jung D., Novoa J. J., Whangbo MH,*Synthetic Metals, 42* (1991) 1983.

3. Oshima K., Urayama H., Yamochi H., Saito G., *Physica C 153-155* (1988) 1148.

4. Oshima K., Mori T., Inokuchi H., Urayama H., Yamochi H., Saito G., *Phys. Rev. B 38*, (1988), 938.

5. Leblanc O.H., Blohm M. L., Messmer R. P., *MRS Symp. Proc. 173*, (1990), 119.

6. Urayama H., Yamochi H., Saito G., Sugano T., Kinoshita M., Inabe T., Mori T., Maruyama Y., Inokuchi H., *Chemistry Letters* (1988), 1057.

7. Mori H., Yamochi H., Saito G., Oshima K., in *The Physics and Chemistry of Organic Superconductors*, (Springer-Verlag 1990), 150.

8. Toyota N., Sasaki T., *Synthetic Metals, 41-43*, (1991) 2235.

9. Cariss C. S., Porter L. C., Thorn R. J., *Solid State Communications 74*, (1990) 1269.

10. We define U_a as the U value leading to a net spin unpairing of 0.005 per site.

11. Gaussian 92, Revision B, M. J. Frisch, G. W. Trucks, M. Head-Gordon, P. M. W. Gill, M. W. Wong, J. B. Foresman, B. G. Johnson, H. B. Schlegel, M. A. Robb, E. S. Replogle, R. Gomperts, J. L. Andres, K. Raghavachari, J. S. Binkley, C. Gonzalez, R. L. Martin, D. J. Fox, D. J. Defrees, J. Baker, J. J. P. Stewart, and J. A. Pople, Gaussian, Inc., Pittsburgh PA, 1992.

12. Carlson KD, Geiser U, Kini AM, Wang H. H., Schultz AJ, Montgomery LK, Kwok WK, Beno M. A., Williams JM, Cariss C. S., Crabtree G. W., Whangbo MH, Evain M., *Inorganic Chemistry, 27* (1988) 967.

13. Vlasova, R.M., Priev, S. Ya., Semkin V. N., Lyubovskaya, R. N., Zhilyaeva, E. I., Yagubskii, E. B., Yartsev V. M., *Synthetic Metals, 48* (1992) 129.

14. Murata K., Ishibashi M., Honda Y., Fortune N. A., Tokumoto M., Kinoshita N., Anzai H., *Solid State Communications 76*, (1990) 377.

15. The Fermi surfaces for $U = 0.685190$ eV and $U = 0.685200$ eV are shown in Figure 3 (e) and (f). For $U = 0.685190$ eV The Fermi surface is open for electrons but for $U = 0.685200$ it is closed. Thus we consider $U_{closed} = 0.685195$ eV. With the 150×102 discrete k points describing the BZ used in our calculations we cannot obtain a Fermi surface that exactly touches the BZ boundary.

16. Sasaki T., Sato H., Toyota N., *Solid State Communications 76*, (1990) 507.

17. Miyagawa K., Kawamoto A., Nakazawa Y., Kanoda K., *Phys. Rev. Lett. 75*, (1995) 1174.

18. Welp U., Fleshler S., Kwok W. K., Crabtree G.W., Carlson K. D., Wang H.H., Geiser U., Williams J. M., Hitsman V. M., *Phys. Rev. Lett. 69*, (1992) 862.

19. Watanabe Y., Sasaki T., Sato H., Toyota N., *Journal of The Physical Society of Japan 60*, (1991)2118.

20. Doi T., Kokichi O., Yamazaki H., Muruyama H., Hironobu M., Koizumi A., Kimura H., Fujita M., Yunoki Y., Mori H., Tanaka S., Yamochi H., Saito G., *Journal of The Physical Society of Japan 60*, (1991) 1441.

21. Kusuhara H., Sakata Y., Ueba Y., Tada K., Kaji M., *Solid State Communications 74*, (1990) 251.

22. Demiralp E., Goddard W. A. III, *J. Phys. Chem., 98*, (1994) 9781.

23. Demiralp E., Goddard W. A. III, *Synthetic Metals, 72*, 297 (1995).

24. Demiralp E., Dasgupta S., Goddard W. A. III, *Journal of American Chemical Society 117*, 8154 (1995).

25. Chaikin P. M., in *Organic Superconductivity*, (Plenum Press 1990), 101.

26. Murata et al.[9] used the lack of an anomaly in R_H around 100K (which could be caused by a change in the number of effective carriers) as an argument against the gap formation model of Toyota et al.[7]

27. Saito G., *Physica C 162-164*, (1989) 577-582.

Table 1: Electron transfer matrix elements
Electron transfer matrix elements (t_{ij}) from GVB calculations on ET dimers (from reference 5). The nomenclature is explained in Figure 8. The units are in meV.

t_1	t_2	t_3	t_4	t_5	t_6
−162.9	−93.6	−92.8	32.3	−73.1	37.6

Table 2: Site densities for up and down spins
Site densities for up and down spins as a function of U. For each case the entries are in the sequence $i = a, a', b, b'$.

U (eV)	$< n_{i\alpha} >$	$< n_{i\beta} >$
0.000	0.7489	0.7489
	0.7511	0.7511
	0.7489	0.7489
	0.7511	0.7511
0.300	0.7493	0.7494
	0.7506	0.7507
	0.7494	0.7493
	0.7507	0.7506
0.670	0.7492	0.7495
	0.7505	0.7508
	0.7495	0.7492
	0.7508	0.7505
0.674	0.7490	0.7497
	0.7503	0.7510
	0.7497	0.7490
	0.7510	0.7503
0.678	0.7469	0.7518
	0.7481	0.7531
	0.7518	0.7469
	0.7531	0.7481
0.678950	0.7403	0.7585
	0.7414	0.7598
	0.7585	0.7403
	0.7598	0.7414
0.679	0.6884	0.8104
	0.6889	0.8123
	0.8104	0.6884
	0.8123	0.6889
0.680	0.6879	0.8110
	0.6883	0.8129
	0.8110	0.6879
	0.8129	0.6883
0.685190	0.6257	0.8733
	0.6250	0.8760
	0.8733	0.6257
	0.8760	0.6250
0.685200	0.6051	0.8941
	0.6038	0.8970
	0.8941	0.6051
	0.8970	0.6038
0.690	0.5898	0.9095
	0.5881	0.9126
	0.9095	0.5898
	0.9126	0.5881
0.698960	0.5704	0.9291
	0.5681	0.9324
	0.9291	0.5704
	0.9324	0.5681
0.800	0.5577	0.9423
	0.5549	0.9451
	0.9423	0.5577
	0.9451	0.5549
1.000	0.5407	0.9599
	0.5376	0.9619
	0.9599	0.5407
	0.9619	0.5376
∞	0.5000	1.0000
	0.5000	1.0000
	1.0000	0.5000
	1.0000	0.5000

Table 3: Characteristics of the band structure as a function of U
Characteristics of the band structure as a function of U. S_{net} is the spin unpairing (see equation 9). N_c is the occupation of the conduction band (it is the same for both up-spin and down-spin bands). δk is the momentum gap between closed orbits (valence band) and open orbits (conduction band) of the Fermi surface; it is in units of $B/2$ (the grid over k space has 75 points for B/2).

U (eV)	N_c	S_{Net}	δk	State
0.000	0.1697	0.0000	$\frac{2}{75}$	Metallic
0.300	0.1697	0.0001	$\frac{2}{75}$	Metallic
0.670	0.1697	0.0003	$\frac{2}{75}$	Metallic
0.674	0.1697	0.0007	$\frac{2}{75}$	Metallic
0.678	0.1697	0.0050	$\frac{2}{75}$	Metallic
0.678950	0.1692	0.0183	$\frac{3}{75}$	Semi-metallic
0.679	0.1434	0.1227	$\frac{16}{75}$	Semi-metallic
0.680	0.1431	0.1238	$\frac{16}{75}$	Semi-metallic
0.685190	0.0796	0.2493	$\frac{35}{75}$	Semi-metallic
0.685200	0.0511	0.2911	-	Semi-metallic
0.690	0.0294	0.3221	-	Semi-metallic
0.698960	0.0000	0.3615	-	Semiconductor
0.800	0.0000	0.3874	-	Semiconductor
1.000	0.0000	0.4218	-	Semiconductor
∞	0.0000	0.5000	-	Insulator

Table 4: Energies from the band calculation

Energies (in meV) from the Hubbard-UHF band calculation on ET. All energies are relative to the bottom of the first (lowest) band $E_1^b = 0$. E_c^t is the top of the fourth (highest) band; this gives the total width of the ET HOMO band structure. E_F is the Fermi energy (the chemical potential μ, for zero temperature), E_c^b is the energy of the bottom of conduction (fourth) band E_v^t is the energy of at the top of the valence (third) band. E_g is the direct energy gap between the third (valence) band and the fourth (conduction) band. All results are for $T = 0°$.

U(eV)	E_c^t	μ	E_C^b	E_V^t	E_g	$\frac{E_g^2}{\mu}$
0.000	844.8029	522.6820	442.4582	648.2950	8.1867	0.1282
0.300	844.8038	522.6751	442.4612	648.4528	7.9128	0.1198
0.670	844.8049	522.6541	442.5829	648.5633	7.7226	0.1141
0.674	844.8050	522.6398	442.6855	648.5620	7.7274	0.1143
0.678[a]	844.8223	522.6239	444.1521	648.3963	8.2140	0.1291
0.678950[b]	845.0467	522.8909	448.8468	646.6708	12.9284	0.3197
0.679	855.3908	534.4193	491.2927	628.7004	67.3640	8.4913
0.680	855.6176	534.5743	491.9001	628.5299	68.0719	8.6682
0.685190[c]	886.6236	571.1884	555.7679	619.9479	122.9906	26.4828
0.685200[c]	900.3870	588.9825	578.9809	620.1448	131.4241	29.3256
0.690	912.3507	603.6132	597.9936	621.2653	139.6652	32.3160
0.698960[d]	929.5836	624.0354	624.0368	624.0339	148.4373	35.2914
0.800	968.6776	657.1822	677.9939	636.3704	158.9976	38.4676
1.000	1052.1515	728.6382	784.9779	672.2984	168.9013	39.1520

[a] U_a.

[b] U_{opt} providing the best fit to the magnetic properties of $\kappa - ET_2Cu(NCS)_2$.

[c] $U_{closed} = 0.685195$ is between these two values.

[d] U_i.

Figure Captions

Figure 1. The bis(ethylenedithio)tetrathiafulvalene molecule. This is denoted as BEDT-TTF or simply as ET.

Figure 2. Experimental properties of $\kappa - ET_2Cu(NCS)_2$.

(a)Electrical resistivity, ρ is in bc plane. The maximum is at $\sim$100 K.[27]

(b) Hall coefficient (R_H) in the c direction with current parallel to b and magnetic field parallel to a*. The large slope is from 20 to 60 K.[14]

(c) The magnetic susceptibility with the field in the a*direction. The superconductor transition is at 10.4 K .[27]

(d) The magnetoresistance oscillations when the current and field are parallel to a*.[4]

(e) High field magnetoresistance oscillations. The arrows show the peak positions of the high frequency F_β oscillations due to magnetic breakdown superimposed on the low frequency F_α oscillations.[16]

(f) The thermoelectric power with the thermal gradient (a) parallel to c and (b) parallel to b.[27]

Figure 3. The calculated Hubbard-UHF band structure as a function of U. Figures a-h show the bands for spin-up electrons. For large U there are very slight differences with the spin-down bands. This is shown in Figure 3j for $U = 1.0$ eV where there are very small differences between the second and third bands for up-spin and down-spin, especially along $M - \Gamma$ in Figures 3i and 3j.

Figure 4. The Fermi surface as a function of U. The conduction (fourth) band (electron states) has its lowest energy at M, and for $U \leq 0.685190$ eV leads to an open Fermi surface in the MY direction, leading to the highest mobility in the c direction. The valence (third) band (holes states) leads to a closed Fermi surface centered around Z, leading to the highest mobility in the b direction. For $U > U_a = 0.678$ eV the momentum gap between the third and fourth bands increases rapidly. For $U > U_i = 0.698960$ eV the lowest fourth band (electron) states (at M) are above the highest third band (hole) states (at Z). This leads to semiconducting behavior.

Figure 5. Various properties as a function of U. (a) The conduction band occupancy (N_c) (for up-spin); the experimental value is about 0.163. Above $U_i = 0.698960$

eV, the system is nonmetallic. (b) The (antiferromagnetic) the net spin density (S_{net}); above $U_a = 0.678$ eV the system is antiferromagnetic. (c) The momentum gap (δk) between the third and fourth bands. (d) The magnetic breakdown factor $\frac{E_g^2}{E_F}$ (assuming $N_c \neq 0.0$).

X marks the data point point for $U_{opt} = 0.678950$ eV.

Figure 6. Density of States for (a) $U = 0$ eV (b) $U_a = 0.6780$ eV (c) $U_{opt} = 0.678950$ eV (d) $U = 0.679$ eV.

The dash lines show the contributions of the valence and the conduction bands.

Figure 7. Temperature dependence of the conduction band occupation for (a) $U = 0$ eV (b) $U_a = 0.6780$ eV (c) $U_{opt} = 0.678950$ eV (d) $U = 0.679$ eV.

Figure 8. Definition of electron transfer matrix elements (t_{ij}) for the band calculations of $\kappa - (BEDT - TTF)_2Cu(NCS)_2$. Here aa' and bb' refer to the two pairs of donors in each unit cell. See reference 5 for more details.

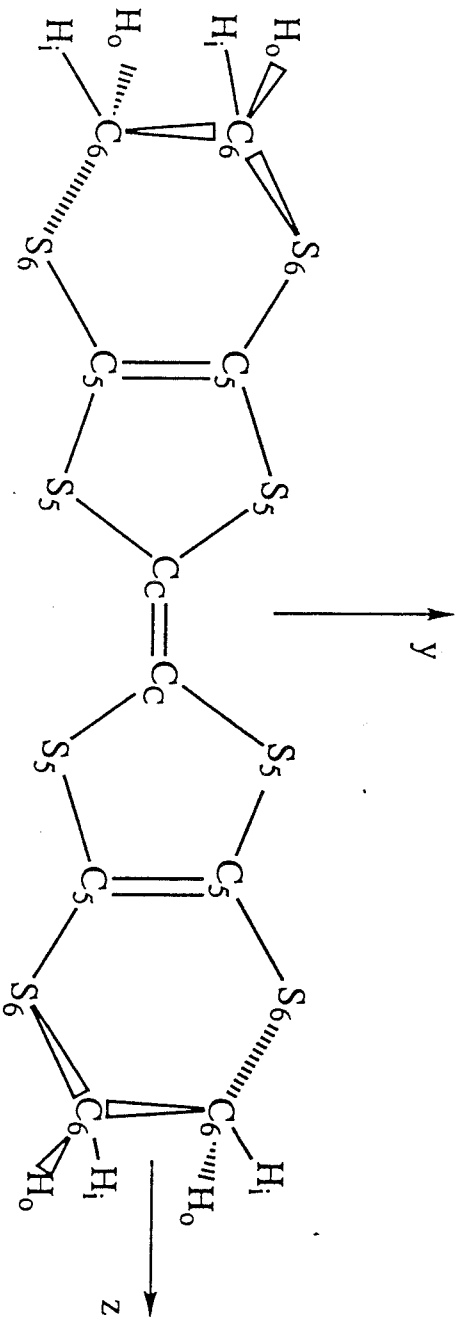

Figure 1. bis(ethylenedithio)tetrathiafulvalene, ET

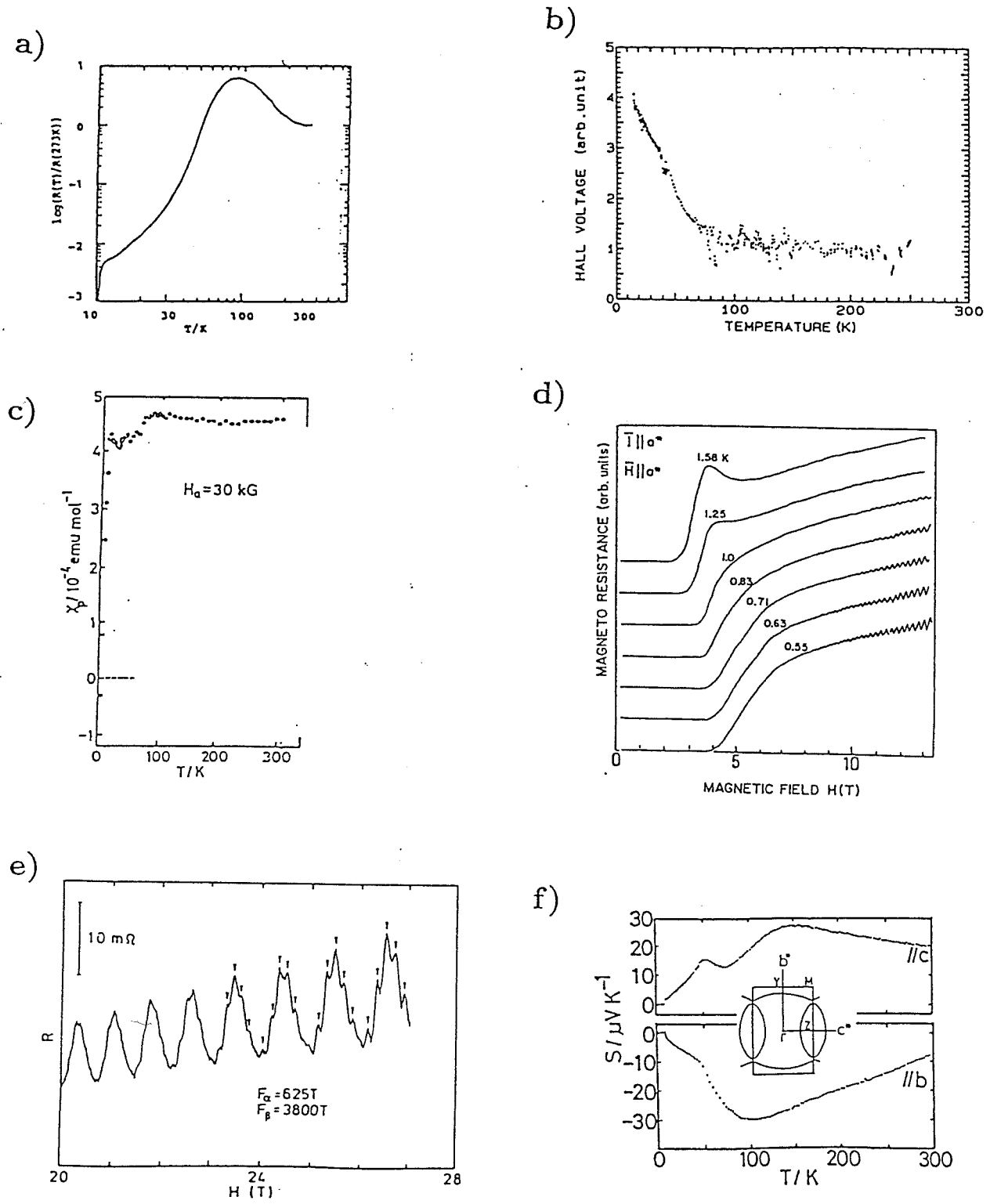
a)
log(R(T)/R(273K))
T/K
b)
HALL VOLTAGE (arb.unit)
TEMPERATURE (K)
c)
H_a=30 kG
$\chi_p/10^{-4}$ emu mol^{-1}
T/K
d)
T||a*
H||a*
1.58 K
1.25
1.0
0.83
0.71
0.63
0.55
MAGNETO RESISTANCE (arb.units)
MAGNETIC FIELD H(T)
e)
10 mΩ
R
F_α=625T
F_β=3800T
H (T)
f)
S/μVK^{-1}
//c
//b
T/K

Figure 2

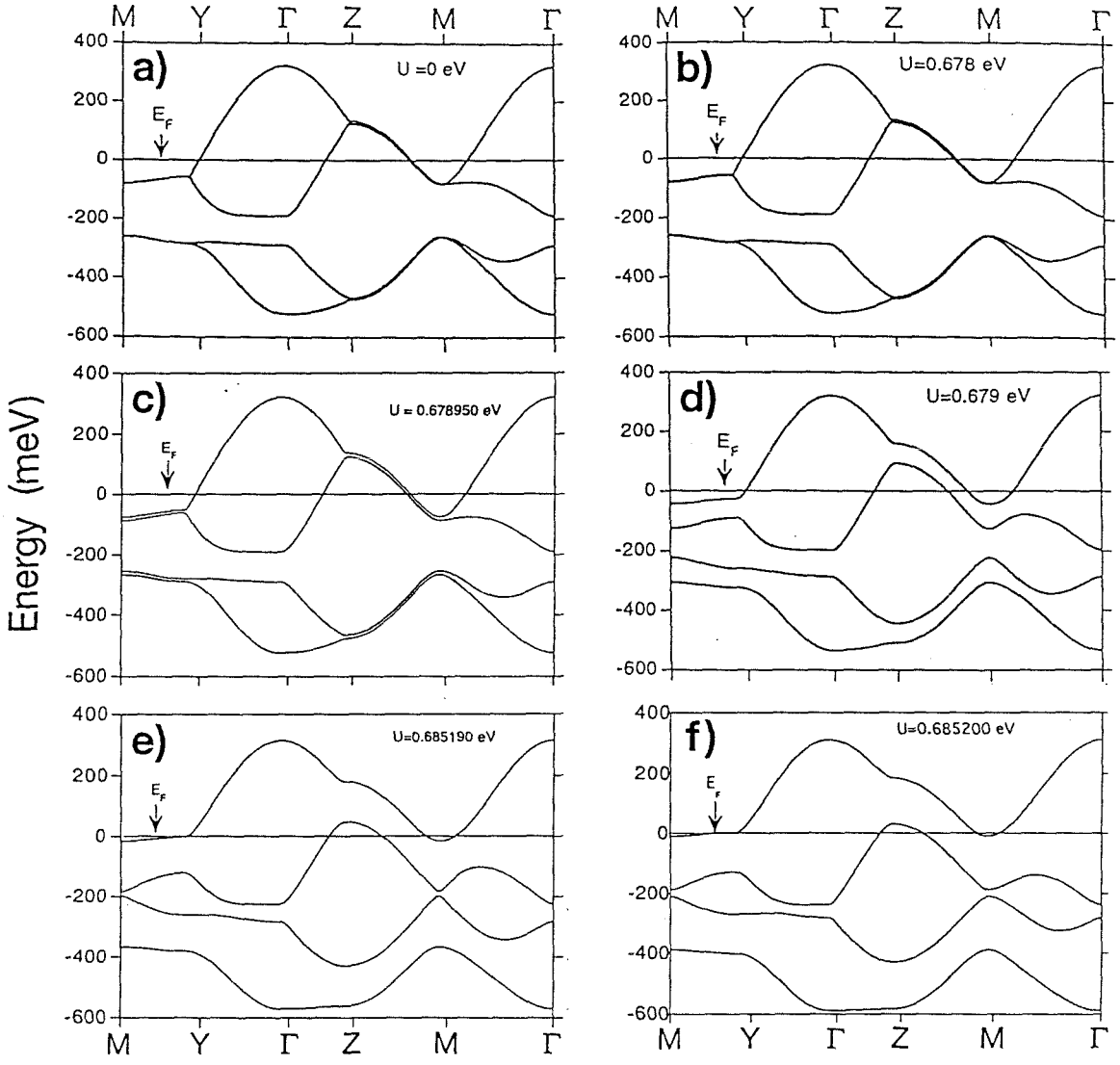
M Y Γ Z M Γ
a)
U =0 eV
b)
U=0.678 eV
c)
U = 0.678950 eV
d)
U=0.679 eV
e)
U=0.685190 eV
f)
U=0.685200 eV
E_F
Energy (meV)
400
200
0
-200
-400
-600

Figure 3

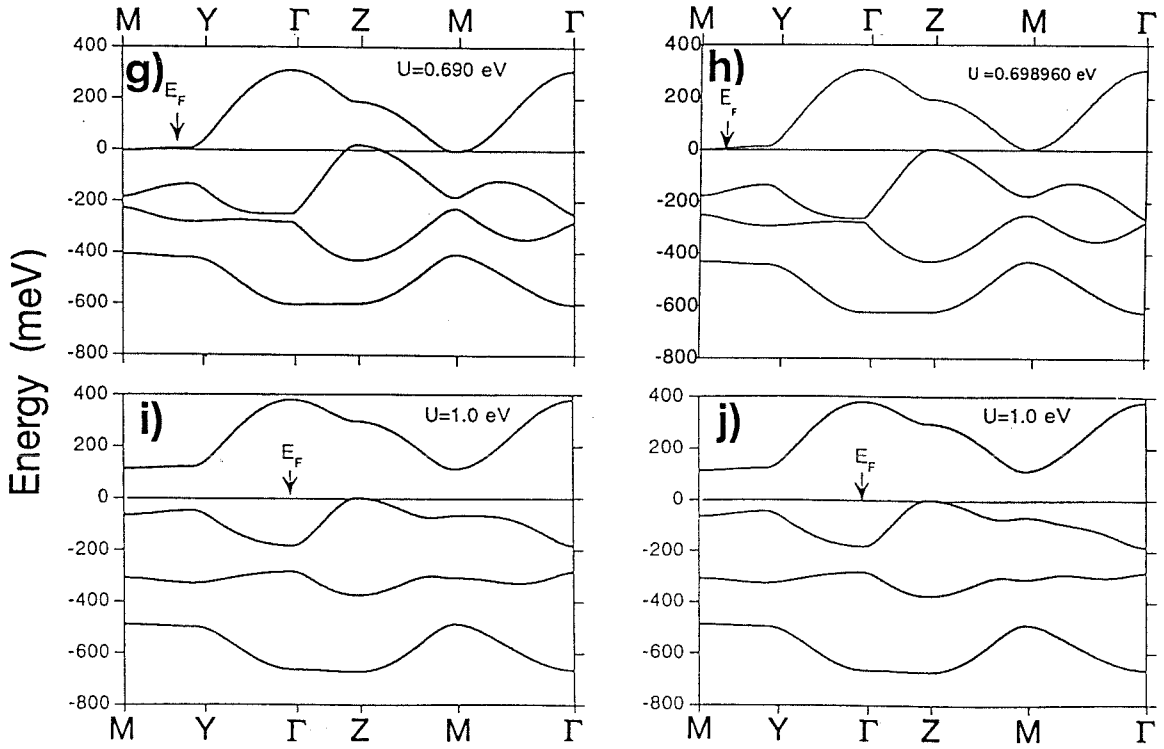
M Y Γ Z M Γ
g)
U=0.690 eV
h)
U =0.698960 eV
i)
U=1.0 eV
j)
U=1.0 eV
E_F
Energy (meV)
400
200
0
-200
-400
-600
-800

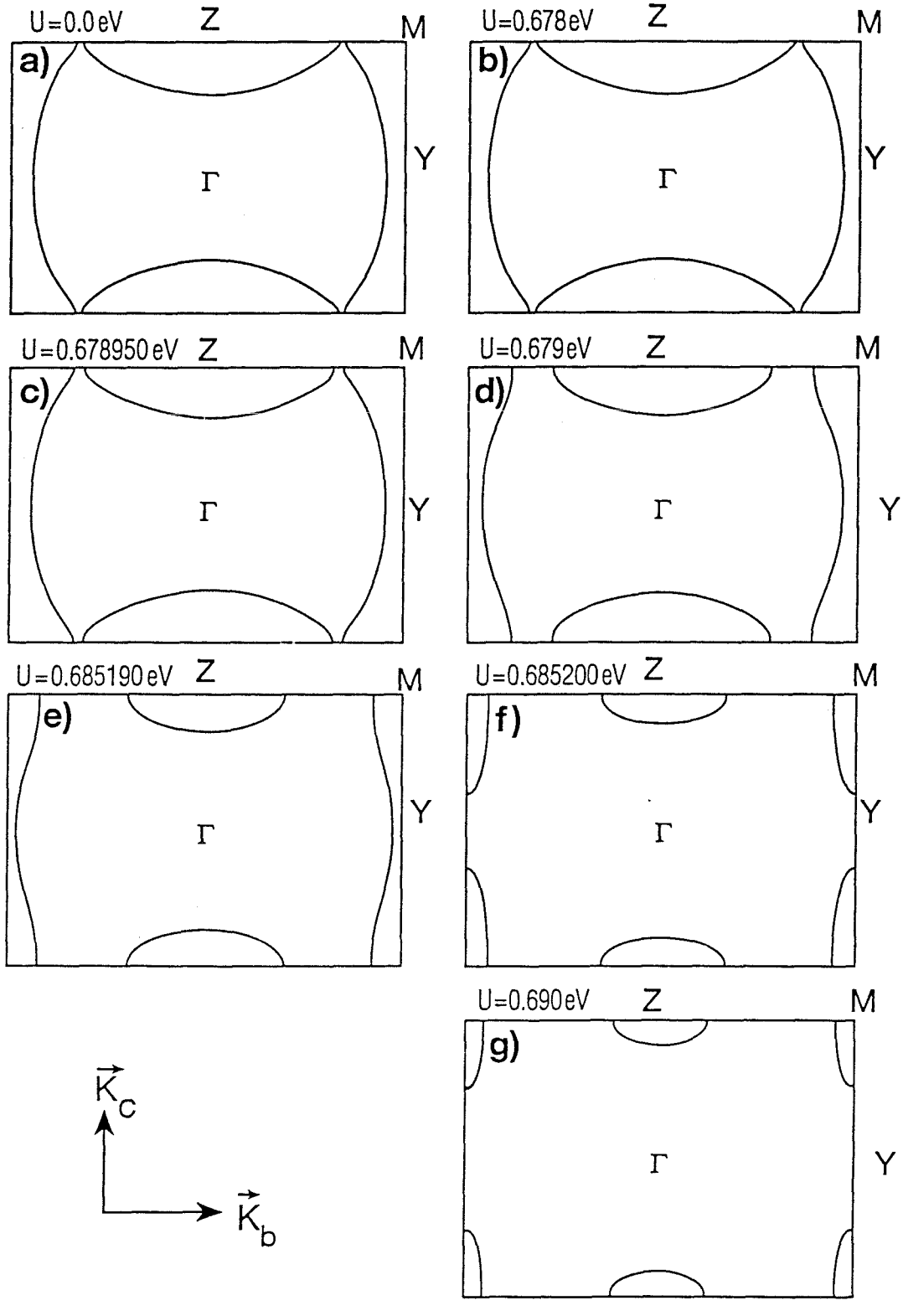
U=0.0eV
Z
M
a)
Γ
Y
U=0.678eV
Z
M
b)
Γ
Y
U=0.678950eV
Z
M
c)
Γ
Y
U=0.679eV
Z
M
d)
Γ
Y
U=0.685190eV
Z
M
e)
Γ
Y
U=0.685200eV
Z
M
f)
Γ
Y
U=0.690eV
Z
M
g)
Γ
Y
$\vec{K}_c$
$\vec{K}_b$

Figure 4

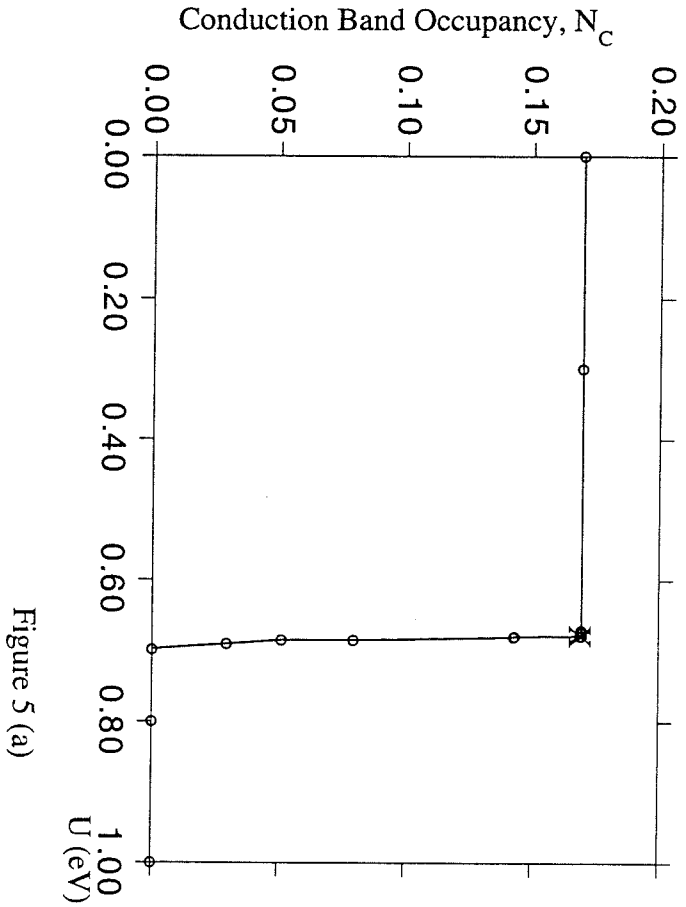
Conduction Band Occupancy, N_C
0.00
0.05
0.10
0.15
0.20
0.00
0.20
0.40
0.60
0.80
1.00
U (eV)

Figure 5 (a)

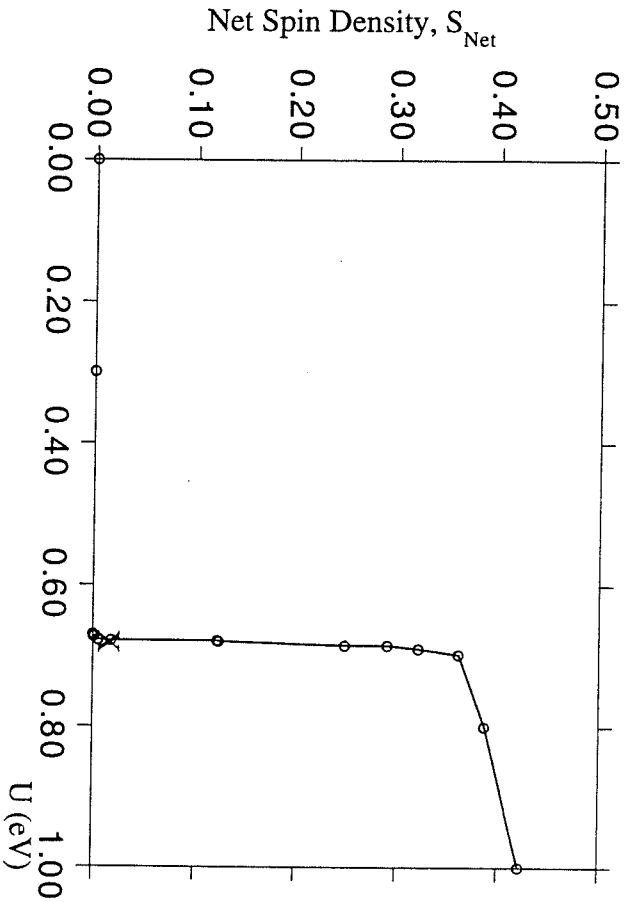
Net Spin Density, S_{Net}
0.00
0.10
0.20
0.30
0.40
0.50
0.00
0.20
0.40
0.60
0.80
1.00
U (eV)

Figure 5 (b)

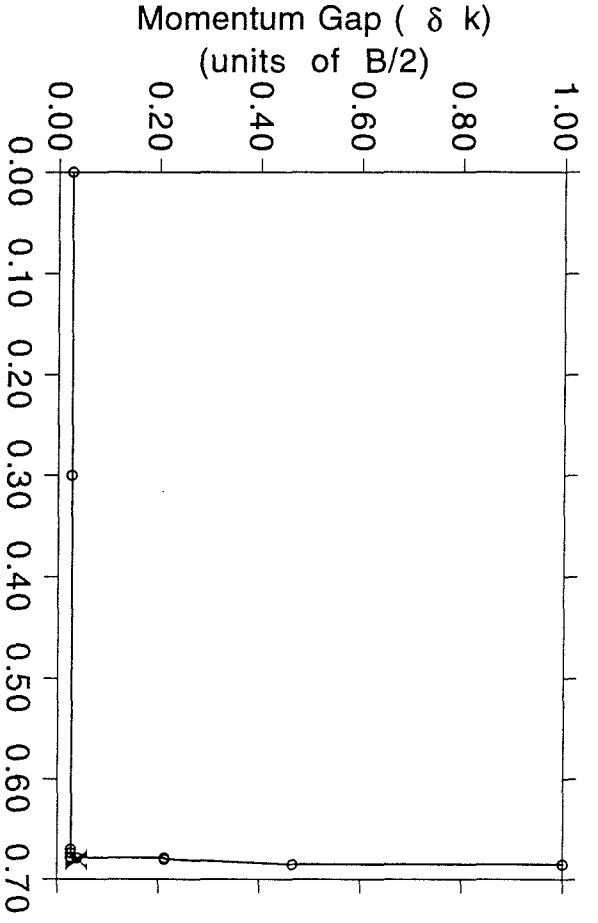
Momentum Gap (δ k)
(units of B/2)
0.00
0.20
0.40
0.60
0.80
1.00
0.00
0.10
0.20
0.30
0.40
0.50
0.60
0.70
U (eV)

Figure 5(c)

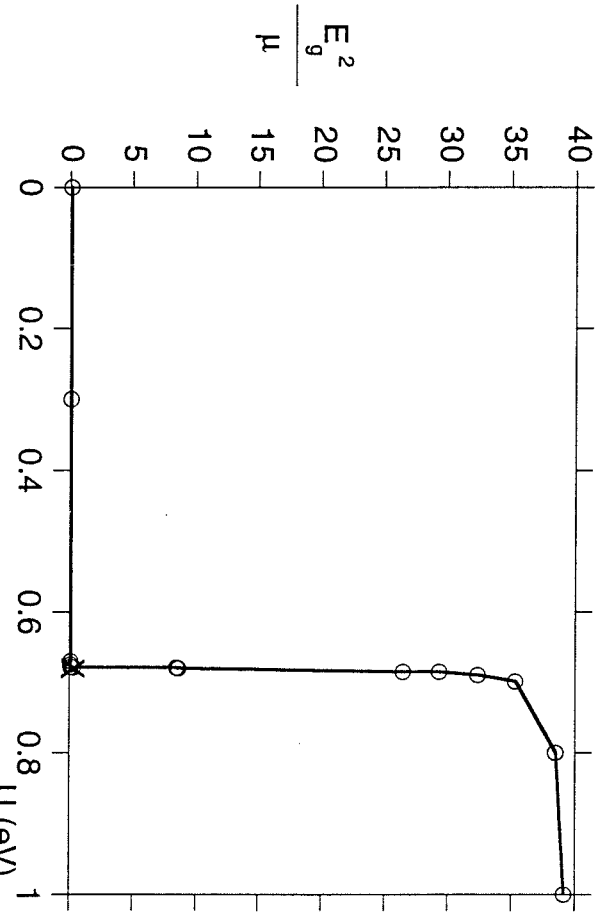

Figure 5 (d)

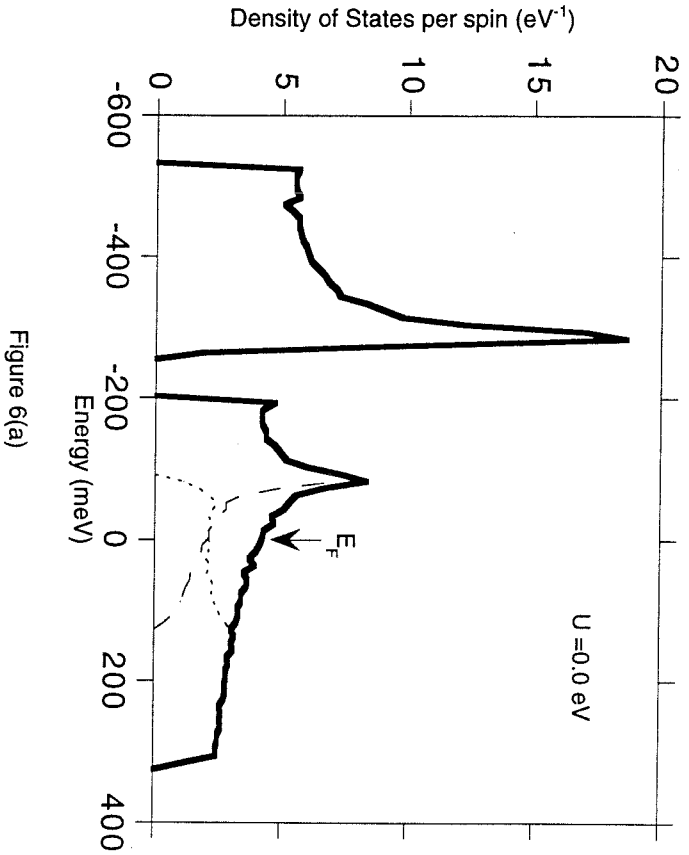
Density of States per spin (eV-1)
0
5
10
15
20
-600
-400
-200
0
200
400
Energy (meV)
EF
U =0.0 eV

Figure 6(a)

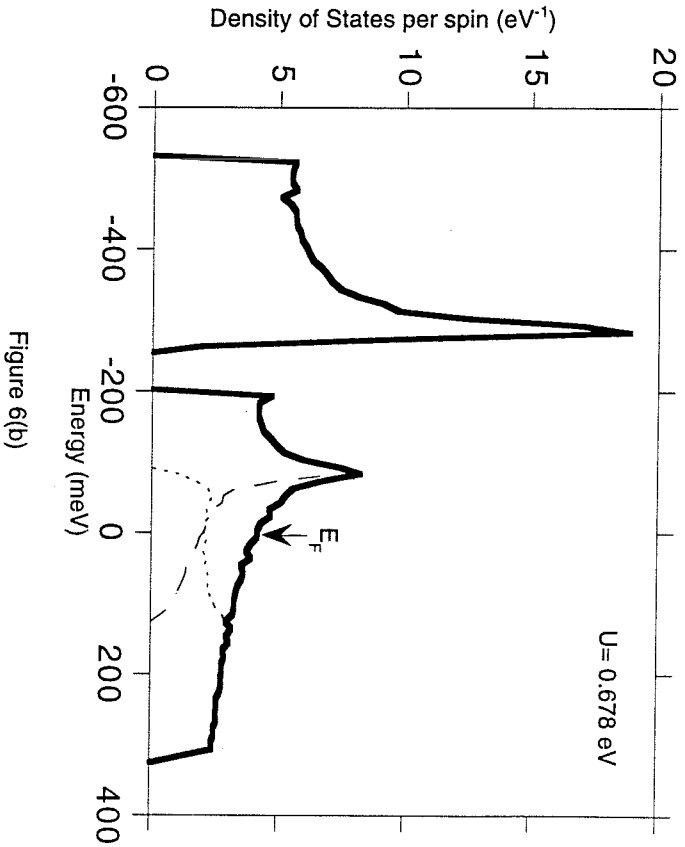
Density of States per spin (eV-1)
0
5
10
15
20
-600
-400
-200
0
200
400
Energy (meV)
EF
U= 0.678 eV

Figure 6(b)

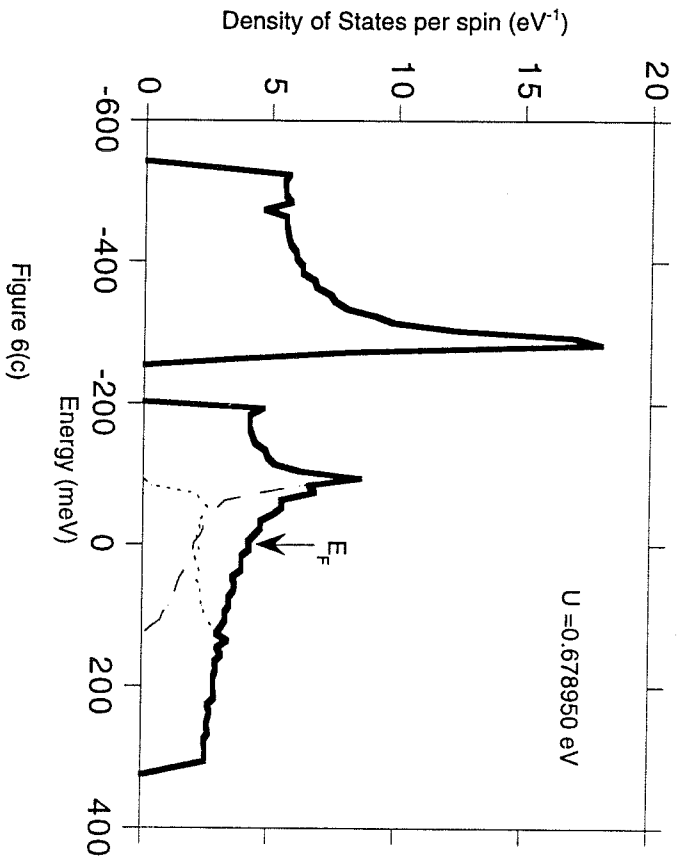
Density of States per spin (eV-1)
0
5
10
15
20
-600
-400
-200
0
200
400
Energy (meV)
EF
U =0.678950 eV

Figure 6(c)

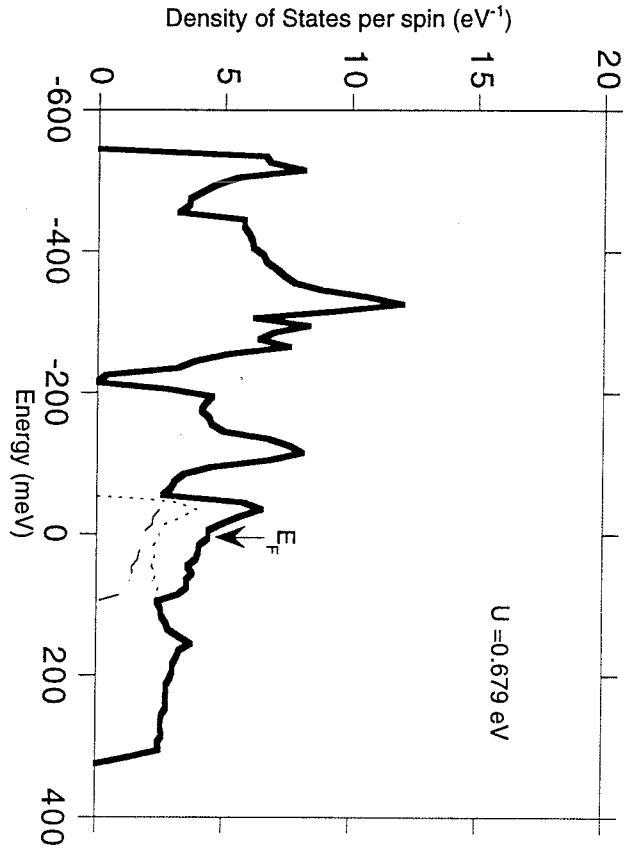
Density of States per spin (eV-1)
0
5
10
15
20
-600
-400
-200
0
200
400
Energy (meV)
EF
U =0.679 eV

Figure 6(d)

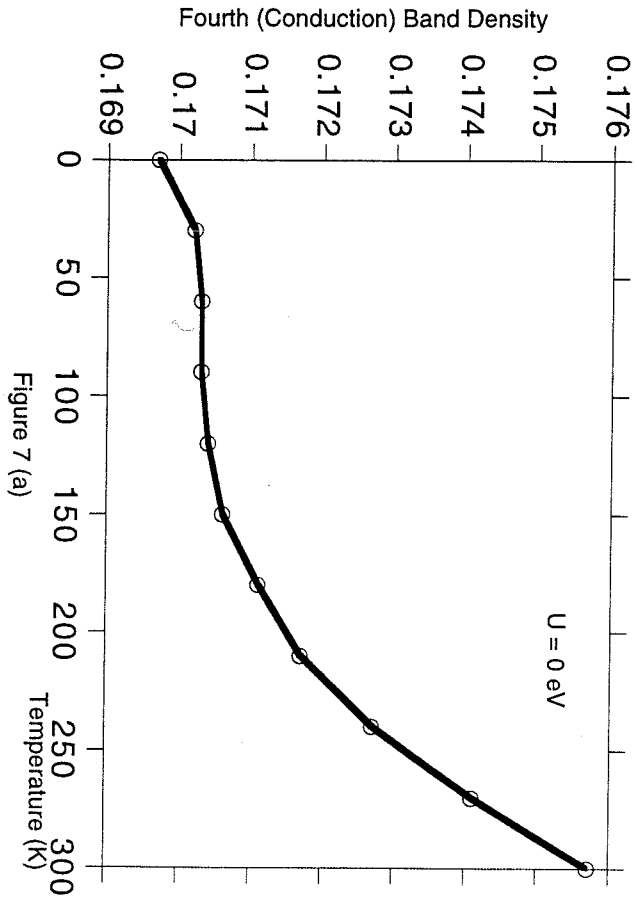
Fourth (Conduction) Band Density
0.169
0.17
0.171
0.172
0.173
0.174
0.175
0.176
0
50
100
150
200
250
300
Temperature (K)
U = 0 eV

Figure 7 (a)

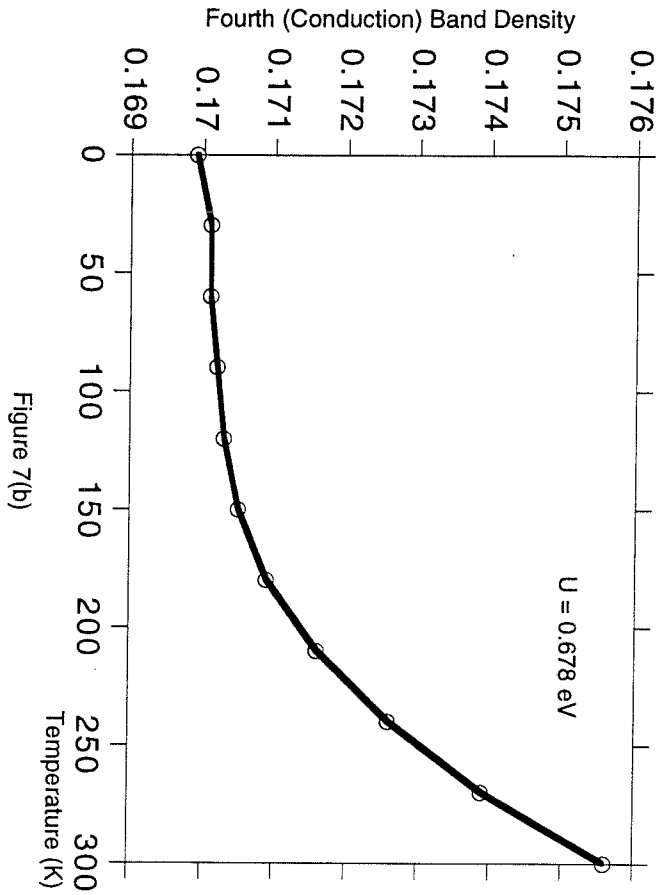
Fourth (Conduction) Band Density
0.169
0.17
0.171
0.172
0.173
0.174
0.175
0.176
0
50
100
150
200
250
300
Temperature (K)
U = 0.678 eV

Figure 7(b)

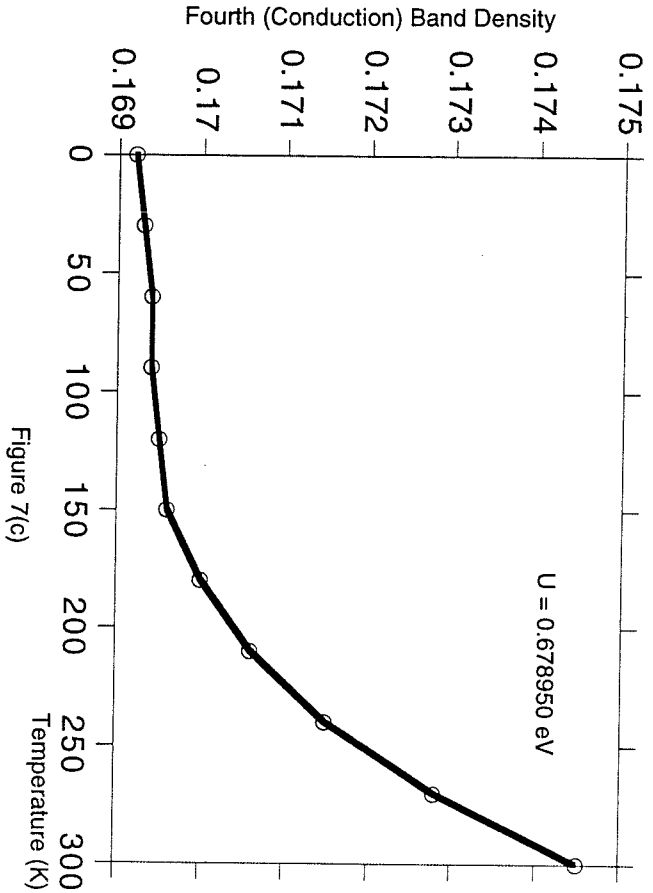
Fourth (Conduction) Band Density
0.175
0.174
0.173
0.172
0.171
0.17
0.169
0
50
100
150
200
250
300
Temperature (K)
U = 0.678950 eV

Figure 7(c)

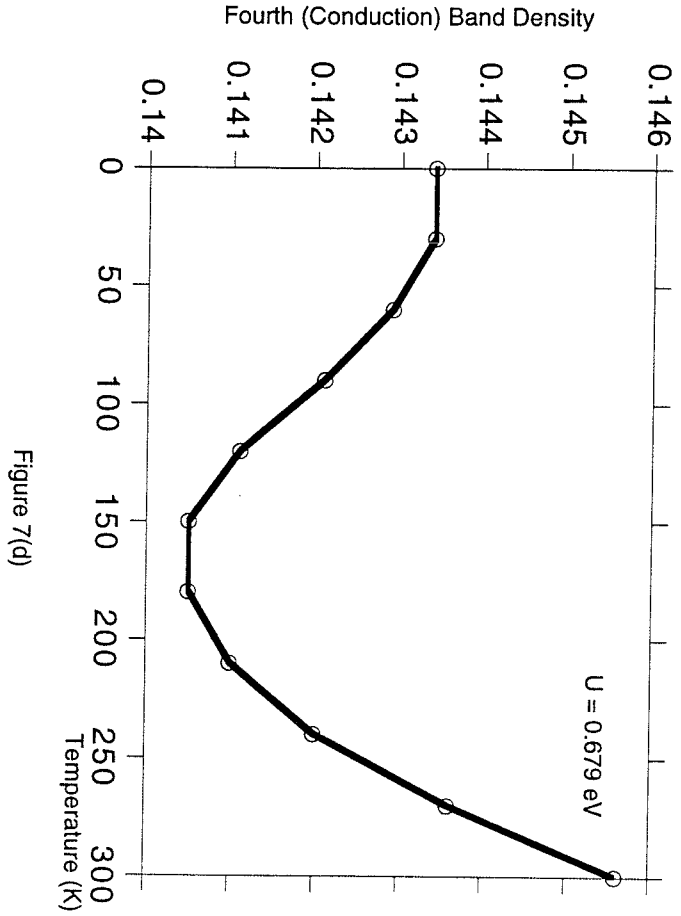
Fourth (Conduction) Band Density
0.14
0.141
0.142
0.143
0.144
0.145
0.146
0
50
100
150
200
250
300
Temperature (K)
U = 0.679 eV

Figure 7(d)

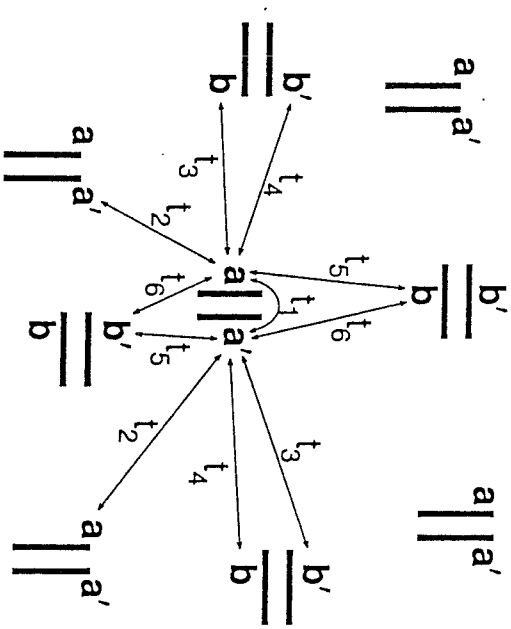

Figure 8

Chapter 3 Structural Calculations for Organic Superconductors

3.1 Ab Initio and Semi-empirical Electronic Structural Studies on $BEDT-TTF$

Abstract

We report electronic structure calculations for the organic molecule bis(ethylenedithio)tetrathiafulvalene (BEDT-TTF or ET), associated with the highest T_c organic superconductors. The experimental structures exhibit considerable disorder in the outer rings and concomitant uncertainty in the structures. We find that Hartree-Fock (6-31G** basis set) calculations lead to results within 0.01Å and 1° of experiment for the ordered regions allowing us to predict to composite structures expected to have this accuracy. We report optimized geometries and atomic charges for ET, ET^{+}, and $ET^{+\frac{1}{2}}$ that should be useful for atomistic simulations.

1.0 Introduction

The transition temperature of organic superconductors has been increasing since the discovery of $(TMTSF)_2PF_6$.[1,2] The highest T_c organic superconductors involve the electron donor bis (ethylenedithio) tetrathiafulvalene (denoted as BEDT-TTF or ET, shown in the Figure 1 in Chapter 2) complexed to appropriate electron acceptors. Such systems show a variety of electronic behaviors (semiconducting, metallic, superconducting), but it is not totally clear how the superconductivity is related to the structure, composition, electronic states, or vibrational states.[7,8] We are carrying out a series of theoretical studies aimed at establishing a basis for such an understanding. In carrying out these studies we found a disturbing variation in experimental structures from various sources. Since structure is the starting point for many of our studies, we optimized the structures for both neutral and cation ET molecules using both the *ab initio* Hartree-Fock (HF) method (with the 6-31G** basis set)[4] and the semi-empirical modified neglect of differential overlap (MNDO) method.[5]

The best organic superconductors have the composition $(ET)_mX_n$ where X is an electron acceptor.[2,3] In most such crystals there are ET_2^+ dimers, but some crystals have ET^+. Consequently, we report properties (structure, HOMO, LUMO levels, atomic charges) for ET, ET^+, and $ET^{+\frac{1}{2}}$. By comparing theory and experiment we were able to extract composite best structures.

2.0 Calculations

Using the HF method with a 6-31G** basis set, we optimized the structures of ET (C_2 symmetry) and ET^+ (D_2 symmetry).[4] With MNDO[5] we also optimized the structures of ET and ET^+, but it was necessary to distort the molecule to C_1. This led to deviations from the strict D_2 symmetry (less than 0.001Å for distances and less than 0.05 degrees for angles for neutral case, less than 0.005Å for distances and less than 0.5 degrees for angles for cation case).

3.0 Structural Results

3.1 Neutral ET

The crystal structure of neutral ET was reported by Kobayashi *et al.*[3] (See Figure 1). The monoclinic unit cell has four molecules grouped into two dimers. Such dimer structures are observed in most crystals containing ET molecules. The structural studies show a planar geometry for the central C_2S_4-like region; however, the terminal $-CH_2-CH_2-$ groups are nonplanar, leading to distortion and (probably) disorder.

Averaging out the small differences of the bond lengths and the angles of the neutral ET with C_2 symmetry , we take 7 independent atoms (See Figure 1 in Chapter 2 for notation): C_C (central double bonded carbon), S_5 (S in 5 membered ring), C_5 (double bonded C in 5 membered ring), S_6 (S in 6 membered ring), C_6 (single bonded C in 6 membered ring), H_o (H bonded to C_6 but out of plane, axial), H_i (H bond to C_6 but nearly in the plane, equatorial). The other atoms are obtained from rotations about the x, y, or z axes.

From Table 1 we see that HF bond distances are within about 0.015Å of experiment while MNDO is within about 0.06Å. The bond angles also agree well, errors of about 1° for HF and about 3° for MNDO. In these comparisons with experiment, we do not use the experimental positions for the terminal $-CH_2-CH_2-$ groups since they are disordered (thus the experimental C_6-C_6 bond distance of 1.46Å is clearly low by 0.07Å). As a result the experimental data on the out-of-plane distortions are not reliable.

Both theory and experiment show the S_6-C_6 bond to be significantly longer than S_6-C_5 (by 0.04 to 0.06Å), indicating partial double bond character for bonding of S_6 to $C_5=C_{5z}$.

3.2 ET^+

There are two crystal structures[5,6] with essentially a full positive charge on ET, $\epsilon-(ET)PF_6$ and $\delta-(ET)PF_6$ (See Figure 2). We carried out full self-consistent optimization of the structure for ET^+ with both HF(6-31G**) and MNDO. The structural parameters are compared with experiment in Table 2. Again there is excellent agreement between HF and experiment. Of the experimental results, the structure for $\epsilon-(ET)PF_6$ seems less reliable since the value obtained for the C_6-C_{6z}

bond is 1.32Å (rather than the expected value of 1.53Å). The $\delta - (ET)PF_6$ crystal leads to $R(C_6 - C_{6z}) = 1.484$Å, short but in agreement with the structural data for the neutral. Thus we compare these to the δ crystal results. Comparing ET and ET^+, we see that the structure changes occur only within the TTF portion, as indicated in Figure 3. This suggests that ionization involves primarily the central $C = C$ bond followed by some delocalization of the S_5 π orbital onto C_C and some delocalization of the $C_5 = C_{5z}$ bond onto S_5.

3.3 $ET^{+\frac{1}{2}}$

The best organic superconductors have an average charge of +0.5 on each ET. Examples include two important κ phase crystals $\{\kappa-(ET)_2Cu(NCS)_2$ (see Figure 2 and 3 in Chapter 1) and $\kappa - (ET)_2Cu[N(CN)_2]Br$ (see Figure 1 in Chapter 1) and $\beta - (ET)_2I_3\}$.[9–11] In Table 3 we compare the average of the calculated structures for ET and ET^+ with the average structural parameters. The 5-membered rings from all three crystal structures agree well with the theory (error of 0.01Å for HF); however, the 6-membered rings disagree substantially. Thus the $C_5 - S_6$ distance of the two κ states have values of 1.744Å and 1.749Å while $\beta - (ET)_2I_3$ has 1.712Å. The experimental studies of ET lead to 1.742Å while ET^+ of $\delta - (ET)PF_6$ leads to 1.736Å. Thus we assume that there is some problem with the value 1.712Å for $\beta-(ET)_2I_3$. Also for the S_6-C_6 distance, the value of 1.740Å for $\kappa-(ET)_2Cu(NCS)_2$ differs substantially from all others (1.811Å for the other κ structure, 1.810Å for $\beta(ET)_2I_3$, 1.809Å for $\delta-(ET)PF_6$, and 1.802Å for neutral ET). As a result only the $\kappa-ET_2Cu[N(CN)_2]Br$ structure seems to be without problems and we will use it for all comparisons. Comparing the crystal structure for $ET^{+\frac{1}{2}}$ and the average experimental values for ET and ET^+ (see Table 3), we find excellent agreement ($C_C = C_{Cx}$ longer by 0.01Å, $S_5 - C_5$ longer by 0.08Å). This justifies the use of the average values from the theory.

Comparing the theoretical values with experiment for $ET^{+\frac{1}{2}}$, we also find excellent agreement: bonds distance within 0.02Å for HF and 0.08Å for MNDO, bond angles within 0.9° for HF and 5.6° for MNDO.

4.0 Charges

There are two ways to evaluate charges from electronic wavefunction. Mulliken charges are based on the MO coefficients. Potential derived charges (PDQ) are based on the electric field derived from the HF density.[15] A set of atomic charges are obtained that reproduce the same electric field outside the vdW radii. Since the charges are used to predict packing energies and geometries in the crystal, PDQ charges should be more useful. In addition we have applied an empirical method, charge equilibration[14] (denoted as QEq), which is based only on atomic parameters.

The PDQ charges were calculated using both the CHELPG model of GAUSSIAN 92 and the PDQ module of the PS-GVB[19] program. (For the latter, the point charges fit not only the potential but also the *ab initio* dipole and quadrupole moments.) There seems to be a numerical problem with GAUSSIAN 92 since the calculated charges do not reflect the symmetry of the molecule (C_2 for neutral ET and D_2 for ET^+) and of the wavefunction. We symmetry averaged the GAUSSIAN 92 results to obtain the values in Figure 4 (top line for each atom). PS-GVB leads to symmetry consistent results (Figure 4, second line for each atom).

The main charge density is around the central part of the molecule. This result is consistent with the STM experiment of $\kappa - (ET)_2Cu(NCS)_2$.[12] The change between ET and ET^+ suggests that during the electron transfer between ET molecules, the vibrational modes of the central part of ET (center carbons and sulfurs on the pentagon ring) may couple with the electrons. However, recent isotope experiments exclude the importance of these kind of couplings for the superconductivity of organic superconductors.[17,18]

5.0 Ionization Potential

The orbital energies from HF and MNDO calculations on ET and ET^+ are shown in Figure 5, 6 and Table 4. The HOMO and LUMO orbitals from HF are plotted in Figure 7 and 8. The experimental gas-phase ionization potential is 6.21 eV.[13] Comparing the total energies from the HF calculations on the ion and neutral leads to $IP = 5.80$ eV whereas the orbital energy of the neutral (Koopmans theorem)

leads to $IP = 7.07$ eV. This is typical, the correlation error is smaller for the positive ion leading to too small an IP. Koopmans theorem assumes that the orbitals do not relax upon ionization, leading to too large a value. The average value of 6.44 eV is in good agreement with the experiment. From MNDO, the total energies leads to an IP of 7.42 eV, whereas the orbital energy leads to IP = 8.09 eV.

6.0 Conclusion

The structures from HF calculations (6-31G** basis) are in excellent agreement (0.01Å and 1°) with the experimental data on the ordered regions of ET, ET^{+}, and $ET^{+\frac{1}{2}}$. Thus one may use the HF structures to obtain full structural parameters. The atomic charges should be useful in molecular dynamics simulations.

References

1. Jerome D., Mazaud A., Ribault M., Bechgaard K., *J. Phys. Lett. 41*, (1980) L95.

2. Williams J. M., Ferraro J. R., Carlson K. D., Geiser U., Wang H. H.,Kini A. M., Whangbo M-H, *Organic Superconductors (Including Fullerenes): synthesis, structure, properties, and theory*, (Prentice-Hall 1992).

3. Kobayashi H., Kobayashi A., Yukiyoshi S., Saito G., Inkuchi H., *Bull. Chem. Soc. Jpn., 59*, (1986) 301.

4. Gaussian 92, Revision B, M. J. Frisch, G. W. Trucks, M. Head-Gordon, P. M. W. Gill, M. W. Wong, J. B. Foresman, B. G. Johnson, H. B. Schlegel, M. A. Robb, E. S. Replogle, R. Gomperts, J. L. Andres, K. Raghavachari, J. S. Binkley, C. Gonzalez, R. L. Martin, D. J. Fox, D. J. Defrees, J. Baker, J. J. P. Stewart, and J. A. Pople, Gaussian, Inc., Pittsburgh PA, 1992.

5. The MNDO calculations used Mopac, Version 6.00: M. J. S. Dewar, *et al.*, Frank J. Seiler Research Laboratories, U.S. Air Force Academy, Colorado Springs, Colorado, 80840.

6. a) Bu, X., Cisarova I., Coppens P., *Acta Cryst. C48* (1992) 1562.

   b) Bu, X., Cisarova I., Coppens P., *Acta Cryst. C48* 1992) 1558.

7. Kozlov M. E., Pokhodnia K. I., Yurchencko A. A., *Spectrochimica Acta 45A* (1989), 323.

8. Kozlov M. E., Pokhodnia K. I., Yurchencko A. A., *Spectrochimica Acta 45A* (1989), 437.

9. Carlson, K. D, Geiser U., Kini A. M., Wang H. H., Montgomery L. K., Kwok W. K., Beno M. A., Williams J. M., Cariss C. S., Crabtree G. W., Whangbo M-H. Evain M. *Inorg. Chem. 27*, (1988), 967.

10. Geiser U., Schultz A. J., Wang H. H., Watkins D. M., Stupka D. L., Williams J. M., Schirber J. E., Overmyer D. L., Jung D., Novoa J.J., Whangbo M-H. *Physica C 174*, (1991), 475.

11. Mori T., Kobayashi A., Yukiyoshi S., Kobayashi H., Saito G., Inkuchi H., *Chem. Lett.*, (1984) 957.

12. Yoshimura M., Shigekawa H., Nejoh H., Saito G., Saito Y., Kawazu A. *Phys. Rev. B 16*, (1991), 13590.

13. Sato N., Saito G., Inokuchi H., *Chem. Phys.*, *76*, (1983),79.

14. Rappé A. K.; Goddard III, W. A. *J. Phys. Chem. 95*, (1991), 3358.

15. Chirlian L. E., Francl M. M., *J. Comp. Chem. 8* (1987), 894.

16. Wang H. H., Carlson K. D., Geiser U., Kini A. M., Schultz A. J., Williams J. M., Montgomery L. K., Kwok W. K., Welp U., Vandervoort, Schirber J. E., Overmyer D. L., Jung D., Novoa J. J., Whangbo M. H., *Synthetic Metals, 42* (1991) 1983.

17. Carlson K. D., Kini A. M., Klemm R. A., Wang H. H., Williams J. M., Geiser U., Kumar S. K., Ferraro J. R. , Flesher S., Dudek J. D., Eastman N. L., Mobley P. R., Seaman J. M., Sutin J. D. B., Yaconi G. A., *Inorg. Chem.*, 1992, 3346.

18. Carlson K. D., Kini A. M., Schlueter J. A., Geiser U., Klemm R. A., Williams J. M., Dudek J. D., Caleca M. A., Lykke K. R., Wang H. H., Ferraro J. R., *Physica C 215*, (1993) 195.

19. M. N. Ringnalda, J-M. Langlois, B. H. Greeley, T. V. Russo, R. P. Muller, B. Marten, Y. Won, R. E. Donnelly, Jr., W. T. Pollard, G. H. Miller, W. A. Goddard III, and R. A. Freisner, PS-GVB v1.0, Schrödinger, Inc., Pasadena, California, 1994.

Figure Captions

Figure 1. Crystal Structure of Neutral ET

Figure 2. Crystal Structure of $\delta - (ET)PF_6$

Figure 3. Distance changes upon ionization: experiment and [theory (HF)].

Figure 4. Calculated charges for ET (right side) and ET^+ (left side). For each atom the top entry is PDQ (Gaussian), the next is PDQ (PS-GVB), followed by Mulliken, and QEq.

Figure 5. Molecular orbital energy levels for ET and ET^+ from HF/(6-31G**) calculations.

Figure 6. Molecular orbital energy levels for ET and ET^+ from MNDO calculations.

Figure 7. The HOMO orbital of neutral ET molecule from HF calculations. The positive lobes are dark gray and the negative lobes are light gray. The isosurfaces are for an amplitude of 0.02 in atomic units.

Figure 8. The LUMO orbital of neutral ET molecule from HF calculations. The positive lobes are dark gray and the negative lobes are light gray. The isosurfaces are for an amplitude of 0.02 in atomic units.

Table 1: Structural Parameters for Neutral ET
From Theory (HF and MNDO) and Experiment (Reference 3) (See Figure 1 in Chapter 2 for notation).

a. Bond distances (Å) for neutral E.

	Number	Xtal	HF/6-31G**	MNDO
$C_C = C_{Cx}$	1	1.319	1.326	1.356
$C_C - S_5$	4	1.758	1.771	1.695
$S_5 - C_5$	4	1.754	1.774	1.688
$C_5 = C_{5z}$	2	1.332	1.323	1.367
$C_5 - S_6$	4	1.742	1.767	1.670
$S_6 - C_6$	4	1.802	1.814	1.737
$C_6 - C_{6z}$	2	(1.462)[a]	1.523	1.530
$C_6 - H_i$	4	-	1.084	1.112
$C_6 - H_o$	4	-	1.081	1.112
RMS Error		0.00	0.017	0.063

b. Bond angles (degrees) for neutral ET .

	Number	Xtal	HF/6-31G**	MNDO
$C_C - C_C - S_5$	4	123.2	123.71	123.38
$C_C - S_5 - C_5$	4	94.5	94.55	97.66
$S_5 - C_5 - C_{5z}$	4	117.3	117.22	115.72
$C_{5z} - C_5 - S_6$	4	126.6	128.45	127.19
$C_5 - S_6 - C_6$	4	100.8	100.81	106.35
$S_6 - C_6 - C_{6z}$	4	(116.8)[a]	113.17	115.91
$C_{6z} - C_6 - H_i$	4	-	109.75	109.43
$C_{6z} - C_6 - H_o$	4	-	110.83	109.97
RMS Error		0.00	0.86	2.96

[a]Crystallographic value is not accurate and was not included in the RMS error calculation.

Table 2: Structural Parameters for ET^+
From Theory (HF and MNDO) and Experiment ($\epsilon-(ET)PF_6$ from Reference 6a and $\delta-(ET)PF_6$ from reference 6b]. (See Figure 1 in Chapter 2 for notation).

a. Bond distances (Å) for ET^+.

	Number	$\epsilon-(ET)PF_6$	$\delta-(ET)PF_6$	HF/6-31G**	MNDO
$C_C=C_{Cx}$	1	1.396	1.381	1.389	1.398
C_C-S_5	4	1.715	1.721	1.721	1.672
S_5-C_5	4	1.743	1.732	1.751	1.676
$C_5=C_{5z}$	2	1.353	1.351	1.336	1.389
C_5-S_6	4	1.727	1.736	1.765	1.663
S_6-C_6	2	1.761	1.809	1.816	1.741
C_6-C_{6z}	4	$(1.32)^a$	$(1.484)^a$	1.523	1.529
C_6-H_i	4	-	-	1.083	1.112
C_6-H_o	4	-	-	1.080	1.112
RMS Error		0.024	0.00	0.017	0.059

b.Bond angles (degrees) for ET^+.

	Number	$\epsilon-(ET)PF_6$	$\delta-(ET)PF_6$	HF/6-31G**	MNDO
$C_C-C_C-S_5$	4	122.1	122.5	122.76	122.65
$C_C-S_5-C_5$	4	95.8	95.9	96.33	97.47
$S_5-C_5-C_{5z}$	4	116.3	116.6	116.42	115.17
$C_{5z}-C_5-S_6$	4	127.3	126.9	128.83	126.95
$C_5-S_6-C_6$	4	116.4	100.6	100.50	106.54
$S_6-C_6-C_{6z}$	4	$(126.9)^a$	$(115.0)^a$	113.10	115.69
$C_{6z}-C_6-H_i$	4	-	-	109.74	109.54
$C_{6z}-C_6-H_o$	4	-	-	111.46	110.34
RMS Error		2.5	0.0	0.9	2.8

[a]Crystallographic value is not accurate and was not included in the RMS error calculation.

Table 3 : Structural Parameters for $ET^{\frac{1}{2}}$
The theory values (HF and MNDO) use the average from ET and ET^{+}. The experimental structures (references 9,10 and 11) are X1= $\kappa-(ET)_2Cu(NCS)_2$, X2= $\kappa-(ET)_2Cu[N(CN)_2]Br$ and X3=$\beta-(ET)_2I_3$. It appears that X2 is most consistent (See Figure 1 in Chapter 2 for notation).

a. Bond distances (Å) for $ET^{\frac{1}{2}}$.

	No.	X1	X2	X3	Av. Exp[a]	HF/6-31G**[c]	MNDO[c]
$C_C=C_{Cx}$	1	1.364	1.360	1.363	1.350	1.358	1.377
C_C-S_5	4	1.742	1.741	1.733	1.740	1.746	1.684
S_5-C_5	4	1.758	1.751	1.770	1.743	1.762	1.682
$C_5=C_{5z}$	2	1.339	1.343	1.360	1.342	1.330	1.378
C_5-S_6	4	1.744	1.749	1.712	1.739	1.766	1.666
S_6-C_6	4	1.740	1.811	1.810	1.806	1.815	1.739
C_6-C_{6z}	2	(1.522)[b]	(1.485)[b]	(1.304)[b]	(1.473)[b]	1.523	1.530
C_6-H_i	4	-	-	-	-	1.084	1.112
C_6-H_o	4	-	-	-	-	1.081	1.112
RMS Error		0.033	0.0	0.020	0.007	0.011	0.066

b.Bond angles (degrees) for $ET^{\frac{1}{2}}$.

	No.	X1	X2	X3	Av. Exp[a]	HF/6-31G**[c]	MNDO[c]
$C_C-C_C-S_5$	4	123.00	122.41	122.39	122.8	123.24	123.02
$C_C-S_5-C_5$	4	96.22	95.14	95.78	95.2	95.44	97.56
$S_5-C_5-C_{5z}$	4	116.75	117.13	116.36	117.0	116.82	115.46
$C_{5z}-C_5-S_6$	4	127.66	128.85	128.93	126.8	128.64	127.07
$C_5-S_6-C_6$	4	102.78	100.86	100.61	100.7	100.66	106.42
$S_6-C_6-C_{6z}$	4	(115.56)[b]	(115.10)[b]	(123.46)[b]	115.9[b]	113.14	115.80
$C_{6z}-C_6-H_i$	4	-	-	-	-	109.74	109.48
$C_{6z}-C_6-H_o$	4	-	-	-	-	111.14	110.16
RMS Error[d]		1.16	0.0	0.43	0.9	0.44	2.94

[a]From neutral ET and $\delta-(ET)^{+}(PF_6)^{-}$ crystals.

[b]Crystallographic value is not accurate and not included in the RMS error calculation.

[c]Average of the optimized ET and ET^{+} structures.

Table 4: Energies for ET and ET^+ from HF and MNDO calculations

	ET		ET^+	
	HF/6-31G**	MNDO[a]	HF/6-31G**	MNDO[a]
Total Energy (Hartree)	-3563.3607	-118.4398	-3563.1476	-118.1670
Orbital Energies (eV)				
HOMO	-7.073	-8.093	-10.929	-12.056
LUMO	2.748	-0.519	-4.540	-6.711
Ionization Potential (eV)				
ET^+-ET (total energy difference)	5.80	7.42		
Koopmans Theorem	7.07	8.09		
Experiment[b]	6.21	6.21		

[a]For MNDO, total energy is the sum of the electronic energy of valence electrons and core-core repulsions.

[b]Reference 13.

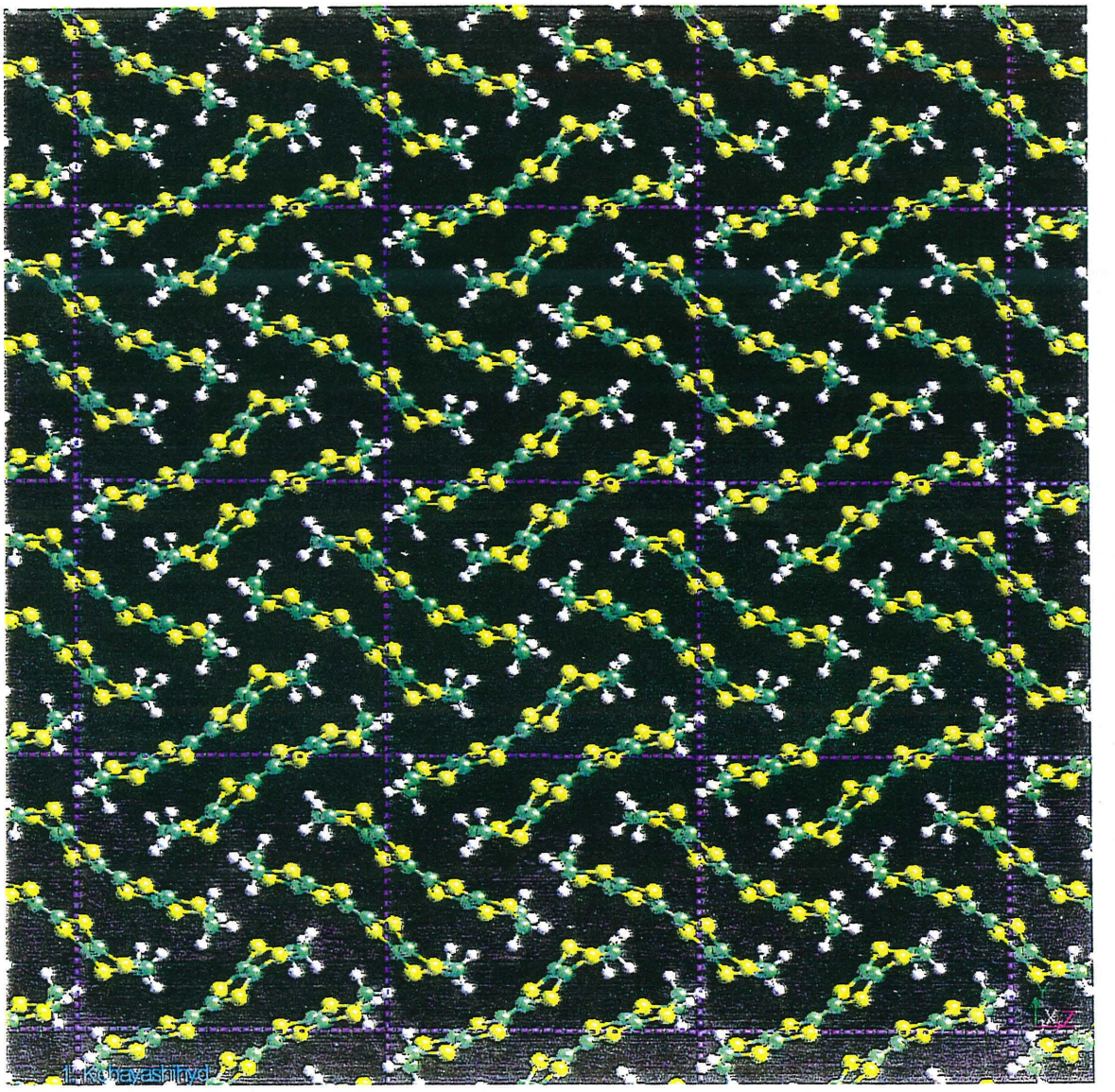
T. Kobayashi/ayd

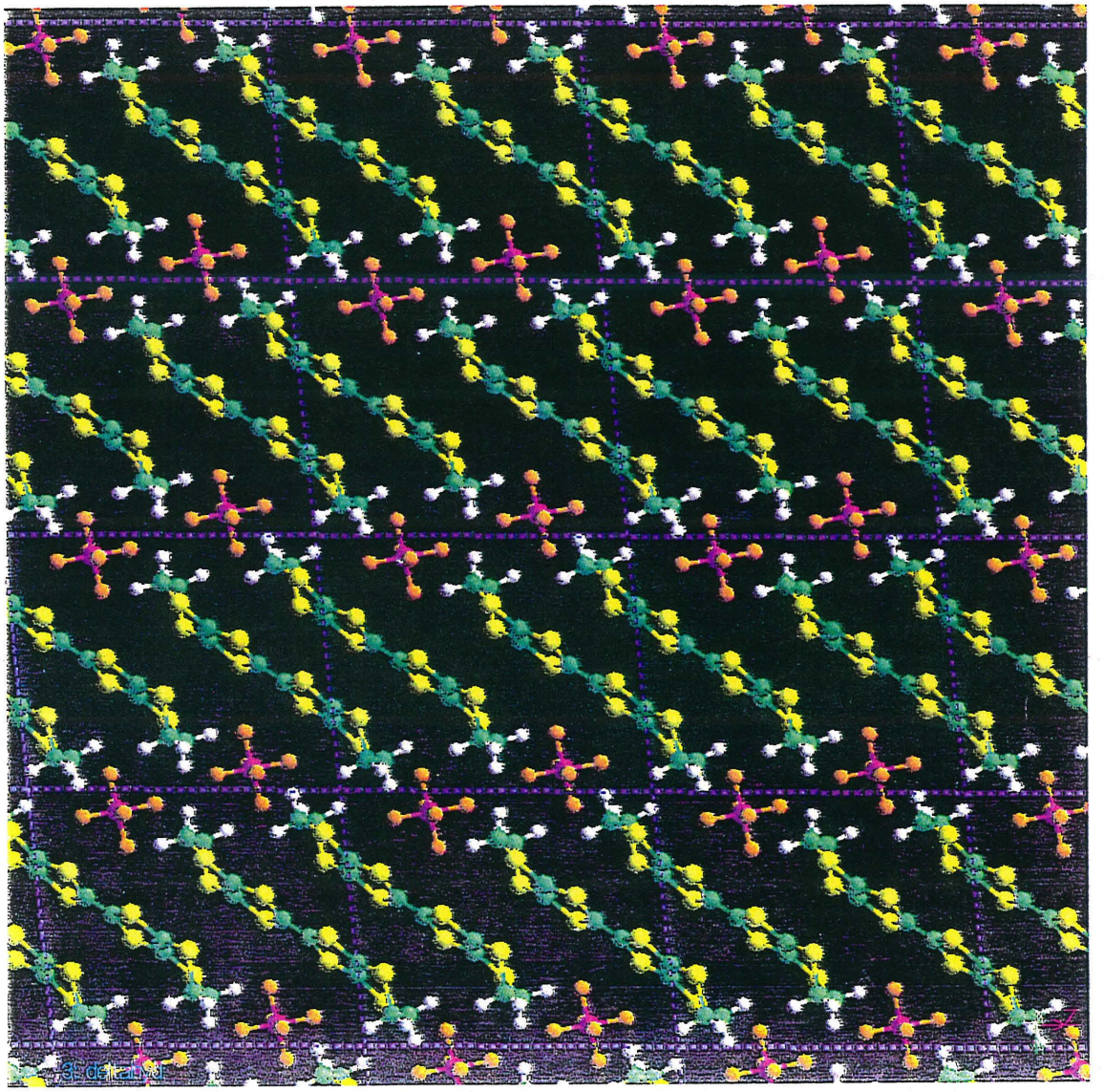

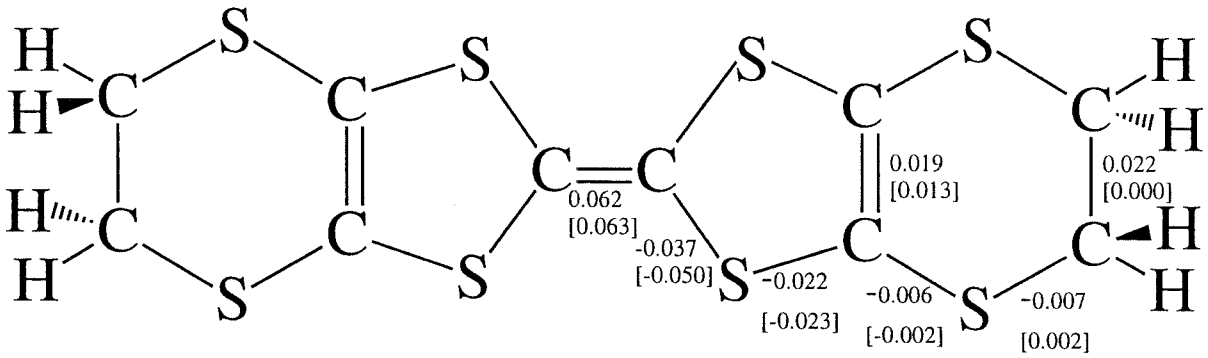

Figure 3. Distance changes (in Å) upon ionization: experiment and [theory (HF)]

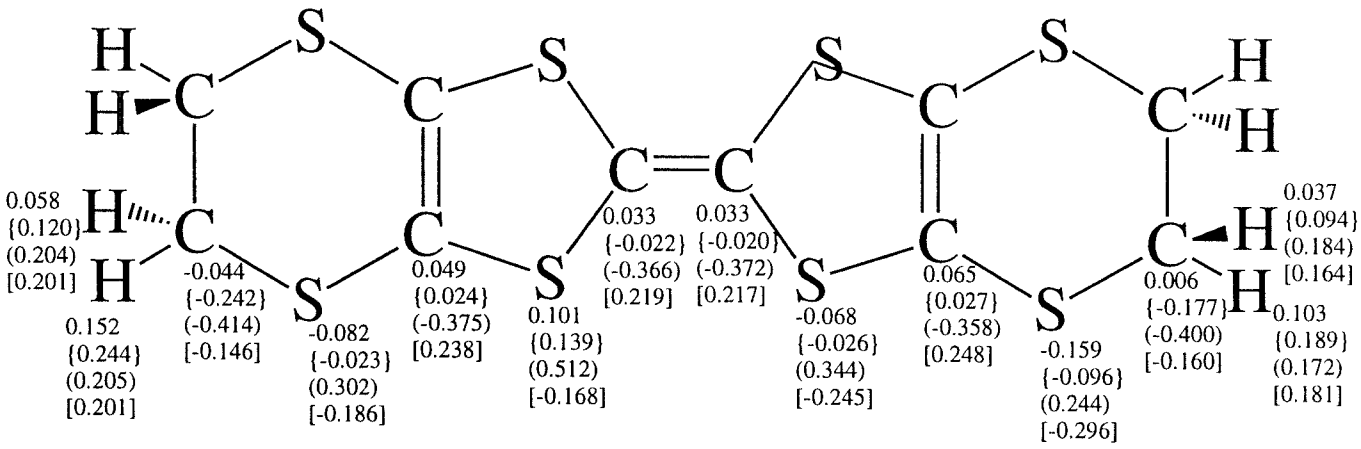

Figure 4. Calculated charges for ET (right side) and ET^+ (left side).

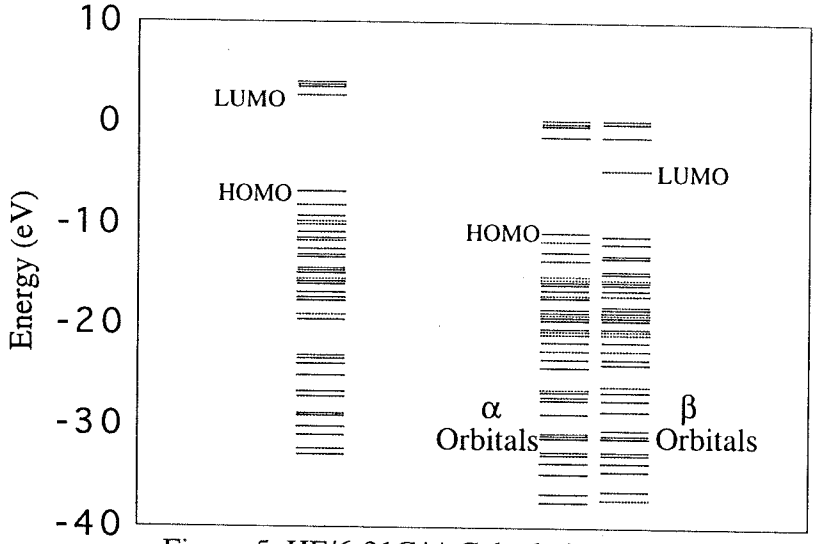

Figure 5. HF/6-31G** Calculations of Molecular Orbital Levels for ET (left) and ET^{+}(right)

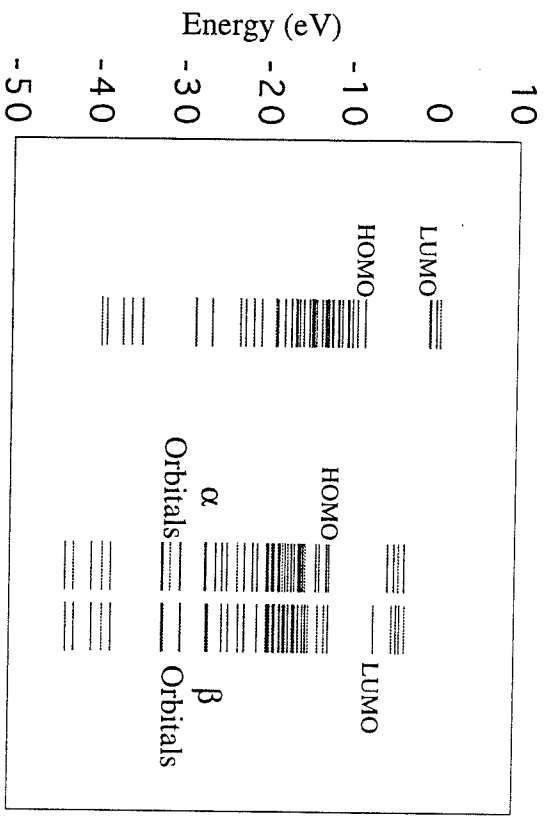

Figure 6. MNDO Calculations of Molecular Orbital Levels for ET (left) and ET^{+} (right)

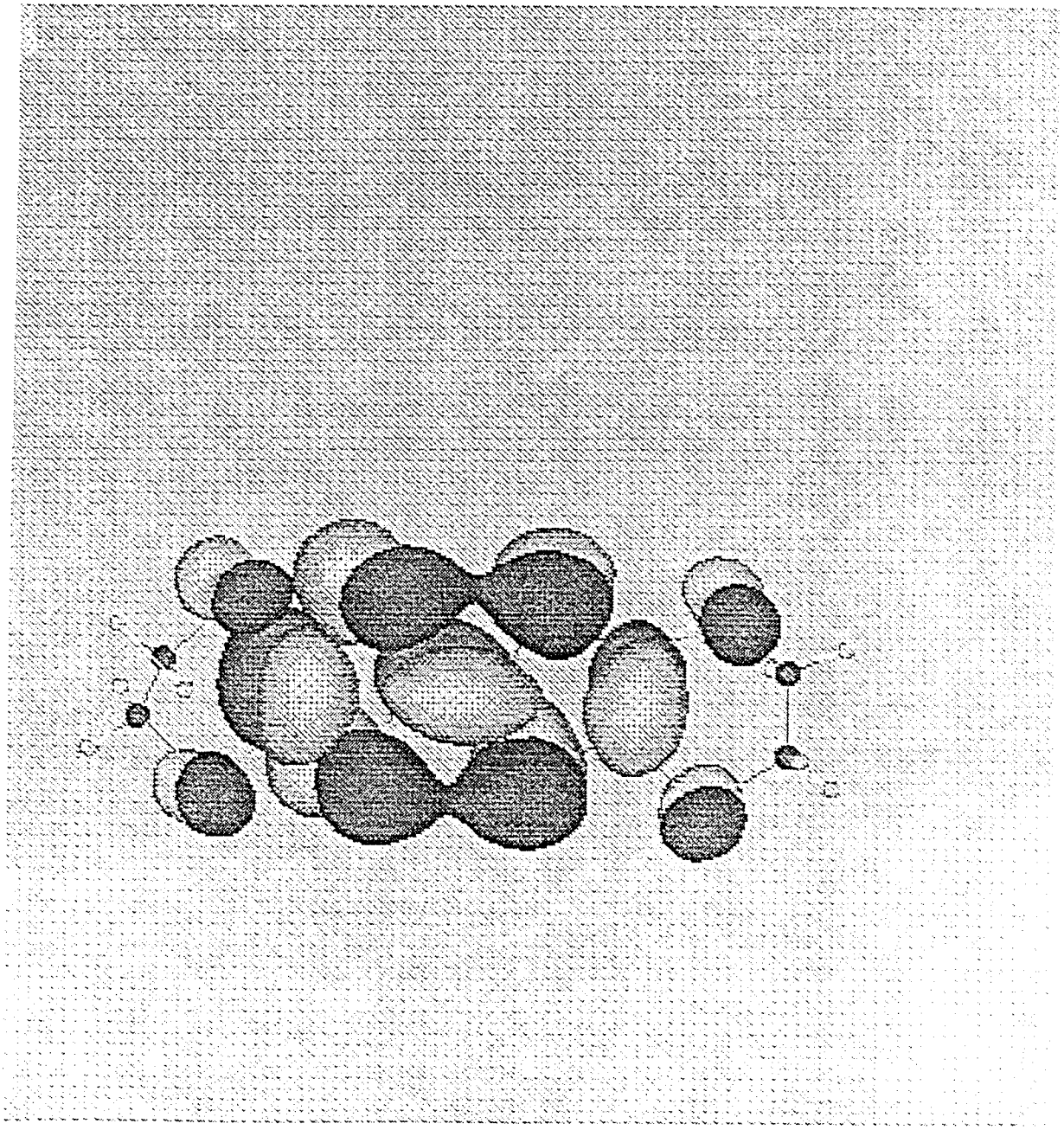

Figure 7

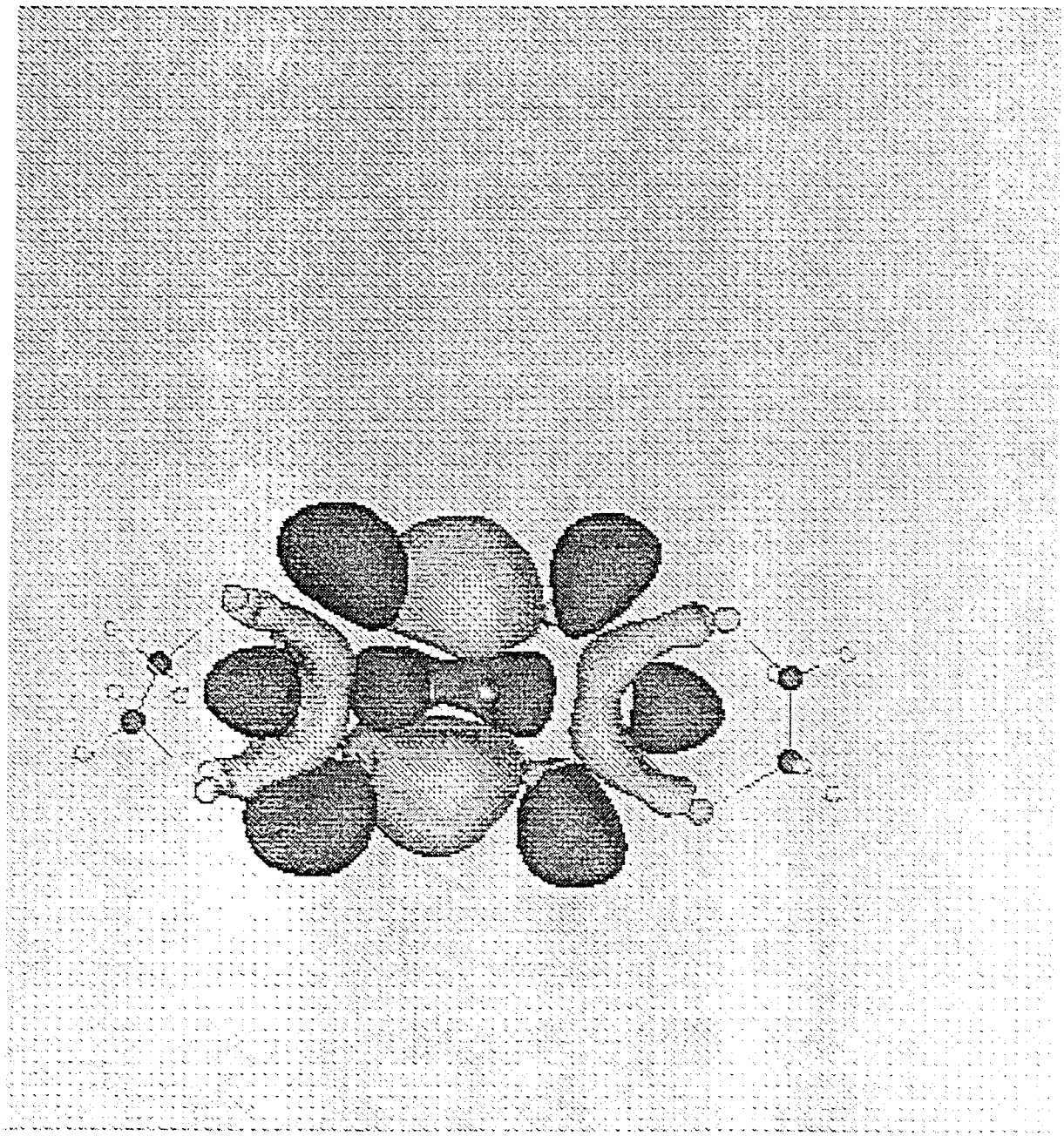

Figure 8

3.2 The Electron-Transfer Boat-Vibration Mechanism For Organic Superconductors

Abstract

The highest T_c organic superconductors all involve the organic molecule bis(ethylenedithio)tetrathiafulvalene (denoted as BEDT-TTF or ET) coupled with an appropriate acceptor. This leads to ET, ET^+, or $(ET)_2^+$ species in the crystal. Using *ab initio* Hartree-Fock calculations (6-31G** basis set), we show that ET deforms to a boat structure with an energy 28 meV (0.65 kcal/mol) lower than planar ET (D_2 symmetry). On the other hand ET^+ is planar. Thus conduction in this system leads to a coupling between charge transfer and the boat deformation vibrational modes at 20 cm^{-1} (ET) and 28 cm^{-1} (ET^+).

We suggest that this electron-phonon coupling is responsible for the superconductivity and predict the isotope shifts (δT_c) for experimental tests of the electron-transfer boat-vibration (ET-BV) mechanism. The low frequency of this boat mode and its coupling to various lattice modes could explain the sensitivity of T_c to defects, impurities, and pressure. We suggest that new higher temperature organic donors can be sought by finding modifications that change the frequency and stability of this boat distortion mode.

[This section is based on the paper "The Electron-Transfer Boat-Vibration Mechanism For Superconductivity In Organic Molecules Based on BEDT-TTF (ET)", Ersan Demiralp, Siddharth Dasgupta and William A. Goddard III, published in *Journal of American Chemical Society 117*, 8154 (1995).]

I. Introduction

Although the T_c's of the quasi one- and two-dimensional organic superconductors have gradually increased[1,2], there is considerable uncertainty concerning the mechanism of superconductivity. The most popular mechanisms involve phonons and BCS theory. Yamaji[3] proposed that the mechanism of superconductivity in organic conductors involves coupling between the Highest Occupied Molecular Orbital (HOMO) and totally symmetric intramolecular vibrational modes. However, the pattern of isotope effects does not support for this view. [9,11,18,19]

We report here *ab initio* quantum chemical calculations (Hartree-Fock with 6-31G** basis set) for the structure, vibrational frequencies, and isotope shifts for the donor molecule bis(ethylenedithio)tetrathiafulvane (denoted as BEDT-TTF or ET) shown in the Figure 1. Based on these calculations, we suggest a special role for the low frequency boat modes (at 19.5 cm^{-1} for ET and 28.1 cm^{-1} for ET^+) in the superconductivity of these organic materials.

2.0 Results

2.1 Structures

The structure of ET is often discussed in terms of D_2 symmetry, which assumes a planar structure for the central TTF moiety. The crystal structures of neutral ET crystal are consistent with planarity but show a distinct boat-like distortion.[4] Some deviations from planarity are also suggested in crystals containing electron acceptors, $(ET)_nX_m$.[25] Here the ET molecules often form dimers $(ET_2)^+$ sharing a single positive charge.

The terminal six membered-rings are nonplanar in order to avoid eclipsing of the $CH_2 - CH_2$ groups at each end. This nonplanarity leads to two possible conformations[25]: (1) The *staggered* conformation indicated in Figure 1a in which the two $C_6 - C_6$ bonds are pointing in opposite directions; assuming a planar TTF central region, this leads to D_2 symmetry. (2) The *eclipsed* conformation indicated in Figure 1b in which the two $C_6 - C_6$ bonds are parallel; with planar TTF, this leads to C_{2h} symmetry. As discussed below these conformations are essentially degenerate,

differing by only 0.0000052 Hartrees = 0.00014 eV = 0.0032 kcal/mol, and we will consider the higher symmetry staggered case.

To determine the structure and vibrational modes of ET, we carried out *ab initio* Hartree-Fock calculations using the 6-31G** basis set.[5,6] Restricting the symmetry to D_2 leads to an optimized structure with two imaginary frequencies vibrational modes (Table 2). We optimized the structure by relaxing the symmetry leading to boat structure with C_2 symmetry. In this case, all vibration frequencies are positive, indicating a stable (boat) structure. Figure 2 shows the side view of the planar and boat structures.

Figure 3 shows the double well potentials along the reaction coordinate of the boat deformation. The boat structure is calculated to be 28 meV (0.65 kcal/mol) lower than planar ET.

In contrast, we find that ET^+ leads to a stable planar D_2 structure (see Figure 3).

Using the HF/6-31G** wavefunction, we calculated all 3N - 6 = 72 molecular vibrations for the boat and planar ET structures and for ET^+. Table 2 compares the lowest four vibrational modes and Figure 4 shows the boat vibrational mode. This mode is the lowest frequency (19.5 cm^{-1} [ET], 28.1 cm^{-1} [ET^+]) and also is the mode converting ET structure to ET^+. As the structure distorts from boat to planar, the boat and chair deformation modes become imaginary while the other 70 modes (3N-8) of neutral ET change slightly. The biggest change is 7 %(21 cm^{-1}) for the 294 cm^{-1} mode (and symmetry D_2). These calculations were used to obtain the vibrationally adiabatic potential curves.

Table 1 : The total energy of the conformations of ET and ET^+
All energies are in Hartree.

Conformation[a]	Staggered	Staggered	Staggered	Eclipsed
Species	Boat ET	Planar ET	Planar ET^+	Boat ET
Symmetry	C_2	D_2	D_2	C_s
	-3563.360692	-3563.359652	-3563.147578	-3563.360697

[a] Orientation of $C_6 - C_6$ bonds of ET, see Figure 1 in this section.

Table 2 : The lowest four vibrational modes of ET and ET^+.
All frequencies are in cm^{-1}.

Species Mode	Boat ET C_2	Planar ET D_2	Planar ET^+ D_2
First Boat	19.5	23.1 i	28.1
First Chair	37.8	24.2 i	36.4
Second Boat	42.6	36.7	42.6
Second Chair	43.8	41.3	49.0

For the lowest energy boat structure of ET, we optimized the neutral molecules for both the eclipsed and staggered conformations of the terminal $-CH_2 - CH_2-$ groups. We found that the eclipsed and staggered conformations have essentially the same energy (with eclipsed lower by 0.0032 kcal/mol, see Table 1), leading to the same bonds and angles. Hence, even at 10 K both forms of the monomers would be nearly equally populated . In the crystals, packing interactions (donor-donor and donor-anion) may lead to preferences for either conformation. For the detailed structural and vibrational calculations of ET and ET^+ performed herein, we focus on the staggered conformation which leads to C_2 symmetry (the results for the eclipsed conformation should be essentially the same).

2.2 Electron Transfer

The fact that ET is nonplanar whereas ET^+ is planar leads to electron-phonon coupling that we believe is critical to the superconductivity. After boat ET loses the electron, ET^+ would relax toward the planar geometry. Simultaneously the planar ET^+ upon accepting the electron would distort to the boat ET conformation. Denoting the adiabatic ionization energy as I_o, the vertical (fixed geometry) ionization from the boat distorted ground state of neutral ET costs an energy of $I_o + 0.177$ eV, while the electron affinity of ET^+ (at its optimum planar geometry) is $I_o - 0.028$ eV. Thus isolated ET and ET^+ molecules with their optimum structures would lead to a hopping barrier of 0.205 eV (ignoring polarization of the environment which might increase the barrier). Figure 5 shows the corresponding Marcus-type electron transfer diagram, using as the abscissa the simultaneous boat distortion in which the structure of boat ET changes to planar simultaneously with the structure of planar ET^+ changing to the stable boat structure of ET. This leads to a net barrier of $\sim$0.205/4 = 0.05 eV and a curvature corresponding to a frequency of $\omega = \sqrt{\frac{1}{2}[\omega_b^2 + (\omega_b^+)^2]} = 24.2\ \mathrm{cm}^{-1}$.

2.3 The ET Dimer

In the organic superconductors $(ET)_nX_m$, ET molecules donate electrons to the anion layer. Thus, in $(ET)_2I_3$, each I_3 accepts one electron from a pair

of ET molecules, forming $(ET)_2^+$ and I_3^-. Ignoring electronic interactions (orbital overlap) and steric interactions, Figure 5 describes the charge transfer between the two ET and ET^+ molecules of the dimer. If the overlap of the HOMO's of this two ET molecules is sufficiently large, the system will lead to a structure (denoted as $ET^{\frac{1}{2}}$) intermediate between ET and ET^+. This requires interaction energies greater than the barrier of 0.05 eV.

The crystals of ET molecules exhibit a wide variety of phases and stackings. Some lead to columnar stacking while others do not. Some lead to quasi-one dimensional conductors, others lead to two-dimensional conductors. The best superconductors are generally two-dimensional. The $S\cdots S$ networks generally increase the intercolumn interactions. Relative orientation of monomers in these dimers and the dimers with respect to the other dimers will change the magnitude of transfer integrals and determine the rate of the electron transfer. In addition, all these structural effects can modify both vibrational and electronic modes which, in turn, may change T_c.

2.4 The Electron-Transfer Boat-Vibration Mechanism For Electron- Phonon Coupling

Figure 6a illustrates the electron transfer for a case in which one extra electron is on one of the $(ET)_2$ dimers (making it neutral). In the limit of slow electron transfer, the system might go through the structures in Figure 6b (for strong coupling within a dimer) or Figure 6c (weak coupling within a dimer). Thus *there is a strong coupling between the boat vibrational distortion and electron transfer.* For a good conductor with rapid electron transfer, the molecules would all remain in conformations close to that for $ET^{\frac{1}{2}}$, but there would be a tendency towards a larger boat distortion as the electron hops onto ET and then a smaller distortion as it hops off. [This discussion implies that the hopping of electrons is directly between the ET dimers; however, electron transfer between the $(ET_2)^+$ and the acceptor (to neutralize each) can also play a role in the conduction.] Thus we believe that it is this coupling of the conduction electrons to the boat vibrational mode that is involved in the BCS mechanism for these systems. We refer to this as the electron-transfer

boat-vibrational (ET-BV) mechanism for superconductivity.

We should emphasize that all vibrational energies are obtained from Hessians involving self-consistent wavefunctions. Thus the frequencies include the effect of changing the wavefunction upon distortion.

Some analyses of the superconductivity of ET molecules have assumed that the molecule is planar and have used a formalism on which the MO's of the equilibrium molecule (assumed planar) are mixed by various symmetric (A_g) intramolecular vibrations.[3] The origins of the electron-phonon coupling responsible for superconductivity have been sought in terms of how the various intramolecular vibrations might couple with the MO's.

Our view is quite different. We find that the ET molecule is distorted and that electron-phonon coupling arises from electron transfer between molecules. The phonons that must couple strongly with electron transfer involve boat vibrations. For the distorted (boat) geometry, the boat vibrational mode, the HOMO, and the LUMO are all of A symmetry (for C_2). However for the full planar geometry (neglecting also the nonplanarity of six membered-rings) these will have B_{1u} , B_{1u} , and A_g symmetry (of D_{2h}), respectively.

3.0 Isotope Effects

3.1 Shifts in the Boat Frequency

The most direct test of the role of the ET-BV mechanism in superconductivity is the effect of isotope substitutions on the superconducting properties, T_c. Crystal effects such as donor-anion and donor-donor interactions can influence the strength of the electron-phonon coupling, leading to substantial changes in T_c for different ET salts. For an accurate estimate of T_c, one should consider all such effects and carry out calculations for the molecular crystals. However to provide a means for rapid testing of the ET-BV model, we present estimates of isotopic shifts on T_c. We find cases where the isotopic shifts should be quite large, allowing direct experimental test of the ET-BV model.

Table 3 : Frequency shifts for the lowest boat vibrational mode
Shifts are in % for the isolated ET and ET^+ molecules. Also listed are the frequency shifts for the coupled vibrational frequency, $\omega = \sqrt{\frac{1}{2}[\omega_b^2 + (\omega_b^+)^2]} = 24.2$ cm^{-1} (see Figure 1 for nomenclature) for various isotopic substitutions.

Substitution	ET (19.5 cm^{-1})	ET^+ (28.1 cm^{-1})	ω(24.2 cm^{-1})
D	-4.10	-6.05	-5.41
$^{13}C_6$	-1.03	-1.07	-1.06
$^{13}C_c$	0.00	-0.36	-0.24
$^{13}C_c + ^{13}C_5$	0.00	-1.42	-0.96
^{34}S	-1.03	-1.07	-1.06
$D + ^{13}C_6$	-5.64	-6.76	-6.39
$D + ^{13}C_6 + ^{34}S$	-6.67	-7.47	-7.20

Using the Hessian (second derivative matrix) of the Hartree-Fock wavefunctions [6-31G** basis set], we calculated the isotopic shifts for the boat modes of ET and ET^+. Table 3 shows the frequency shifts for a number of isotope substitutions. These results will be used to test of the role of the ET-BV mechanism in the superconductivity.

In all cases, we find that an increase in the isotopic mass decreases the frequency of the boat mode. We obtain the largest frequency shifts for H to D substitutions $\{(\delta\omega_b/\omega_b) = -0.041[-0.060]\}$ for ET [ET^+]; smaller shifts for $^{12}C_6$ to $^{13}C_6$ $\{(\delta\omega_b/\omega_b) = -0.010[-0.011]\}$ and ^{32}S to ^{34}S $\{(\delta\omega_b/\omega_b) = -0.010[-0.011]\}$; and very small shifts for $^{12}C_c \rightarrow {}^{13}C_c$ $\{(\delta\omega_b/\omega_b) = -0.000[-0.004]\}$ and $^{12}C_5 \rightarrow {}^{13}C_5$ $\{(\delta\omega_b/\omega_b) = -0.000[-0.014]\}$. Table 4 shows that multiple isotopic substitutions give almost additive frequency shifts for the "boat mode." These trends

that H, C_6, S_6 atoms on the outer rings of ET provide the biggest shifts in ω_b are consistent with the character of the boat mode in Figure 4.

3.2 Effect of $\delta\omega$ on δT_c

Assuming that the electron-phonon matrix elements are dominated by the boat phonon mode and using the weak coupling formulation of BCS theory, leads to [24] the equation (1) for T_c,

$$kT_c = 1.14\hbar\omega \exp[-\frac{1}{(N_0 V)}] = 1.14\hbar\omega \exp[-\frac{1}{\lambda}] \quad , \tag{1}$$

where ω is the frequency for the coupled boat phonon mode ($\omega = 24.2\ cm^{-1}$), N_0 is the density of states of the electrons at Fermi surface, and V is the attractive interaction between electrons. However, using $\omega = 24.2\ cm^{-1}$ and $T_c = 10\ K$ in equation (1) gives $\lambda = 0.73$. Thus we use the Kresin strong-coupling formulation[22] (2):

$$T_c = 0.25\sqrt{<\omega^2>}\left[exp\left(\frac{2}{\lambda_{eff}}\right) - 1.0\right]^{-1/2} \quad . \tag{2}$$

Assuming that an isotope substitution which changes ω by $\delta\omega$ also changes λ_{eff} by $\delta\lambda$, equation (2) leads to

$$\frac{\delta T_c}{T_c} = \frac{\delta\omega}{\omega} + \frac{\delta\lambda}{\lambda_{eff}^2}\left(1 + 16\frac{T_c^2}{\omega^2}\right) \quad . \tag{3}$$

The magnitude of λ_{eff} should be related to the boat frequency ω and to the energy barrier (0.05 eV) which in turn depends on ω. In the crystal these quantities also depend on the packing of the other molecules (particularly the dimer pairing) and on the pressure.

In order to estimate the effect of the isotope substitutions on λ_{eff}, we write

$$\lambda_{eff}(\omega) = \lambda_0 + \lambda_1\delta\omega + \lambda_2(\delta\omega)^2 + ...$$

This will likely lead to a linear dependence

$$\delta\lambda = \lambda_1 \delta\omega \quad , \tag{4a}$$

but because of the double well nature of the boat mode, the net dependence might be

$$\delta\lambda = \lambda_2 (\delta\omega)^2 \quad . \tag{4b}$$

We will estimate λ_1 or λ_2 by using the experimental δT_c for H to D substitutions. Using λ_1 or λ_2 with the predicted ω allows the prediction of δT_c for other isotopic substitutions.

Combining terms leads to

$$\delta T_c = \frac{\delta T_D}{\delta\omega_D}\delta\omega \quad , \tag{5a}$$

and

$$\delta T_c = \frac{T_c}{\omega}\delta\omega + \left\{ -\frac{T_c}{\omega(\delta\omega_D)} + \frac{\delta T_D}{(\delta\omega_D)^2} \right\} (\delta\omega)^2 \quad , \tag{5b}$$

for approximations (4a) and (4b), respectively. Here δT_D and $\delta\omega_D$ are the shifts for H to D substitution.

3.3 Observed δT_c for H to D Substitutions

Recent isotopic shift experiments show the following results for replacing the hydrogen atoms of ET with deuterium

(i.) $\kappa - (ET)_2Cu[N(CN)_2]Br$ ($T_c = 11.8\ K$) leads to a normal isotope effect of $\delta T_c = -0.09\ K$.[7] In addition, Andres et al.[13] found a "normal" isotope shift for the "high T_c" phase of $\beta^* - (ET)_2I_3 (T_c = 8\ K)$; however, they considered the significance uncertain because of the sensitivity of T_c to pressure.

(ii.) On the other hand the following systems (1) $\kappa - (ET)_2Cu(NCS)_2$ ($T_c = 10.4\ K$), (2) $\kappa - (ET)_2Cu[N(CN)_2]Cl$ ($T_c = 12.8\ K$), (3) $\kappa - (ET)_2Cu(CN)[N(CN)_2] (T_c = 11.2K)$, (4) $\kappa - (ET)_2Ag(CN)_2H_2O (T_c = 5.0\ K)$, and (5) $\beta - (ET)_2I_3 (T_c = 1.15\ K)$ all showed inverse isotope effects, with $\delta T_c \sim$ 0.7, 0.5-1.5, 1.1, 1.0, 0.28 K

respectively.[8,14,23,15,16]

3.4 Predicted δT_c for Other Isotopic Substitutions

Using the experimental δT_c (denoted δT_D) and the calculated $\delta\omega$ (denoted $\delta\omega_D$) from Table 3, we estimated the parameters in (9). This leads to the predicted isotopic effects in Table 4. These results are generally in agreement with experiment. Thus

(i.) in $\kappa-(ET)_2Cu(NCS)_2$, the substitution $^{12}C_6$ to $^{13}C_6$ leads to a T_c "just between those of H and D salts,"[17] This inverse effect is expected from (5) (see Table 4).

(ii.) Carlson et al.[9] checked the controversial "giant isotope effect" results of Merzhanov et.al.[10] and found no isotopic shifts (within the standard deviations $\delta T_c = 0.1\ K$) for the substitutions of:

(1.) $^{12}C_c$ with $^{13}C_c$ in $\beta^* - (ET)_2I_3$, $\kappa - (ET)_2Cu(NCS)_2$, and $\kappa - (ET)_2Cu[N(CN)_2]Br$,[9,11]

(2.) all $^{12}C_c$ and $^{12}C_5$ with ^{13}C in $\beta^* - (ET)_2I_3$.[18,19]

Indeed as shown in Table 4, we find very small shifts (δT_c less than 0.06 K) for all C_c substitutions with ^{13}C. In addition, we find δT_c less than 0.20 K for simultaneous $^{12}C_c$ and $^{12}C_5$ substitutions with ^{13}C.

(iii.) Carlson et al.[9] found a very small isotopic shift, $\delta T_c = -0.08 \pm 0.07$ K, upon substituting all ^{32}S with ^{34}S in $\kappa-(ET)_2Cu[N(CN)_2]Br$. As shown in Table 4 we estimate that $\delta T_c = -0.18$ to -0.13 K in reasonable agreement. In $\kappa-(ET)_2Cu(NCS)_2$ "less detailed" studies[12] indicate no isotope effect whereas we find $+0.14$ to -0.06 K.

From Table 4 we see that the largest isotope shifts are for H, C_6, and S_6. Indeed (a) simultaneously substituting for both H and C_6 should increase δT_c by $\sim$ 18 to 57 % over that for H alone, while (b) simultaneously substituting H, C, and S_6 leads to an increase in δT of $\sim$ by 33 to 113 % over that for H only. Thus multiple isotope substitution experiments should provide a clear cut test of the ET-BV mechanism.

4.0 Summary

The stable structure of ET is boat-like whereas ET^+ is planar. The

energy of boat distortion is 28 meV (for ET) and the boat frequency is 19.5 cm^{-1}. We propose that the mechanism for superconductivity of these materials involves the coupling of charge transfer to the boat deformation mode. This boat mechanism can be tested by measuring the isotopic shifts for specific simultaneous isotopic substitutions.

This ET-BV mechanism provides some guidance for modifying ET to obtain new higher T_c materials. Thus, we require donor molecules that distort into the boat form for the neutral form, but change significantly (becoming planar) upon ionization. We expect T_c to be sensitive to the boat frequency ω, and to the magnitude of the distortion energy. Based on these ideas, one can postulate various modifications of ET that would increase T_c. Consequently, we are carrying out quantum mechanical calculations for some such cases.

Table 4. Predicted isotopic shifts (δT_c) based on the coupled boat phonon model for organic superconductors (see Figure 1 for nomenclature). The experimental deuterium isotopic shift (δT_D) was used with $\delta\omega_D$ in equation (5a) to obtain the values listed while equation (5b) was used for the values in parentheses.

	T_c	D	$^{13}C_6$	$^{13}C_c$	$^{13}C_c + ^{13}C_5$	^{34}S	$D + ^{13}C_6$	$D + ^{13}C_6 + ^{34}S$
$\kappa-(ET)_2Cu[N(CN)_2]Br$	11.8[a]	-0.90	-0.18(-0.13)	-0.04(-0.03)[h]	-0.16(-0.12)	-0.18(-0.13)[i]	-1.06(-1.12)	-1.20(-1.31)
$\kappa-(ET)_2Cu(NCS)_2$	10.4[b]	+0.70	+0.14(-0.06)[g]	+0.03(-0.02)[h]	+0.12(-0.06)	+0.14(-0.06)[j]	+0.83(+1.10)	+0.93(+1.49)
$\kappa-(ET)_2Cu(CN)[N(CN)_2]$	11.2[c]	+1.10	+0.21(-0.05)	+0.05(-0.02)	+0.19(-0.05)	+0.21(-0.05)	+1.30(+1.66)	+1.46(+2.22)
$\kappa-(ET)_2Ag(CN)_2H_2O$	5.0[d]	+1.00	+0.20(+0.00)	+0.04(-0.01)	+0.18(-0.01)	+0.20(+0.00)	+1.18(+1.45)	+1.33(+1.89)
$\beta-(ET)_2I_3$	1.15[e]	+0.28	+0.05(+0.00)	+0.01(+0.00)	+0.05(0.00)	+0.05(+0.00)	+0.33(+0.40)	+0.37(+0.52)
$\kappa-(ET)_2Cu[N(CN)_2]Cl$	12.8[f]	1.0[f]	+0.20(-0.07)	+0.04(-0.03)	+0.18(-0.07)	+0.20(-0.07)	+1.18(+1.54)	+1.33(+2.08)

[a] Reference 7.

[b] Reference 8.

[c] Reference 23.

[d] Reference 15.

[e] Reference 16.

[f] Reference 14. The isotopic shifts were observed in the range 0.5-1.5K for different samples. We used 1.0 K.

[g] For substitutions of $^{12}C_6$ with $^{13}C_6$ in $\kappa-(ET)_2Cu(NCS)_2$, T_c was found "just between those of H and D salts." See reference 17.

[i] $\delta T_c = -0.08 \pm 0.07$ was observed with ^{34}S substitutions (see reference 12).

[j] No isotope effect (within standard deviations) was observed with ^{34}S substitutions (see reference 12).

[h] No isotope effect (within standard deviations $\delta T_c = 0.1K$) was observed with $^{13}C_c$ substitutions (see references 9,11).

References

1. Jerome D., Mazaud A., Ribault M., Bechgaard K., *J. Phys. Lett. 41*, (1980) L95.

2. Wang HH, Carlson KD, Geiser U, Kini AM, Schultz AJ, Williams JM, Montgomery LK, Kwok WK, Welp U, Vandervoort, Schirber J.E., Overmyer D.L., Jung D., Novoa J. J., Whangbo MH,*Synthetic Metals, 42* (1991) 1983.

3. Yamaji K., *Solid State Communications, 61*, (1987), 413.

4. Kobayashi H., Kobayashi A., Yukiyoshi S., Saito G., Inkuchi H., *Bull. Chem. Soc. Jpn., 59*, (1986) 301.

5. Demiralp E., Goddard W. A. III, *Journal of Physical Chemistry*, 98, (1994) 9781.

6. The quantum chemical calculations were carried out using Gaussian 92, Revision B, M. J. Frisch, G. W. Trucks, M. Head-Gordon, P. M. W. Gill, M. W. Wong, J. B. Foresman, B. G. Johnson, H. B. Schlegel, M. A. Robb, E. S. Replogle, R. Gomperts, J. L. Andres, K. Raghavachari, J. S. Binkley, C. Gonzalez, R. L. Martin, D. J. Fox, D. J. Defrees, J. Baker, J. J. P. Stewart, and J. A. Pople, Gaussian, Inc., Pittsburgh PA, 1992.

7. Tokumoto M., Konishito N., Tanaka Y., Anzai H., *Journal of the Physical Society of Japan, 60*, (1991) 1426.

8. Oshima K., Urayama H., Yamochi H., Saito G., *Synthetic Metals, 27* (1988) A473.

9. Carlson K. D., Williams J.M., Geiser U., Kini A. M., Wang H. H., Klemm R. A., Kumar S. K., Schlueter J. A., Ferraro J. R., Lykke K. R., Wurz P., Parker H., Sutin J. D. B., *Mol. Crsyt. Liq. Cryst. 234*, (1993), 127.

10. Merzhanov V., Auban-Senzier P., Bourbonnais C., Jerome D., Lenoir C., Batail P., Buisson J.P., Lefrant S, *C.R. Acad. Sci. Paris,314* (1992), 563.

11. Carlson K. D., Kini A. M., Klemm R. A., Wang H. H., Williams J.M., Geiser U., Kumar S. K., Ferraro J. R., Lykke K. R., Wurz P., Fleshler S., Dudek J. D., Eastman N. L., Mobley P. R., Seaman J. M., Sutin J. D. B., Yaconi G. A., *Inorg. Chem. 31*, (1992), 3346.

12. Carlson K. D., Kini A. M., Schlueter J. A., Geiser U., Klemm R. A., Williams J.M.,Dudek J. D., Caleca M. A., Lykke K. R., Wang H. H., Ferraro J. R., *Physica C 215*, (1993), 195.

13. Andres K., Schwenk H., Veith H., *Physica 143B*, (1986), 334.

14. Schirber J. E., Overmyer D. L., Carlson K. D., Williams J.M., Kini A. M., Wang H. H., Charlier H. A., Love B. J., Watkins D. M., Yaconi G. A., *Phys Rev B 44*, (1991), 4666.

15. Mori H., Hirabayashi I., Tanaka S., Mori T., Maruyama Y., Inokuchi H., *Synthetic Metals, 55-57* (1993)2437.

16. Heidmann C. P., Andres K., Schweitzer D., *Physica 143B*, (1986), 357.

17. Saito G., Yamochi H., Komatsu T., Ishiguro T., Nogami Y., Ito Y., Mori H., Oshima K., Nakashima M., Takagi H., Kagoshima S., Osada T., *Synthetic Metals, 41-43* (1991) 1993.

18. Carlson K. D., Kini A. M., Schlueter J. A., Wang H. H., Sutin J. D. B., Williams J.M., Schirber J. E., Venturini E. L. , Bayless W. R., *Physica C 227*, (1994), 10.

19. Carlson K. D., Williams J.M., Geiser U., Kini A. M., Wang H. H., Klemm R. A., Kumar S. K., Schlueter J. A., Ferraro J. R., Lyyke K. R., Wurz P., Parker D. H., Sutin J. D. B. *Mol. Cryst. Liq. Cryst. 234*, (1993), 127.

20. Kozlov M.E., Pokhodnia K. I., Yurchencko A. A., *Spectrochimica Acta 45A* (1989), 323.

21. Ferraro J. R., Kini A. M., Williams J.M., Stout P., *Applied Spectroscopy 48*, (1994) 531.

22. Kresin V. Z., *Physics Letters A 122*, (1987) 434

23. Saito G., Yamochi H., Nakamura T., Komatsu T., Matsukawa N., Inoue T., Ito H.,Ishiguro T., Kusunoki M., Sakaguchi K., Mori T., *Synthetic Metals, 55-57* (1991) 2883.

24. See for example , P. G. de Gennes, *Superconductivity of Metals and Alloys*, (Addison-Wesley Pub. Co. Inc., 1989).

25. Williams J.M., Ferraro J. R., Carlson K. D., Geiser U., Wang H. H., Kini A. M., Whangbo M-H, *Organic Superconductors (Including Fullerenes): synthesis, structure, properties, and theory*, (Printice-Hall 1992)

Figure Captions

Figure 1. Bis(ethylenedithio)tetrathiafulvalene (denoted as BEDT-TTF or ET) (a) Staggered (C_2 symmetry) (b) Eclipsed (C_s symmetry).

Figure 2. Side view of the optimized structure for ET. a) D_2 symmetry (planar). (b) C_2 symmetry (boat). Carbons are the solid circles, hydrogens are the open circles, and sulfurs are the hatched circles.

Figure 3. (a) Energy of the boat structure of ET as a function of the boat distortion. The pathway for boat is obtained from a three point fit to the planar, + boat, and - boat structures. (b) The energy for ET^+ using the boat structures of ET (based on the Koopmans theorem).

Figure 4. Boat deformation mode of the boat structure ($\omega_b = 19.5cm^{-1}$).

Figure 5. The Marcus-type electron transfer diagram for $ET\ ET^+ \rightarrow ET^+ET$. Electron transfer from $ET\ ET^+$ to ET^+ET is couplied to simultaneous boat distorsions for both molecules, $\omega = \sqrt{\frac{1}{2}[\omega_b^2 + (\omega_b^+)^2]} = 24.2\ \mathrm{cm}^{-1} = 0.0030eV$.

Figure 6. Illustration of electron transfer in $(ET)_2^+$ superconductors. (a) The case of one extra electron. (b) The structural changes for fast transfer. (c) The structural changes for slow transfer.

a) Staggered

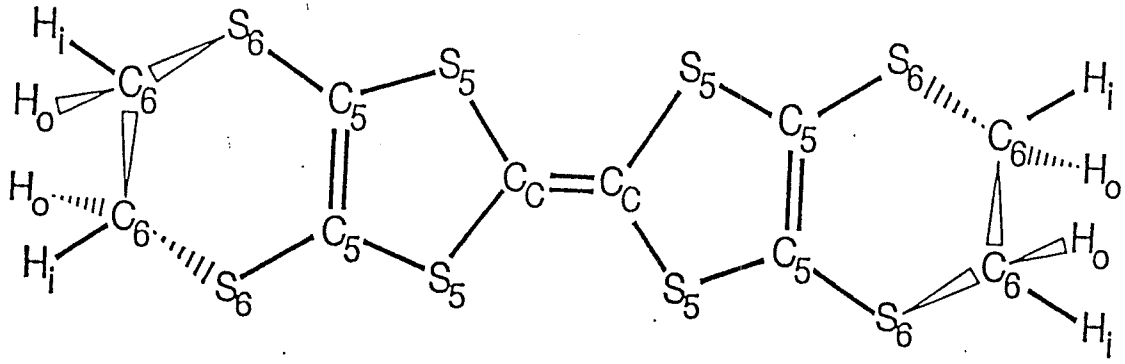

b) Eclipsed

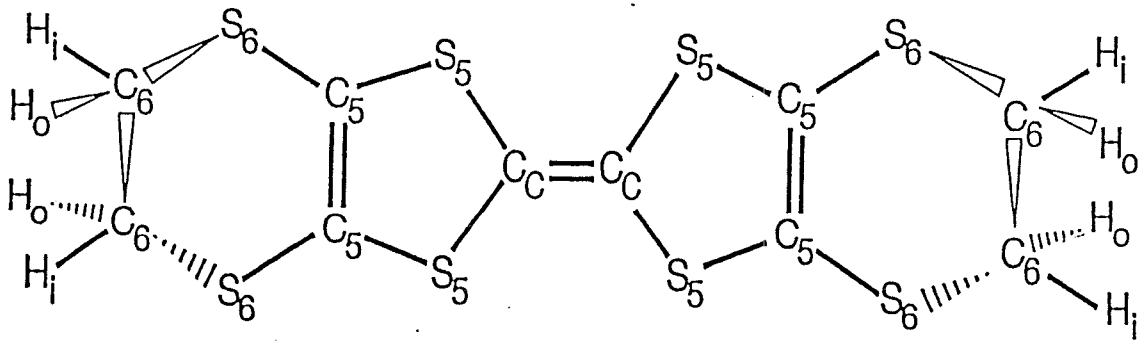

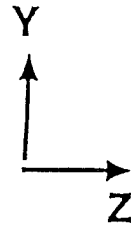

bis(ethylenedithio)tetrathiafulvalene, ET

Figure 1

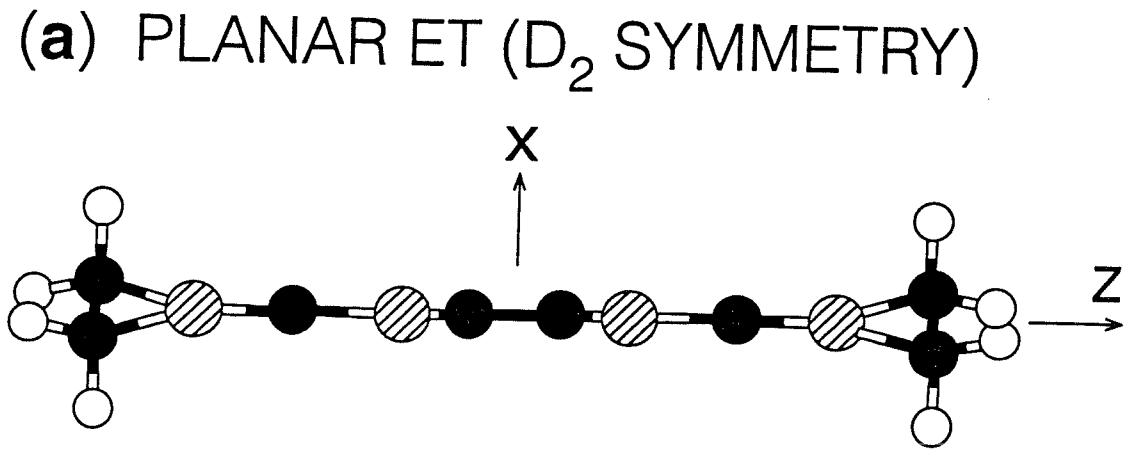

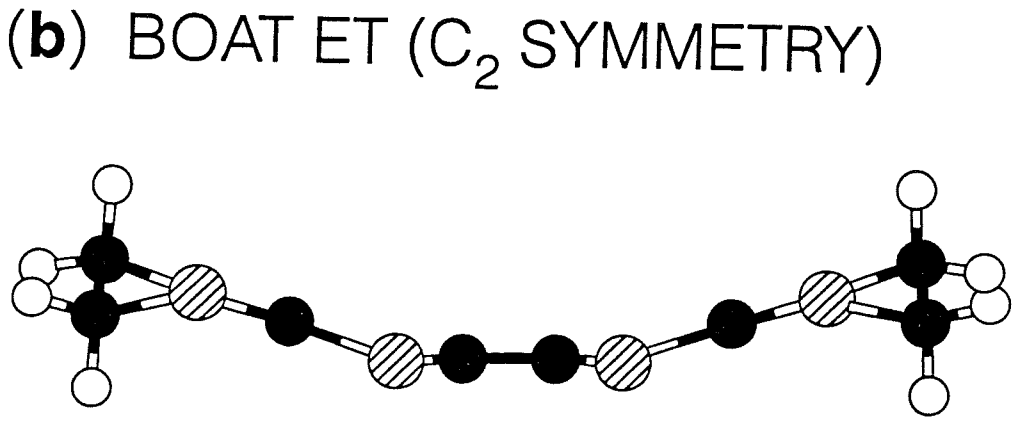

Figure 2

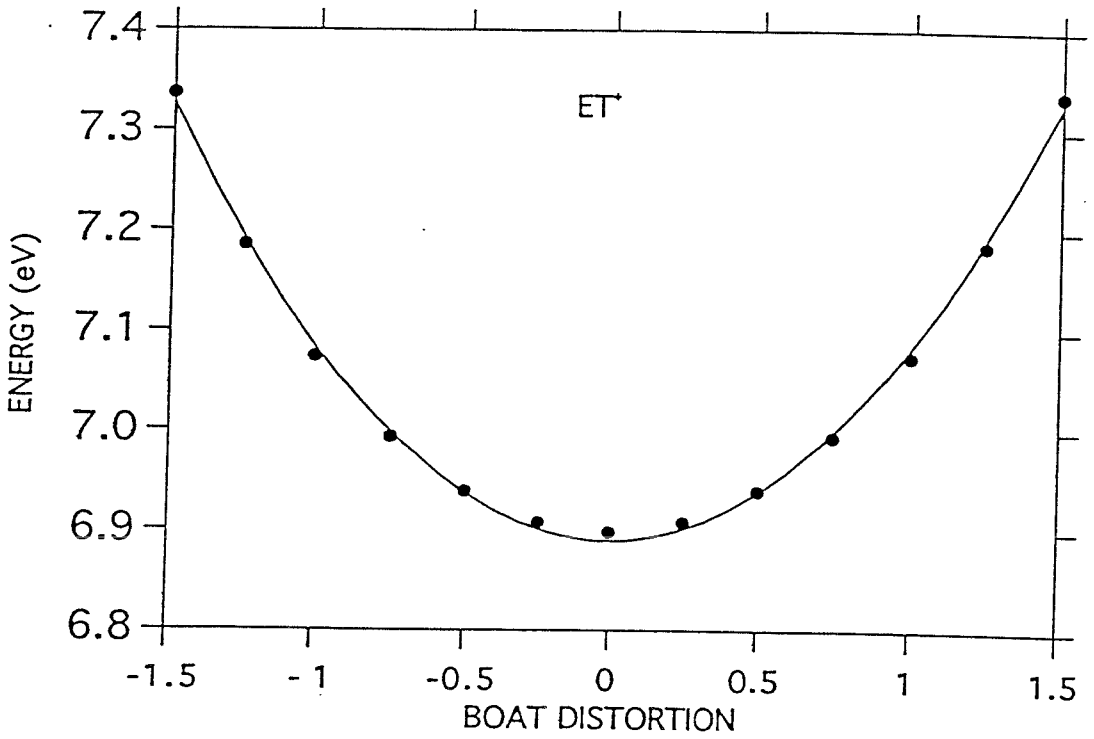
7.4
7.3
7.2
7.1
7.0
6.9
6.8
ENERGY (eV)
ET*
-1.5
-1
-0.5
0
0.5
1
1.5
BOAT DISTORTION

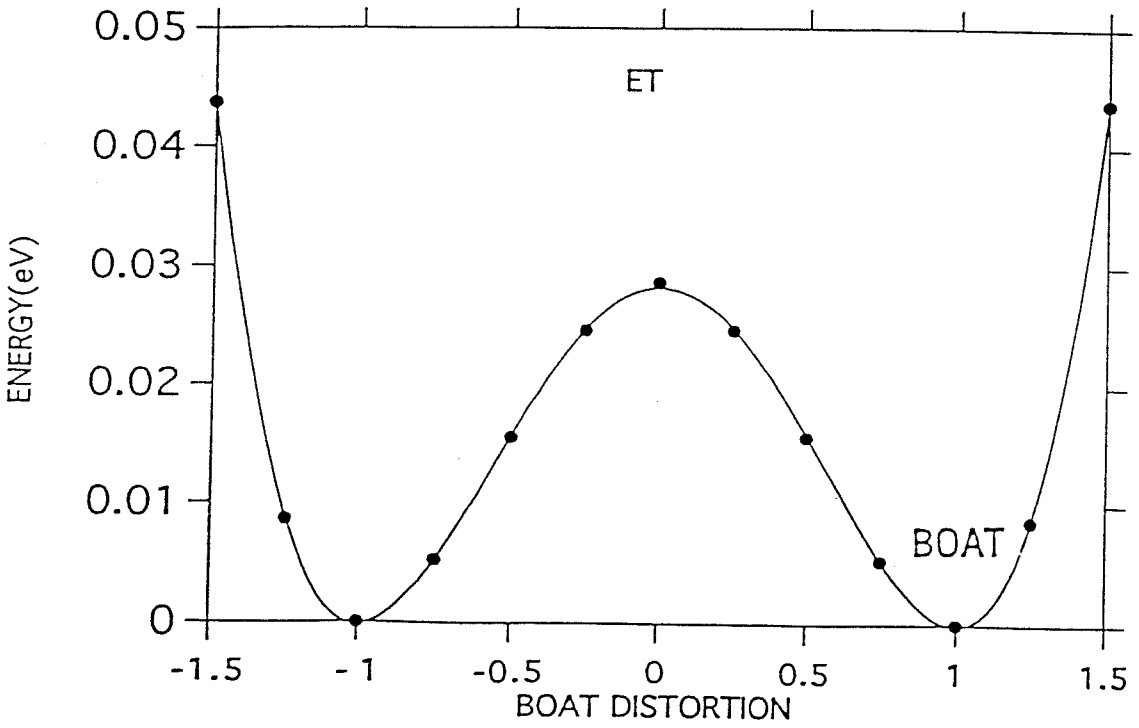
0.05
0.04
0.03
0.02
0.01
0
ENERGY(eV)
ET
BOAT
-1.5
-1
-0.5
0
0.5
1
1.5
BOAT DISTORTION

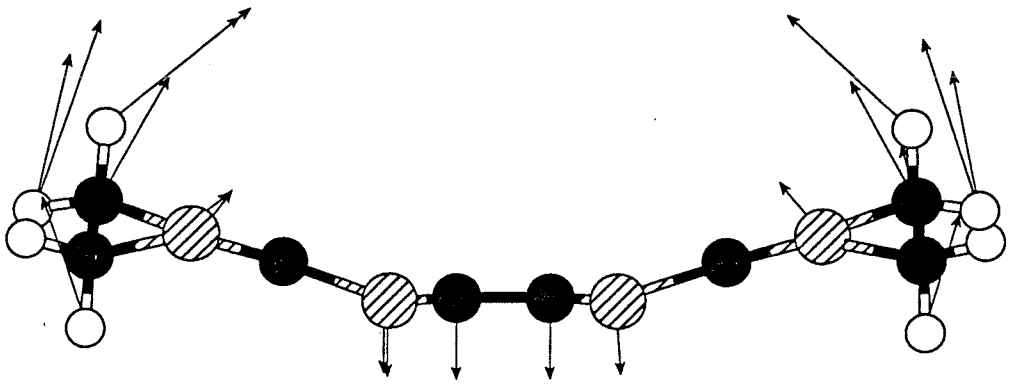

BOAT VIBRATION MODE of ET

Figure 4

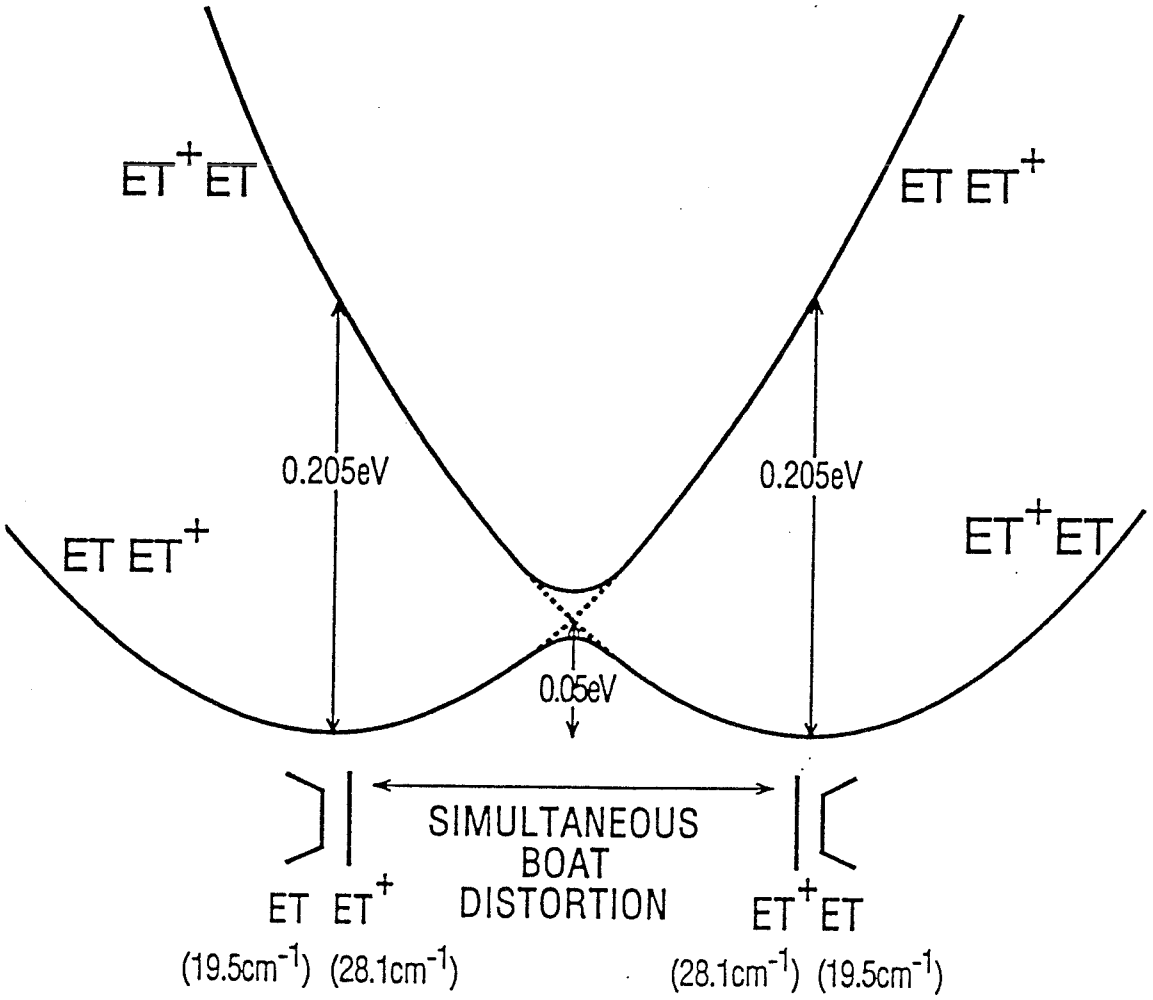
ET+ET
ET ET+
0.205eV
0.205eV
ET ET+
ET+ET
0.05eV
SIMULTANEOUS
BOAT
DISTORTION
ET ET+
ET+ET
(19.5cm-1) (28.1cm-1)
(28.1cm-1) (19.5cm-1)

Figure 5

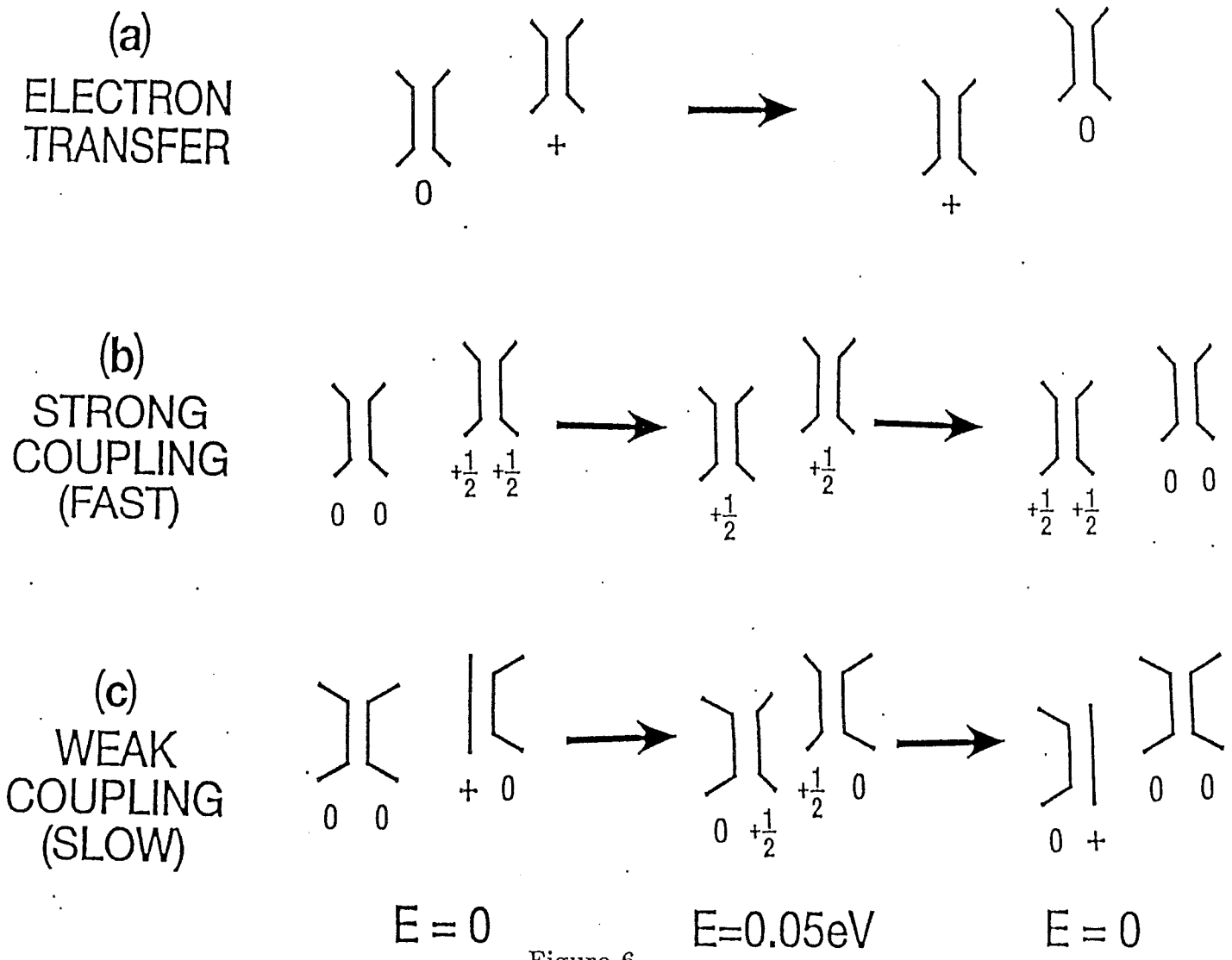
(a)
ELECTRON
TRANSFER
0
+
+
0
(b)
STRONG
COUPLING
(FAST)
0 0
+½ +½
+½
+½
+½ +½
0 0
(c)
WEAK
COUPLING
(SLOW)
0 0
+ 0
0 +½
+½ 0
0 +
0 0
E = 0
E=0.05eV
E = 0

Figure 6

3.3 Prediction of New Donors for Organic Superconductors

Abstract

The donors of all known one or two dimensional organic superconductors are based on a core organic molecule that is either tetrathiafulvalene (denoted as TTF) or tetraselenafulvalene (denoted as TSeF) or some mixture of these two molecules. Coupling X, with appropriate acceptors, Y, leads to superconductivity. The oxidized form of X may be X^+ or X_2^+ species in the crystal. From *ab initio* quantum mechanical calculations (HF/6-31G**), we find that all known organic superconductors involve an X that deforms to a boat structure while X^+ is planar. This leads to a coupling between charge transfer and the boat deformation phonon modes that we believe is responsible for the superconductivity of these materials. Based on this idea we have developed similar organic donors having the same properties and suggest that with appropriate electron acceptors they will also lead to superconductivity.

A number of organic superconductors have been developed using the donors in Figures 1b-d coupled with appropriate acceptors.[1–3] These are all based on S or Se containing fulvalenes (tetrathiafulvalene, TTF, and related molecules in Figure 1a). The superconducting transition temperatures, T_c, range up to 12.8K and have improved slowly over the years. Despite the advances in T_c, progress in developing new materials is impeded by the lack of an understanding of how the superconductivity is related to fundamental structural quantities. Herein we identify what we believe is the salient structural issue in the superconducting coupling mechanism and use this insight to suggest a number of new donors, all of which are expected to show superconductivity when coupled with appropriate acceptors. These donors are simpler than the current ones and some may lead to higher T_c.

In most systems the donors form dimers X_2 so that there is one hole per dimer. The holes on the dimers result in overlapping valence and conduction bands, leading to electrical conduction involving both positive and negative charge carriers.

We have used *ab initio* quantum mechanics[4–6] (Hartree-Fock, 6-31G** basis) to examine the structures for a number of donors in both the oxidized (X^+) and neutral (X) states and find that *all known donors for superconductors lead to a distorted boat conformation (see Figure 2) for X and a planar conformation for X^+*. The change in structure upon ionization from nonplanar X to planar X^+ leads to electron-phonon coupling that we believe is critical for the electronic behavior of molecular crystals based on these donors. After boat X loses the electron to form X^+, the structure would start to relax toward the planar geometry. Simultaneously the planar X^+ upon accepting the electron would tend to distort toward the boat conformation of X. The idea is illustrated in Figure 3 in this section. Thus this charge transfers tends to couple the electrons to the boat deformation modes.

In analyzing these transfers, we define:

I_o = the adiabatic ionization energy,

U = the relaxation energy for X^+ from the optimum boat structure of X to the optimum structure of X^+,

W = the relaxation energy for neutral X from the planar to the boat structure.

Thus, the vertical (fixed geometry) ionization from the boat distorted ground state of X costs an energy of $I_o + U$, while the vertical electron affinity of X^+ (at its optimum planar geometry) is $I_o - W$.

Isolated neutral and cation donor molecules with their optimum structures would lead to a hopping barrier of $U + W$ (ignoring polarization of the environment which might increase the barrier). Figure 5 shows the corresponding Marcus-type electron transfer diagram, using as the abscissa the simultaneous boat distortion in which the structure of the neutral boat molecule changes to planar simultaneously with the structure of the planar cation molecule changing to the stable boat structure of the neutral molecule. This leads to a net barrier of $\frac{(U+W)}{4}$ and an approximate curvature corresponding to $\omega = \sqrt{\frac{1}{2}[\omega_b^2 + (\omega_b^+)^2]}$, where ω_b is the boat deformation frequency for the neutral and ω_b^+ is for X^+. Of course in a metal, we do not have such localized states. In this case the structure will tend to remain near that of $X^{\frac{1}{2}}$ (in between X^+ and X). However the coupling between electrons and the boat deformation will remain. We believe that the coupling of conduction electrons to these deformation modes is critical for the superconductivity of these organic materials.

Based on these considerations we hypothesize that TTF-like molecules which lead to boat-distorted neutral donors (but a planar positive ion) will result in superconductivity when combined with suitable acceptors. Here we use this idea to suggest several new donors as candidates for forming superconductors. The simplicity of these new donors might lead to improved properties.

The donors for the known superconductors Figures 1b-d (all based on TTF, TSeF, or a mixture) are all expected have distorted neutral donors. However, we find that the parent compounds of Figure 1a, are all planar in the neutral (and

oxidized) forms. Thus none of the donors in Figure 1a would lead to the coupling such as in Figures 3 , responsible for superconductivity. Only upon replacing the hydrogens of the TTF and TSeF molecules with bulky groups do we get distortions.

The results of calculations for several substitutions are summarized in Table 1. We expect that the superconducting T_c is related to the distortion angle Θ, boat stabilization ΔE_{boat}, and boat vibrational frequency, ν_{boat}. Generally we expect that larger Θ, ΔE_{boat}, and ν_{boat} will lead to higher T_c (as long as the positive ion is planar and the system is a conductor).

Replacing the H in TTF with Cl or F leads to substantial distortions (14° and 11°, respectively, see Figure 4). Cl-TSeF leads to a distortion larger by 1.2° but Cl-TOF is planar. These results are consistent with the studies on BEDT-TTF (i.e., ET) where S or O in the six membered ring (the same position as the Cl in Cl-TTF) leads to distortion. In addition, replacing the S in the five-membered ring with Se leads to larger distortions, but replacing S with O in the five-membered ring leads to no distortion. For TTF and TSeF replacing the H with CH_3 also leads to a small distortion (6° and 8° respectively), but little energy lowering.

The origin of these distortions is found in the bond angle preferences of the atoms involved. The bond angles in OH_2, SH_2, and SeH_2 are 104.5°, 92.1°, and 90.6°, respectively.[7] On the other, hand the average angle in the five-membered rings is 540/5=108°. Indeed for the molecules in Figure 1a, the optimum angles are 105.01° and 95.09° at O and S, respectively. Thus S and Se lead to a significant strain energy. Although planar, these molecules (with S or Se) are spring loaded, needing only additional steric interactions to tip the balance toward nonplanar. Although not calculated, TTeF is expected to yield even larger distortions (probably $\sim$ 17°) for Cl substitution.

Cl-TTF has a distortion 3° larger than F-TTF, and Br-TTF, I-TTF should lead to even larger distortions. This is consistent with the results on BEDT-TTF where replacing S_6 with O_6 leads to much smaller distortions. Thus for BEDT-TTF, replacing S_6 with Se_6 or Te_6 should lead to increased distortions. Similarly although CH_3 leads to only a small distortion for TTF and TSeF, we expect that tBu

[i.e., $C(CH_3)_3$] would lead to much larger distortions.

We have ignored packing issues. The ET based systems crystallize into structures with two-dimensional layers of ET dimers separated by a two- dimensional layer of acceptor molecules. The positive hydrogens of ET interacting with the negative acceptor layer probably play a role in stabilizing this structure. The modified molecules such as Cl-TTF are halogen terminated, leading to a net negative charge in the region of the acceptor. This would likely require hydrogen on the acceptors to electrostatically attract the negative halogens. Thus I_3 and $Cu(NCS)_2$ would likely *not* be good acceptors for Cl-TTF. On the other hand with tBu groups the standard acceptors might be satisfactory.

Summarizing,

(i.) We indicate a criterion for determining new classes of donors, namely that the neutral molecule distort into a boat form while the cation species is planar.

(ii.) We suggest several new candidate donors for organic superconductors each involving simple modifications of TTF and related molecules.

Tests of these suggestions should provide additional insights into the mechanism of superconductivity and might lead to improved properties.

Table 1: The deformation angles, energy differences and the boat vibrational frequency for various organic donors
The deformation angle is Θ (see Figure 2); energy difference between boat and planar structures is ΔE_{boat}, and the lowest boat deformation vibrational frequency is ν_{boat}.

Species	Substitutions[a]	Θ^b degrees	ΔE_{boat} (meV)	ν_{boat} (cm^{-1})
TOF	-	0.0	POS[d]	76.1
	Cl	0.0	POS[d]	29.7
TTF	-	0.0	+14.39[d,e]	17.7
	F	11.3	NEG[c]	18.6
	Cl	14.3	−5.87	18.1
	CH_3	5.8	−0.18	10.3
TSeF	Cl	15.5	−5.74	na[f]
	CH_3	7.9	−0.40	na[f]
BEDT-TTF	-	21.1	−28.36	19.5
	Se_5	24.4	NEG[c]	na[f]
	O_6	8.5	NEG[c]	10.5
	O_5	0.0	POS[d]	21.5

[a]For TTF or TSeF, all substitutions replace H atoms with the corresponding substituents. For BEDT-TTF, the subscripts show that the sulfurs in the five or six member rings are replaced by Se or O.

[b]For ET-derived molecules with C_2 symmetry, Θ is the average angle on both sides of central plane.

[c]NEG indicates that starting with C_2 symmetry, the structure optimizes to a boat structure, hence the energy of the boat structure is lower than planar structure. However, we did not separately optimize the planar structure to obtain ΔE_{boat}.

[d]POS indicates that starting with C_2 symmetry, the optimized structure becomes planar structure, hence the energy of the boat structure is higher than planar structure.

[e]To obtain the positive ΔE_{boat} we started with the optimized planar and boat structures containing Cl and replaced each Cl with H as the appropriate distance.

[f]Frequencies not yet calculated.

References

1. Jerome D., Mazaud A., Ribault M., Bechgaard K., *J. Phys. Lett. 41* (1980) L95.

2. Wang H. H., Carlson K. D., Geiser U., Kini A. M., Schultz A. J., Williams J. M., Montgomery L.K., Kwok W. K., Welp U., Vandervoort, Schirber J.E., Overmyer D. L., Jung D., Novoa J. J., Whangbo M. H.,*Synthetic Metals, 42* (1991) 1983.

3. Mori H., *Int. J. of Modern Physics B, 8* (1994) 1-45.

4. Demiralp E., Goddard W. A. III, *Journal of Physical Chemistry 98* (1994) 9781.

5. Demiralp E., Dasgupta S., Goddard W. A. III, submitted *J. Am. Chem. Soc.*.

6. The quantum chemical calculations were carried out using Gaussian 92, Revision B, M. J. Frisch, G. W. Trucks, M. Head-Gordon, P. M. W. Gill, M. W. Wong, J. B. Foresman, B. G. Johnson, H. B. Schlegel, M. A. Robb, E. S. Replogle, R. Gomperts, J. L. Andres, K. Raghavachari, J. S. Binkley, C. Gonzalez, R. L. Martin, D. J. Fox, D. J. Defrees, J. Baker, J. J. P. Stewart, and J. A. Pople, Gaussian, Inc., Pittsburgh PA, 1992.

7. Harmony M. D., et al. , *Journal of Physical Chemistry Ref. Data*, Vol. 8, No. 3, 1979.

Figure Captions

Figure 1. (a) Tetrathiafulvalene (TTF), tetraselenafulvalene (TSeF), and tetraoxafulvalene (TOF).

(b) TTF based donors of organic superconductors.

(c) TSeF based donors of organic superconductors.

(d) TTF-TSeF mixed donors (DMET) of organic superconductors.

Figure 2. Side view of the boat structure for Cl-TTF. The optimum angle is $\Theta = 14.3°$.

Figure 3. The Marcus-type electron transfer diagram for $X\ X^+ \rightarrow X^+X$. Electron transfer from $X\ X^+$ to X^+X is couplied to simultaneous boat distorsions for both molecules, $\omega = \sqrt{\frac{1}{2}[\omega_b^2 + (\omega_b^+)^2]}$

Figure 4. (a) Donors of organic superconductors.

(b) Donors with no superconducting structure.

(c)Predicted new donors for organic superconductors.

(a)

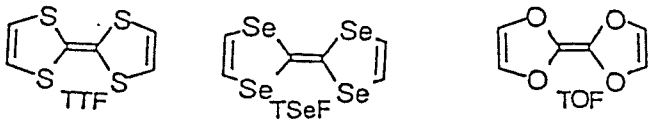

(b)

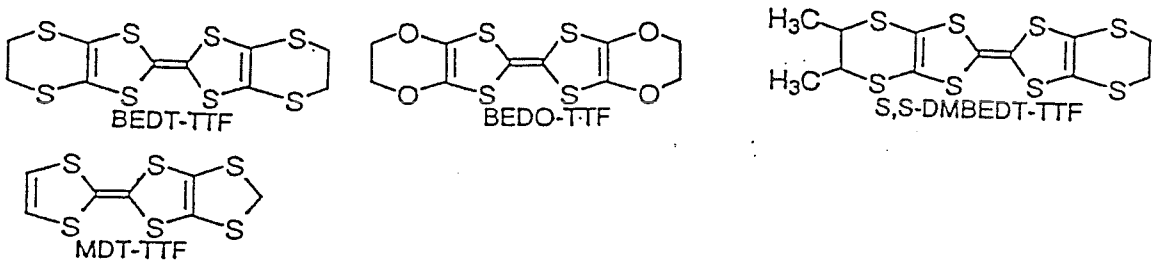

(c)

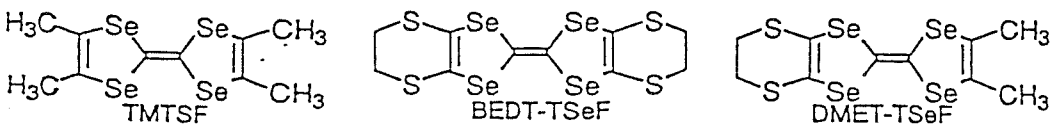

(d)

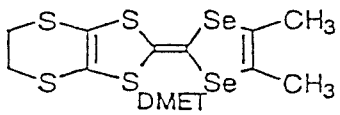

Figure 1

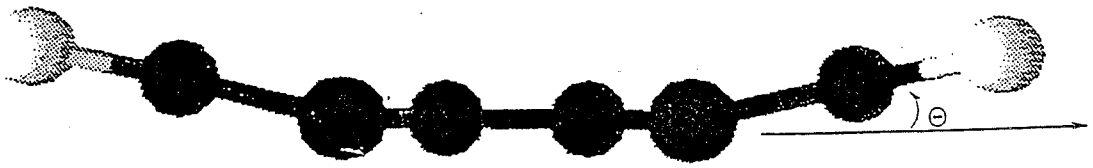

Figure 2

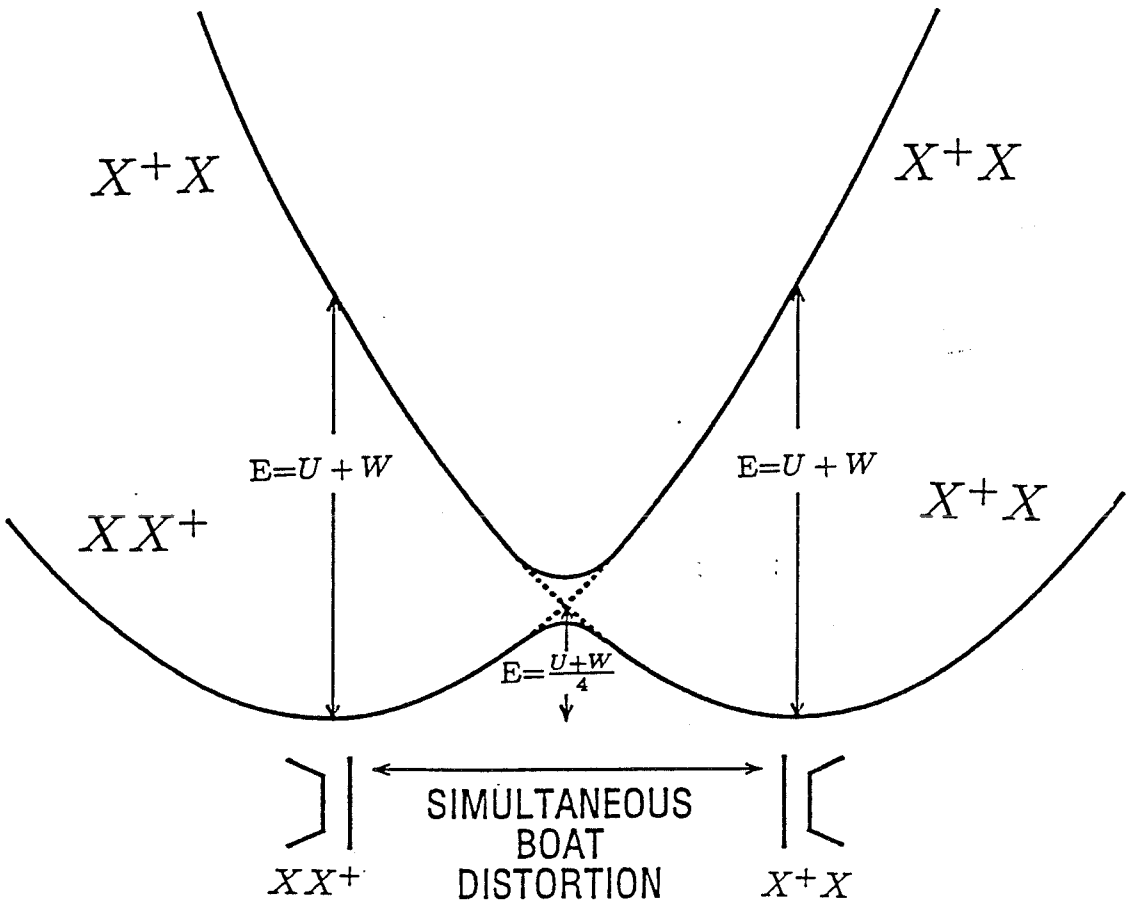
X^+X
X^+X
E=$U+W$
E=$U+W$
XX^+
X^+X
E=$\frac{U+W}{4}$
SIMULTANEOUS
BOAT
DISTORTION
XX^+
X^+X

Figure 3

a)

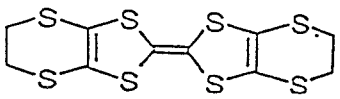

BEDT-TTF
$\Theta = 21.1°$

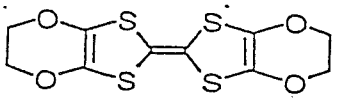

BED0-TTF
$\Theta = 8.5°$

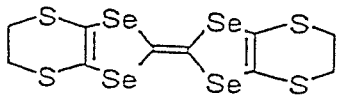

BEDT-TSEF
$\Theta = 24.4°$

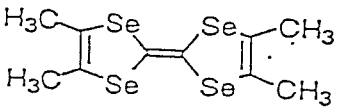

TMTSF
$\Theta = 7.9°$

b)

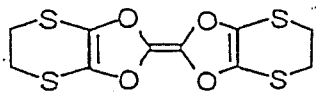

BEDT-TOF
$\Theta = 0°$

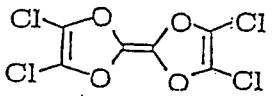

TOF-Cl
$\Theta = 0°$

c)

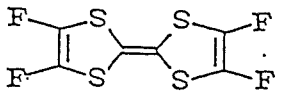

TTF-F
$\Theta = 11.3°$

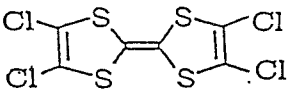

TTF-Cl
$\Theta = 14.3°$

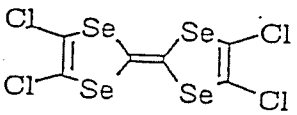

TSeF-Cl
$\Theta = 15.5°$

Figure 4

3.4 Ab Initio Studies of TTF-based Donors of Organic Superconductors

Abstract

We report the structures and properties of TTF-based organic donors of organic superconductors. From *ab initio* quantum mechanical calculations (HF/6-31G**) for the neutral (X) and cation (X^+), we find that X^+ is planar but that X deforms to a boat structure for all cases that are superconductors. Various characteristics of these donors are also discussed.

I. Introduction

Most organic superconductors are based on the TTF-like donors in Figure 1 in Section 3.3.[1] The electronic structures of the molecular crystals involving ET show a wide variety of electronic behavior leading to semiconductors, metals or superconductors, etc. depending on the anion and the packing. For metallic behavior of ET salts, the intermolecular $S \cdots S$ contacts seem important. Hence, the conformations and packing of these donors are very important for understanding the electronic behavior of these materials.

Recently, we reported[2] that known donors for superconductors all lead to a distorted boat conformation for X and a planar conformation for X^+. We indicated[2] that this is a criterion for determining new classes of donors and suggested new TTF-based donors. As an electron hops from X to X^+, the original X distorts from boat to planar while the original X^+ distorts from planar to boat. Thus conduction in this system leads to a coupling between charge transfer and the boat deformation phonon modes, which we suggest that is the electron-phonon coupling responsible for the superconductivity.

In this paper, we report other structures and properties of the TTF-based organic donors of organic superconductors. We used *ab initio* quantum mechanics[3] (Hartree-Fock, 6-31G** basis) to study the structures of these donors in both the oxidized (X^+) and neutral (X) states. The changes in the properties of these molecules upon chemical modification (structure, ionization potential, shape and energy of the molecular orbitals) are important for understanding the electronic and crystal structures of materials containing these organic donors.

2.0 Results

2.1 Structures

It is often assumed that the TTF region of the TTF-related donors for organic superconductors are flat.[4] For neutral ET crystal[5] and for $ET_4PtCl_6 \cdot C_6H_5CN$,[6] some deviations from planarity are suggested in the X-ray structure. However there was no suggestion that these deviations from planarity are related to the in-

trinsic properties of the donor molecules. The crystal structure of $ET_4PtCl_6 \cdot C_6H_5CN$ exhibits a first-order transition at 250 K. Doublet et al.[6] found that there are two donor layers before the transition and only one donor layer after the transition. By comparing with the neutral ET crystal for ET and with $ETAg_4(CN)_5$ for ET^+, they found that one of the layers (A) contains $(ET^+)_2$ and $(ET)_2$ dimers and the other layer (B) contains two different $(ET^{\frac{1}{2}})_2$ dimers. After the transition, the $(ET^{\frac{1}{2}})_2$ dimers of (B) disproportionate to form $(ET^+)_2$ and ET_2 dimers.

We determined the structures by carrying out *ab initio* Hartree-Fock calculations using the 6-31G** basis set.[3] We find that the parent TTF molecule is planar but all the TTF-based neutral molecules deform to a boat conformation when H in TTF is replaced with F, Cl or bulky (CH_3) groups. Similarly, substituting S for Se to form TSeF leads to a planar structure, but again neutral molecules with similar substitutions for H are boat-like.[2] On the other hand, substituting S for O to form TOF leads to planar structure for all similar substitutions of H.[2]

The propensity for distortion is easily understood. The average angles are 105.0° for O on TOF, 95.1° for S in TTF and 93.2° for Se in TSeF. This is related to the normal preferences in bond angles: thus, H_2O has 104.5°, H_2S has 92.1° and H_2Se has 90.6°.[7] However for a five membered ring, the average angle is 108°. Thus for S and Se, there are strains trying to obtain a smaller bond angle. By going nonplanar, the angle at the S and Se is allowed to be $\sim 95°$ without strain on the rest of the five-membered ring. However it is only when an electronegative or bulky ligand is attached that the TTF-like moiety snaps to a distortion structure.

Charge transfers from the TTF region to the end groups reduces the strains in the pentagonal rings, leading to a positive center and negative ends for these molecules. The neutral molecule deforms to the boat conformation. This charge transfer is reversed upon ionization, leading to a planar molecule.

The energy difference between the stable boat mode and optimized planar structure varies up to 0.65 kcal/mol (see Table 1), leading to a doubly well potential along the boat coordinate. For ET molecules with the staggered ethylene conformation, the deformation of the 6-membered rings lowers the symmetry to C_2,

leading to degenerate chiral molecules. There is also the eclipsed ethylene conformation leads to ET molecules with C_s symmetry. These ethylene conformations have almost same energy (the eclipsed conformation has an energy 5 μHartree lower).[8] In this section, we used the staggered conformation with C_2 symmetry for the detailed structural calculations for neutral and cation ET molecule.

2.2 Ionization Potential

The total energy and orbital energies of from HF calculations are shown in Table 3. The HOMO and LUMO orbitals of TTF-Cl from HF calculations are plotted in Figure 1,2. Two ways of estimating ionization potentials (IP) are:

i. ΔE: using the total energy differences of neutral and cation molecules because the correlation error is smaller for the positive ion than the neutral this usually leads to too small an IP, and

ii. Koopmans' theorem (KT): using the orbital energy of the HOMO level this assumes that the orbitals do not relax upon ionization and hence usually leads to too large a value.

Table 2 shows that the available experimental gas-phase IP's are in between these estimates, as expected. The average of the ΔE and KT values, which often gives a good estimate for the IP, leads to the order $BEDT-TTF$ (6.44 eV) $> TTF$(6.31 eV) $> BEDO-TTF$ (6.26 eV). This is consistent with the gas-phase experimental results $BEDT-TTF \approx TTF(6.7\ eV) > BEDO-TTF(6.46\ eV)$.[9] (The order from Ref. 10 is different, $TTF(6.4\ eV) > BEDT-TTF(6.21eV)$ (see Table 2 in this section). The IP's are very close so that the relative donor abilities are affected by the molecular environment.[9] Thus, the oxidation potentials in solution are ordered $BEDT-TTF > BEDO-TTF > TTF$, which differs from the order of the gas-phase first ionization potentials. Such polarization effects should also be important in crystals. Hence, the structures and packing should influence the charge transfer properties of the salts of TTF-based donors. This information should help in understanding the wide variety of electronic properties of the molecular crystals based on TTF donors.

4. Summary

The results of *ab initio* HF calculations (6-31G** basis) show that TTF-based molecules have boat conformations for X and planar conformation for X^+. This leads to coupling of charge transfer with the boat deformation modes of these molecules. These results should be important for understanding the crystal and electronic properties of molecular crystals based on TTF-based molecules. The ionization potentials should be useful for the comparisons of the relative electron donor abilities these molecules in the synthesis of donor-acceptor systems.

References

1. Mori H., Intl. J. of Modern Physics B, **8**, 1 (1994).

2. Demiralp E. and Goddard W. A. III, *Synthetic Metals, 72*, (1995) 297.

3. The quantum chemical calculations were carried out using Gaussian 92, Revision B, M. J. Frisch, G. W. Trucks, M. Head-Gordon, P. M. W. Gill, M. W. Wong, J. B. Foresman, B. G. Johnson, H. B. Schlegel, M. A. Robb, E. S. Replogle, R. Gomperts, J. L. Andres, K. Raghavachari, J. S. Binkley, C. Gonzalez, R. L. Martin, D. J. Fox, D. J. Defrees, J. Baker, J. J. P. Stewart, and J. A. Pople, Gaussian, Inc., Pittsburgh PA, 1992.

4. Cowan D.O, Fortkort J. A., Metzger R. M., in Lower-Dimensional Systems and Molecular Electronics, (Plenum Press 1991), 1.

5. Kobayashi H., Kobayashi A., Yukiyoshi S., Saito G., Inkuchi H., *Bull. Chem. Soc. Jpn., 59*, (1986) 301.

6. Doublet, M-L., Canadell E., Shibaeva R. P., *J. Phys. I France 4* (1994) 1479.

7. M. D. Harmony, V. W. Laurie, R. L. Kuczkowski, R. H. Schwendeman, D. A. Ramsay, F. J. Lovas, W. J. Lafferty, A. G. Maki, J. Phys. Chem. Ref. Data, 8 (3) (1979) 619.

8. Demiralp E., Dasgupta S., Goddard W. A. III, *Journal of American Chemical Society 117*, (1995) 8154.

9. Lichtenberger D. L., Johnston R. L., Hinkelmann K., Suzuki T., Wudl F., *Journal of American Chemical Society, 112*, (1990) 3302.

10. Sato N., Saito G., Inokuchi H., *Chemical Physics 76*, (1983) 79.

Figure Captions

Figure 1. The HOMO molecular orbital of the neutral TTF-Cl molecule. Results are from HF calculations. The positive lobes are dark gray and the negative lobes are light gray. The isosurfaces are for an amplitude of 0.02 in atomic units.

Figure 2. The HOMO molecular orbital of the neutral TTF-Cl molecule. Results are from HF calculations. The positive lobes are dark gray and the negative lobes are light gray. The isosurfaces are for an amplitude of 0.02 in atomic units.

Table 1 : The deformation angles, energy differences and the boat vibrational frequencies for various TTF-based organic donors

The deformation angle is Θ (see Figure 2 in Section 3.3); energy difference between boat and planar structures is ΔE_{boat}, and the lowest boat deformation vibrational frequency is ν_{boat}.

Species	Substitutions[a]	Θ^b degrees	ΔE_{boat} (Kcal/Mol)	ν_{boat} (cm^{-1})
TTF	-	0.0	+0.332[c]	17.7
	F	11.3	−0.046	18.6
	Cl	14.3	−0.135	18.1
TMTTF	-	5.8	−0.004	10.3
BEDT-TTF	-	21.1	−0.654	19.5
BEDO-TTF	-	8.5	−0.017	10.5
MDT-TTF	-	21.5(7.6)[d]	NEG[e]	29.8
S,S-DMBEDT-TTF	-	21.8(21.5)[d]	NEG[e]	na[f]
TSeF	-	0.0	POS[g]	na[f]
	Cl	15.5	-0.132	na[f]
TOF	-	0.0	POS[g]	76.1
	Cl	0.0	POS[g]	29.7

[a]For TTF, TSeF and TOF, all substitutions replace H atoms with the corresponding substituents.

[b]For ET-derived molecules with C_2 symmetry, Θ is the average angle on both sides of central plane.

[c]To obtain the positive ΔE_{boat} we started with the optimized planar and boat structures containing Cl and replaced each Cl with H as the appropriate distance.

[d] For these asymmetric molecules, Θ is the average angle of left and right angles for each part of the molecule.

[e]NEG indicates that starting with C_2 (or C_{2v}) symmetry, the structure optimizes to a boat structure, hence the energy of the boat structure is lower than planar structure. However, we did not separately optimize the planar structure to obtain ΔE_{boat}.

[f]Frequencies not yet calculated.

[g]POS indicates that starting with C_2 (or C_{2v}) symmetry, the structure optimizes to a planar structure with D_2 (or D_{2h}) symmetry, hence the energy of the boat structure is higher than planar structure.

Table 2 : Ionization potentials (eV) for organic donors.

Species	Substitutions[a]	$X^+ - X$ (eV)	Koopmans Theorem (eV)	Experiment (eV)
TTF	-	5.821	6.806	6.7[b], 6.4[c]
	F	6.803	7.833	na[d]
	Cl	6.599	7.807	na[d]
TMTTF	-	5.491	6.579	6.03[c]
BEDT-TTF	-	5.799	7.073	6.7[b], 6.21[c]
BEDO-TTF	-	5.725	6.791	6.46[b]
MDT-TTF	-	5.954	7.055	na[d]
S,S-DMBEDT-TTF	-	na[e]	7.022	na[d]
TSeF		6.289	7.099	6.68[c]
	Cl	7.005	8.024	na[d]
TOF		5.389	6.940	na[d]
	Cl	6.249	7.952	na[d]

[a]For TTF, TSeF and TOF, all substitutions replace H atoms with the corresponding substituents.

[b]Data from Ref. 9

[c]Data from Ref. 10

[d]No experimental data available.

[e]Not yet calculated.

Table 3 : Energies for various organic donors

			X			X^+		
Species	Conformation	Symmetry	Total (H)	HOMO (eV)	LUMO (eV)	Total (H)	HOMO (eV)	LUMO (eV)
TTF	planar	D_{2h}	-1819.5165	-6.806	3.070	-1819.3026	-11.641	-4.768
F[g]	boat	C_{2v}[a]	-2214.8467	-7.833	1.853	-2214.5967	-12.513	-5.752
Cl[g]	boat	C_{2v}[a]	-3655.0704	-7.807	1.988	-3654.8279	-12.143	-5.397
TMTTF	boat	C_{2v}[a]	-1975.6844	-6.579	3.151	-1975.4826	-11.092	-4.342
BEDT-TTF[b]	boat	C_2	-3563.3607	-7.073	2.748	-3563.1476	-10.929	-4.541
BEDO-TTF[c]	boat	C_2	-2272.7063	-6.791	2.798	-2272.4959	-11.071	-4.612
MDT-TTF	boat	C_1[d]	-2652.3944	-7.055	2.816	-2652.1756	-11.299	-4.833
S,S-DMBEDT-TTF	boat	C_1[d]	-3641.4361	-7.022	2.811	na[e]	na[e]	na[e]
TSeF[g]	planar	D_{2h}	-265.4650	-7.099	2.060	-265.2339	-11.747	-5.330
Cl[f,g]	boat	C_{2v}	-2098.1371	-8.024	1.034	-2097.8796	-12.210	-5.902
TOF	planar	D_{2h}	-528.8507	-6.940	5.278	-528.6526	-12.948	-3.676
Cl[g]	planar	D_{2h}	-2364.4078	-7.953	4.329	-2364.1781	-13.160	-4.291

[a] There is only one negative curvature from the Hessian matrix for the planar conformation, indicating that the only stable structure is boat.
[b] The staggered ethylene conformation is used. There is also an eclipsed ethylene conformation with C_s symmetry and an energy 5 μHartree lower than the staggered conformation (See Ref. 8).
[c] The staggered ethylene conformation is used. We did not do detailed conformation calculations for BEDO-TTF, but we expect that the conformations of BEDO-TTF should be similar to BEDT-TTF.
[d] Molecule is asymmetric (See Figure 1 in Section 3.3).
[e] Not yet calculated.
[f] Effective Core Potential is used for Se atoms.
[g] For TTF, TSeF and TOF, all substitutions replace H atoms with the corresponding substituents.

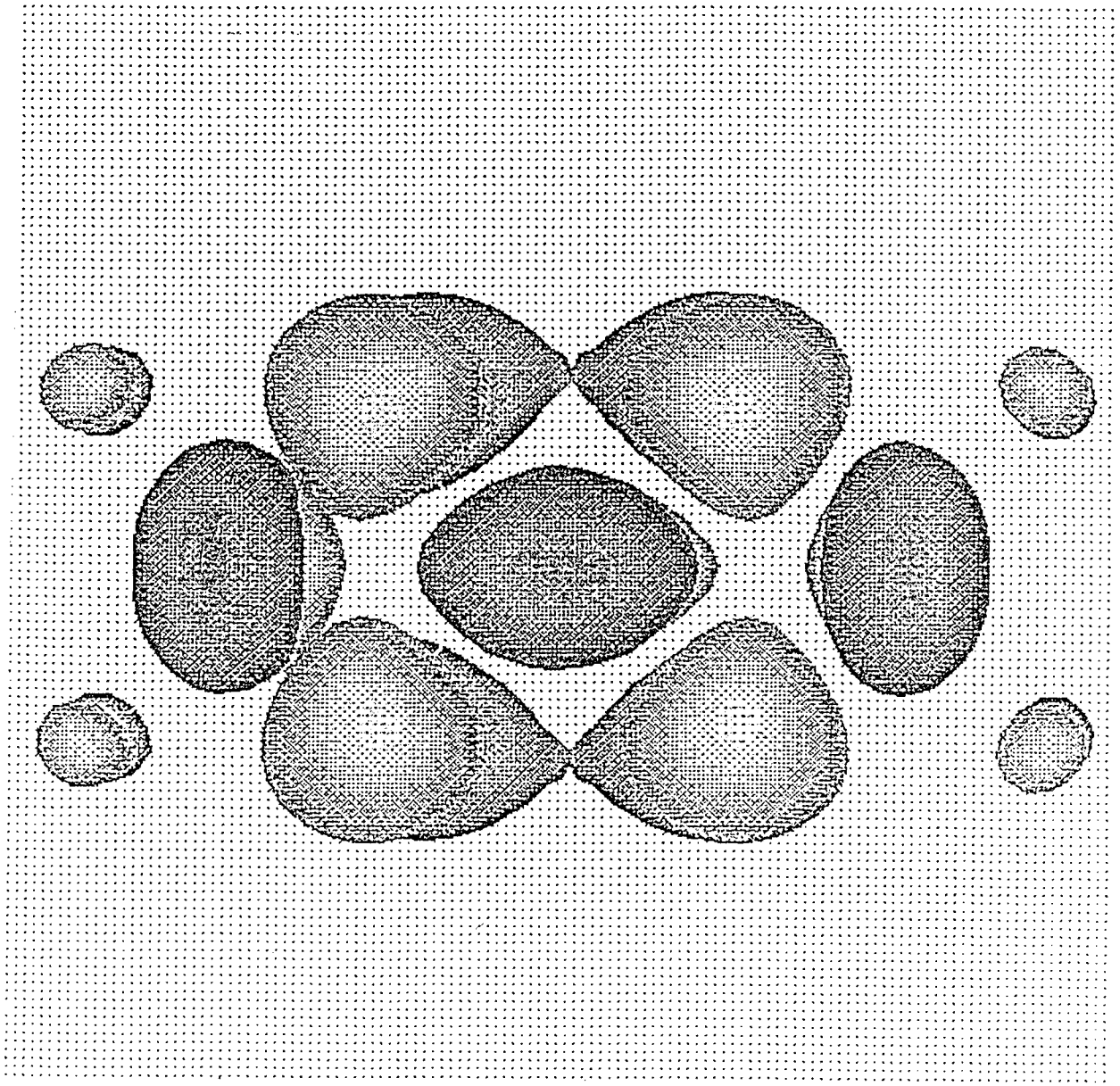

Figure 1

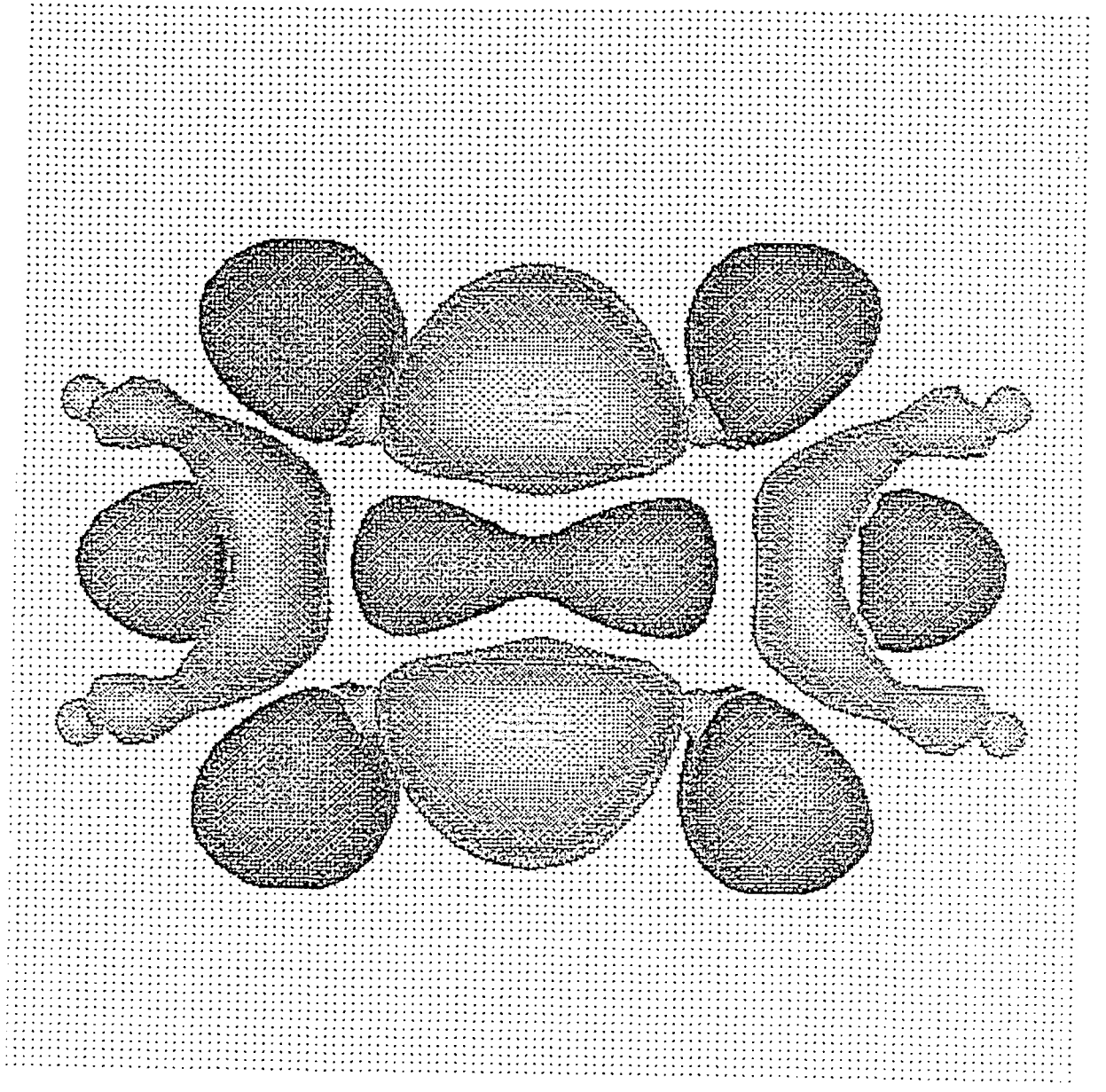

Figure 2

Chapter 4 Molecular Mechanical Calculations for $BEDT-TTF$ and $BEDT-TTF^{+}$

Force Field and Vibrational Frequency Calculations for the Neutral and Cation BEDT-TTF

Abstract

BEDT-TTF is the donor of the best T_c organic superconductors. Isotopic shift experiments support electron-phonon coupling mechanism for the superconductivity; however, the vibrational levels have been only partially observed and assigned. In order to provide a complete consistent description of all levels, we carried out Hartree-Fock calculations (6-31G** basis set) for all fundamental vibrational frequencies of BEDT-TTF and BEDT-TTF$^+$ and obtained the Hessians for these structures. With these Hessians and available experimental frequencies, we develop the force fields for the neutral and cation BEDT-TTF molecules by using Hessian-biased method. Calculated frequencies are compared with the available experimental frequencies for the neutral and cation BEDT-TTF molecule.

1.0 Introduction

The organic superconductors all involve derivatives of the organic donor molecules tetrathiafulvalene (denoted as TTF), tetraselenafulvalene (denoted at TSeF), or some mixture of these two molecules, packed into quasi one- and two-dimensional arrays and complexed to appropriate electron acceptors.[1] Figure 1 shows BEDT-TTF (denoted also as ET) is the donor of the best organic superconductors. Using ET, more than 20 organic superconductors have been synthesized with T_c up to 12.8K. Changes in T_c for various isotope shifts indicate that electron-phonon coupling is important for the superconductivity of these materials. However, experimental data on the vibrational modes is incomplete and does not supply clear evidence about the vibrational modes that are important for superconductivity. Thus, we perform *ab initio* HF and force field calculations to obtain all modes of neutral ET and of ET^+.

With appropriate electron acceptors some modifications of ET show superconductivity and some do not. The relation between superconductivity and the molecular or crystal structures of these molecules is not yet clearly identified by the experiments. Yamaji[2] proposed that the superconductivity in organic conductors involves coupling between the Highest Occupied Molecular Orbital (HOMO) and total symmetric intramolecular vibrational modes. However, the pattern of isotope effects does not support for this view. Isotopic shift experiments with deuterium substitutions showed that the electron-phonon coupling plays a role in the superconductivity of these materials.[3,4,5,6] We found that[7] *the neutral donor distorts into a boat structure whereas the cation is planar* for all known organic superconductors. We suggested that the coupling between charge transfer and the lowest boat deformation vibrational mode is responsible for the superconductivity and predicted the isotope shifts (δT_c) for experimental tests of this coupling.[8] Although incomplete, current experimental isotopic shifts are consistent with this charge transfer boat deformation (ET-BV) coupling for the mechanism of the superconductivity.[8]

In this paper, we present the calculated vibrational spectra for the equilibrium structures of ET (boat) and ET^+ (planar). Using calculated structures, Hessians and available experimental frequencies we develop the force fields for the

neutral and cation ET molecules. These frequencies are compared with the available experimental frequencies.[9,10]

2.0 Results

2.1 Structures

The structure of ET is often discussed in terms of D_2 symmetry, which assumes a planar structure for the central TTF moiety. The crystal structures of neutral ET crystal are consistent with planarity but show a distinct boat-like distortion.[11] Some deviations from planarity are also suggested in crystals containing electron acceptors, $(ET)_nX_m$.[12] Here the ET molecules often form dimers $(ET_2)^+$ sharing a single positive charge.

Recently we reported *ab initio* quantum chemical calculations [Hartree-Fock (HF) with 6-31G** basis set] for the structures of neutral and cation ET.[7,8] These results show that *neutral ET is nonplanar.* It deforms to boat conformation with a well depth of 0.654 kcal/mol. However, the cation, ET^+, is planar.

The terminal six membered-rings are nonplanar in order to avoid eclipsing of the $CH_2 - CH_2$ groups at each end. This nonplanarity leads to two possible conformations[12]:

1. The *staggered* conformation indicated in Figure 1a in Section 3.2 in which the two $C_6 - C_6$ bonds are pointing in opposite directions; assuming a planar TTF central region, this leads to D_2 symmetry.
2. The *eclipsed* conformation indicated in Figure 1b in Section 3.2 in which the two $C_6 - C_6$ bonds are parallel; with planar TTF, this leads to C_{2h} symmetry.

These conformations are essentially degenerate, differing by only 0.0000052 Hartrees(with eclipsed lower). We will consider the higher symmetry staggered case.

To determine the structure and vibrational modes of ET, we carried out *ab initio* Hartree-Fock calculations using the 6-31G** basis set.[13] Restricting the symmetry to D_2 leads to an optimized structure with two imaginary frequency vibrational modes. The stable conformation is the boat structure with C_2 symmetry. The optimized boat structure has vibration frequencies positive, indicating a stable

structure.

2.2 Vibrational Analysis

Previously, assignments of the vibrational spectra of ET assumed planar molecule for both the neutral and cation cases. Planar ET would have D_2 symmetry for the staggered conformation and C_{2h} for the eclipsed conformation. For the staggered conformation this leads to fundamental modes with the following symmetries:

$$\Gamma(D_2) = 19A + 17B_1 + 18B_2 + 18B_3 \quad . \tag{1}$$

To simplify assignments, Kozlov et al.[11,12] considered the ET to be totally flat leading to D_{2h} symmetries (they were aware that only the central C_2S_4 group is planar). This leads to the fundamental mode distribution

$$\Gamma(D_{2h}) = 12A_g + 7A_u + 6B_{1g} + 11B_{1u} + 7B_{2g} + 11B_{2u} + 11B_{3g} + 7B_{3u} \quad . \tag{2}$$

Thus D_{2h} leads to g and u branching of the D_2 symmetry modes. However, the stable boat structure of ET has C_2 symmetry, leading to the mode distribution

$$\Gamma(C_2) = 37A + 35B \quad . \tag{3}$$

Consequently, some modes become both infrared and Raman active. Table 1 shows that this is consistent with data of Kozlov et al.[9] The two-fold axis of B_3 symmetry of the planar molecule and C_2 axis of the boat molecule are perpendicular to the central plane of the molecule. The reduction of symmetry, is as follows:

$$12A_g + 7A_u + 11B_{3g} + 7B_{3u} \rightarrow 19A + 18B_3 \rightarrow 37A \tag{4a}$$

and

$$11B_{1u} + 6B_{1g} + 11B_{2u} + 7B_{2g} \rightarrow 17B_1 + 18B_2 \rightarrow 35B \quad . \tag{4b}$$

Table 4 shows all calculated frequencies plus available experimental frequencies for neutral ET. Calculated Raman and IR intensities are also given for all

the vibrational modes. We used the symmetry of the modes for assigning experimental frequencies to the HF modes. The calculated IR and Raman intensities are in good agreement with experimental intensities.

ET^+ molecules is planar (D_2 symmetry) leading to the distribution of fundamental mode in equation (1). Table 5 shows all the vibrational modes of ET^+ compared to the available experimental frequencies.

3.0 The Force Field

The ET molecules appear to be distorted in the crystal structures, removing all symmetry. The assignment of frequencies for ET and ET^+ molecules by Kozlov et al.[9,10] assumed D_{2h} symmetry. We used the optimized HF geometries of the neutral and cation ET to develop the force fields. Neutral ET has C_2 symmetry and cation ET has D_2 symmetry. The optimized geometric parameters(distances, angles, dihedrals) for the neutral and cation ET molecules are given in Table 1. We use these structures when we optimize our force field (FF). (For the neutral molecule, the optimized HF structure is minimized to reduce the total force by using FF. The rms difference between HF and minimized structure (FF) are 0.002 $\AA$ for bonds, 0.680° for angles). We calculated the Hessian (second derivative of energy with respect to the 3N coordinates) at the HF optimized geometry. This Hessian was used to develop the force field by using Hessian-Biased (HBFF) approach.[14]

The potential energy of the molecule is:

$$E = \sum_{bonds} E_b + \sum_{angles} E_a + \sum_{torsions} E_t + \sum_{inversions} E_i + \sum_{cross} E_X + \sum_{vdW} E_{vdW} + \sum_{Charges} E_Q \quad , \tag{5}$$

where the terms are defined below. In the HBFF approach, the potential energy is expressed as a sum of valence, nonbonded interactions. We optimize the force field terms by fitting the experimental frequencies and the calculated geometries.

a. Valence Interactions

We used the following valence terms:

i. the harmonic bond stretch

$$E_b(R) = \frac{1}{2}k_b(R - R_b)^2 \quad , \tag{6}$$

where (R_b) is the equilibrium bond distance and (k_b) is the force constant.

ii. the harmonic angle bend

$$E_a(\theta) = \frac{1}{2}k_\theta(\theta - \theta_0)^2 \quad , \tag{7}$$

where θ_0 is the equilibrium angle and k_θ is the force constant.

iii. angle-stretch cross terms

$$E_{ab} = k_{R\theta}(\theta - \theta_0)(R - R_b) \quad , \tag{8}$$

where $k_{R\theta}$ is the force constant.

iv. stretch-stretch cross terms

$$E_{bb} = k_{R_bR'_b}(R - R_b)(R' - R'_b) \quad , \tag{9}$$

where $k_{R_bR'_b}$ is the force constant for the bonds R_b and R'_b that share a common atom.

v. the torsional potential

$$E_t(\phi) = V_1 cos\phi + V_2 cos2\phi + V_3 cos3\phi \quad , \tag{10}$$

where V_1, V_2, V_3 are in kcal/mol and the angle ϕ is defined as the angle between the JKL plane and the IJK plane of the any two bonds IJ and KL attached to a common bond JK.

vi. the inversion potential

$$E_i(\omega) = K_\omega(1 - cos\omega) \quad , \tag{11}$$

with a minimum for planar structure ($\omega_0 = 0°$). ω is the angle between the IL axis and the IJK plane for an atom I with exactly three bonds IJ, IK and IL.

b. Charges

Partial atomic charges for the various atoms were obtained using the Potential Derived Charge method(PDQ).[15] The electron density from Hartree-Fock wavefunction is used to calculate the electrostatic potential around the molecule. Then, a set of atomic point charges is obtained that reproduces the *ab initio* electrostatic potential and dipole and quadrupole moments. Table 2 shows the atomic charges for the neutral and cation molecules.

We write total electrostatic energy as

$$E_{Coulomb} = C_0 \sum_{ij} \frac{Q_i Q_j}{\epsilon R_{ij}} \quad , \tag{12}$$

where ϵ is the dielectric constant, R_{ij} is the distance in $\AA$ and the conversion factor $C_0 = 332.0637$ puts the energy in kcal/mol. We take $\epsilon = 1$ (i.e. vacuum value).

c. van der Waals Parameters

We used the van der Waals parameters [16] previously determined from empirical fits to lattice parameters. The exponential-6 potential is used for van der Waals interactions:

$$E_{vdW} = D_0[(\frac{6}{\zeta - 6})e^{\zeta(1-\frac{R}{R_0})} - (\frac{\zeta}{\zeta - 6})(\frac{R_0}{R})^6] \quad . \tag{13}$$

In Table 3 we give the bond strength (well depth) D_0 (in kcal/mol) and the bond length R_0 (in Å) and ζ are given for C, S and H.

The electrostatic and van der Waals interactions are excluded for 1-2, 1-3 and 1-4 interactions since they are considered to be already included in the bond stretch, angle bend and torsion terms.

4.0 Hessian-biased Method[14]

The potential energy can be expanded around the equilibrium geometry.

$$E = E_0 + \sum_{i=1}^{3N} (\frac{\partial E}{\partial R_i})(\delta R_i) + \frac{1}{2} \sum_{i,j=1}^{3N} (\frac{\partial^2 E}{\partial R_i \partial R_j})(\delta R_i)(\delta R_j) + ... \tag{14}$$

where

$$F_i = -\frac{\partial E}{\partial R_i} \tag{15}$$

is the force on the i^{th} component and

$$H_{ij} = \frac{\partial^2 E}{\partial R_i \partial R_j} \tag{16a}$$

is the Hessian. Using the mass weighting

$$H_{ij} = H_{ij}(M_i M_j)^{-1/2} \tag{16b}$$

and diagonalizing (16b)

$$H\mathbf{U} = \mathbf{U}\lambda \quad , \tag{17}$$

where λ contains the 3N vibrational frequencies(6 of which are zero for a free nonplanar molecule).

In the Hessian-biased method, the theoretical Hessian (H_t) is biased with the experimental frequencies. From (17) the theoretical Hessian can be written

$$H_t = \mathbf{U}_t \lambda_t \mathbf{U}_t^T \quad , \tag{18}$$

where $\mathbf{U}_t^T$ is the transpose of $\mathbf{U}_t$. We then modify λ_t by replacing λ_t with the experimental λ_x. This leads to the *experimental biased Hessian* defined as

$$H_{xt} = \mathbf{U}_t \lambda_x \mathbf{U}_t^T \quad . \tag{19a}$$

The biased Hessian has the property that

$$H_{xt}\mathbf{U}_t = \mathbf{U}_t \lambda_x \quad . \tag{19b}$$

That is, it leads to the theoretical modes ($\mathbf{U}_t$) and the experimental frequencies (λ_x). If the λ_x is not available from experiment, it can be obtained from the theory using appropriate scaling rules.

We optimized the force field parameters that gave the best fit to H_{xt} while leading to correct(theoretical) equilibrium geometry. The van der Waals parameters and charges were fixed during optimization of the valence parameters. The charges (Table 2) were based on Potential Derived Charges (PDQ) by using quantum mechanical potentials and the vdW parameters (Table 3) were from previous fits to various crystals. The final force field parameters for the neutral and cation ET are shown in the first two columns of Table 3.

Calculated frequencies for ET and ET^+ are compared with the available experimental frequencies by Kozlov et al.[9,10] (frequencies for both neutral and cation molecules) and Eldridge et al.[17] (only frequencies for neutral molecule) in Table 4 and 5. Kozlov et al. reported more modes for neutral ET and Eldridge et al. did not report for the frequencies of ET^+, hence we use the experimental frequencies by Kozlov et al.[9,10] for rms error calculations. The rms error between theory and experiment frequencies are $\sim 32\ cm^{-1}$ for ET and $\sim 20\ cm^{-1}$ for ET^+.

5.0 Summary

We develop force fields for the neutral, cation ET molecules including the valence and nonbonded interactions. The Hessian-biased approach is used to get the force field which reproduces experimental frequencies for the neutral and cation ET. The calculated frequencies are compared with the available experimental frequencies for the neutral, cation ET molecules. It is shown that there is good agreement between calculated and experimental frequencies.

References

1. Jerome D., Mazaud A., Ribault M., Bechgaard K., *J. Phys. Lett. 41*, (1980) L95.

2. Yamaji K., *Solid State Communications, 61*, (1987), 413.

3. Carlson K. D., Williams J.M., Geiser U., Kini A. M., Wang H. H., Klemm R. A., Kumar S. K., Schlueter J. A., Ferraro J. R., Lykke K. R., Wurz P., Parker H., Sutin J. D. B., *Mol. Crsyt. Liq. Cryst. 234*, (1993), 127.

4. Carlson K. D., Kini A. M., Klemm R. A., Wang H. H., Williams J.M., Geiser U., Kumar S. K., Ferraro J. R., Lykke K. R., Wurz P., Fleshler S., Dudek J. D., Eastman N. L., Mobley P. R., Seaman J. M., Sutin J. D. B., Yaconi G. A., *Inorg. Chem. 31*, (1992), 3346.

5. Carlson K. D., Kini A. M., Schlueter J. A., Wang H. H., Sutin J. D. B., Williams J.M., Schirber J. E., Venturini E. L. , Bayless W. R., *Physica C 227*, (1994), 10.

6. Carlson K. D., Williams J.M., Geiser U., Kini A. M., Wang H. H., Klemm R. A., Kumar S. K., Schlueter J. A., Ferraro J. R., Lyyke K. R., Wurz P., Parker D. H., Sutin J. D. B. *Mol. Cryst. Liq. Cryst. 234*, (1993), 127.

7. Demiralp E. and Goddard III, W. A., *Synthetic Metals, 72*, (1995), 297.

8. Demiralp E.,Dasgupta S. and Goddard III, W. A., *Journal of American Chemical Society 117*,(1995), 8154 .

9. Kozlov M.E., Pokhodnia K. I., Yurchencko A. A., *Spectrochimica Acta 45A* (1989), 323.

10. Kozlov M.E., Pokhodnia K. I., Yurchencko A. A., *Spectrochimica Acta 45A* (1989), 437.

11. Kobayashi H., Kobayashi A., Yukiyoshi S., Saito G., Inkuchi H., *Bull. Chem. Soc. Jpn.*, *59*, (1986) 301.

12. Williams J.M., Ferraro J. R., Carlson K. D., Geiser U., Wang H. H., Kini A. M., Whangbo M-H, *Organic Superconductors (Including Fullerenes): synthesis, structure, properties, and theory*, (Printice-Hall 1992)

13. The quantum chemical calculations were carried out using Gaussian 92, Revision B, M. J. Frisch, G. W. Trucks, M. Head-Gordon, P. M. W. Gill, M. W. Wong, J. B. Foresman, B. G. Johnson, H. B. Schlegel, M. A. Robb, E. S. Replogle, R. Gomperts, J. L. Andres, K. Raghavachari, J. S. Binkley, C. Gonzalez, R. L. Martin, D. J. Fox, D. J. Defrees, J. Baker, J. J. P. Stewart, and J. A. Pople, Gaussian, Inc., Pittsburgh PA, 1992.

14. Dasgupta, S.; Goddard III, W. A.*J. Phys. Chem. 95,* (1989) 7207.

15. M. N. Ringnalda, J-M. Langlois, B. H. Greeley, T. V. Russo, R. P. Muller, B. Marten, Y. Won, R. E. Donnelly, Jr., W. T. Pollard, G. H. Miller, W. A. Goddard III, and R. A. Freisner, PS-GVB v1.0, Schrödinger, Inc., Pasadena, California, 1994.

16. Mayo S.L, Olafson B. D., Goddard III, W. A., , *Journal of Physical Chemistry*, 94, (1990) 8897.

17. Eldridge J. E., Homes C. C., Wang H. H., Kini A. M., Williams J.M., *Synthetic Metals, 70*, (1995) 983.

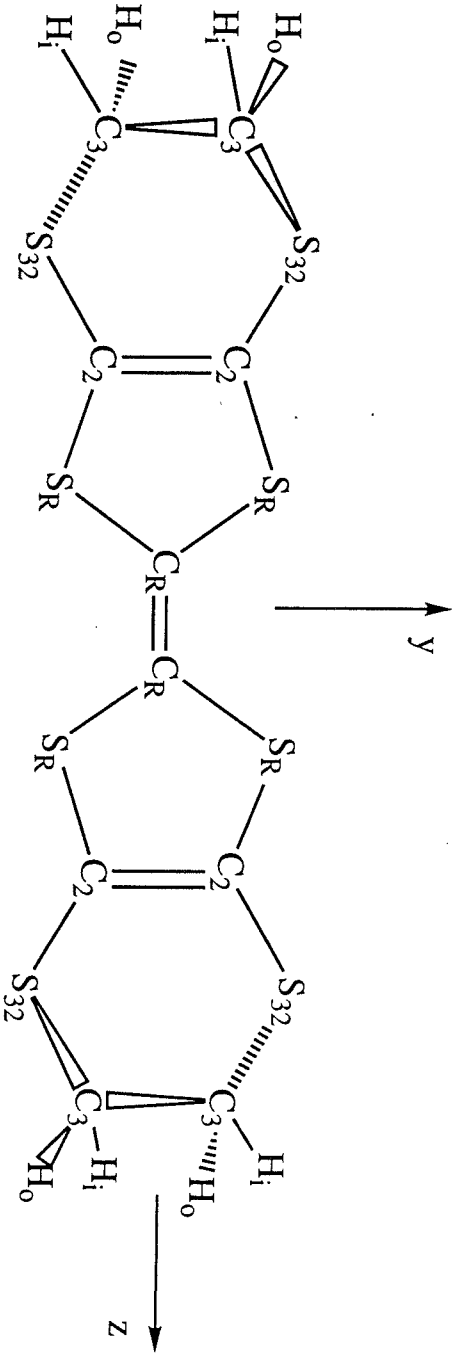

Figure 1 : Definition of the atomic types for the atoms of ET

Table 1a. Optimized distances(in $\AA$) for boat and planar ET conformations and experimental distance (See Figure 1 for notation).

		ET		ET^+	
		FF*	HF	FF	HF
$C_R - C_R$	1	1.325	1.326	1.389	1.389
$S_R - C_2$	4	1.773	1.774	1.751	1.751
$S_{32} - C_3$	4	1.812	1.814	1.816	1.816
$S_R - C_R$	4	1.769	1.771	1.721	1.721
$C_2 - C_2$	2	1.325	1.323	1.336	1.336
$S_{32} - C_2$	4	1.769	1.767	1.765	1.765
$C_3 - C_3$	2	1.523	1.523	1.523	1.523
$C_3 - H$	8	1.083	1.082	1.082	1.082

Table 1b. Optimized angles (in degrees)

		ET		ET^+	
		FF	HF	FF	HF
$S_{32} - C_2 - C_2$	4	128.68	128.45	128.83	128.83
$S_R - C_2 - S_{32}$	4	113.80	114.29	114.75	114.75
$S_R - C_R - S_R$	2	112.74	112.55	114.49	114.49
$C_R - S_R - C_2$	4	94.41	94.55	96.33	96.33
$S_{32} - C_3 - C_3$	4	112.87	113.17	113.10	113.10
$S_R - C_2 - C_2$	4	117.22	117.22	116.42	116.42
$S_R - C_R - C_R$	4	123.63	123.71	122.76	122.76
$C_2 - S_{32} - C_3$	4	100.74	100.81	100.50	100.50
$H - C_3 - H$	4	108.58	108.48	108.51	108.51
$S_{32} - C_3 - H$	8	107.18	107.15	106.84	106.84
$C_3 - C_3 - H$	8	110.36	110.31	110.60	110.60

* For the neutral molecule, the optimized HF structure is minimized to reduce the total force by using FF. The rms force is less than 0.1 (kcal/mol)/A for ET and ET^+.

Table 2. Calculated charges by using Potential Derived Charge Method (See Figure 1 in this chapter for notation).

	Number of Cases	Neutral	Cation
C_R	2	-0.0200	-0.0220
S_R	4	-0.0260	0.1390
C_2	4	0.0265	0.0240
S_{32}	4	-0.0955	-0.0230
C_3	4	-0.1770	-0.2420
H_i	4	0.1885	0.2440
H_o	4	0.0935	0.1200
Net Charge		0.0	1.0

Table 3. Force-field parameters used in this calculations. Units are kcal/mol for energies, Å for length, and degrees for angles. Angular force constants use radians.

van der Waals Parameters		
H	R_o	3.19500
	D_o	0.01520
	ζ	12.38200
C	R_o	3.89830
	D_o	0.09510
	ζ	14.03400
S	R_o	4.03000
	D_o	0.34400
	ζ	12.00000

Table 3. (Continued) Force-field parameters used in this calculations. Units are kcal/mol for energies, Å for length, and degrees for angles. Angular force constants use radians (See Figure 1 in this chapter for notation).

		Neutral	Cation
Bond Stretch			
$C_3 - H$	R_b	1.084	1.081
	k_b	636.386	636.530
$C_3 - C_3$	R_b	1.526	1.523
	k_b	613.257	606.042
$C_2 - C_2$	R_b	1.300	1.329
	k_b	1280.633	1073.148
$C_R - C_R$	R_b	1.319	1.399
	k_b	1120.168	995.272
$S_{32} - C_3$	R_b	1.821	1.825
	k_b	312.535	304.720
$S_{32} - C_2$	R_b	1.827	1.766
	k_b	361.172	479.499
$S_R - C_2$	R_b	1.788	1.753
	k_b	836.525	674.396
$S_R - C_R$	R_b	1.736	1.721
	k_b	483.850	547.649

Table 3. (Continued)

		Neutral	Cation
Angle Bend			
$H - C_3 - H$	θ_0	109.12	108.65
	k_θ	92.818	72.886
$C_3 - C_3 - H$	θ_0	110.79	110.38
	k_θ	80.057	109.365
$S_{32} - C_3 - H$	θ_0	107.44	105.85
	k_θ	74.392	60.653
$S_{32} - C_3 - C_3$	θ_0	114.35	113.57
	k_θ	193.274	364.201
$S_{32} - C_2 - C_2$	θ_0	121.64	127.48
	k_θ	96.121	77.349
$S_R - C_2 - C_2$	θ_0	113.62	115.72
	k_θ	130.018	233.544
$S_R - C_2 - S_{32}$	θ_0	108.09	114.96
	k_θ	89.224	90.533
$S_R - C_R - C_R$	θ_0	130.18	121.61
	k_θ	98.621	129.464
$S_R - C_R - S_R$	θ_0	128.78	116.13
	k_θ	154.837	148.992
$C_2 - S_{32} - C_3$	θ_0	100.03	100.67
	k_θ	198.691	191.985
$C_R - S_R - C_2$	θ_0	98.32	96.85
	k_θ	250.173	322.658

Table 3. (Continued)

		Neutral	Cation
Angle Cross Terms			
$H-C_3-H$	$k_{R_1\theta}$	-75.260	-27.305
	$k_{R_2\theta}$	-75.260	-27.305
	$k_{R_1R_2}$	-38.305	-22.977
C_3-C_3-H	$k_{R_1\theta}$	7.847	6.245
	$k_{R_2\theta}$	3.295	86.784
	$k_{R_1R_2}$	1.546	-0.226
$S_{32}-C_3-H$	$k_{R_1\theta}$	48.635	39.139
	$k_{R_2\theta}$	18.933	-10.670
	$k_{R_1R_2}$	-13.325	-0.371
$S_{32}-C_3-C_3$	$k_{R_1\theta}$	-0.964	-6.689
	$k_{R_2\theta}$	-4.778	68.070
	$k_{R_1R_2}$	20.436	34.745
$S_{32}-C_2-C_2$	$k_{R_1\theta}$	96.007	119.264
	$k_{R_2\theta}$	-47.517	-31.109
	$k_{R_1R_2}$	10.424	-2.801
$S_R-C_2-C_2$	$k_{R_1\theta}$	178.792	162.888
	$k_{R_2\theta}$	81.403	82.593
	$k_{R_1R_2}$	408.025	264.133
$S_R-C_2-S_{32}$	$k_{R_1\theta}$	54.907	35.455
	$k_{R_2\theta}$	113.414	135.257
	$k_{R_1R_2}$	86.875	91.696
$S_R-C_R-C_R$	$k_{R_1\theta}$	40.592	69.328
	$k_{R_2\theta}$	36.508	104.725
	$k_{R_1R_2}$	63.775	29.613
$S_R-C_R-S_R$	$k_{R_1\theta}$	79.702	126.993
	$k_{R_2\theta}$	79.702	126.993
	$k_{R_1R_2}$	60.025	19.556

$C_2 - S_{32} - C_3$	$k_{R_1\theta}$	49.887	148.984
	$k_{R_2\theta}$	46.465	33.800
	$k_{R_1R_2}$	-11.975	-69.191
$C_R - S_R - C_2$	$k_{R_1\theta}$	52.029	124.512
	$k_{R_2\theta}$	59.718	43.796
	$k_{R_1R_2}$	10.704	25.593

Table 3. (Continued)

		Neutral	Cation
Torsion Terms			
$H-C_3-C_3-H$	V_3	5.958	7.164
$S_{32}-C_3-C_3-H$	V_3	19.558	9.641
$S_{32}-C_3-C_3-S_{32}$	V_3	-73.125	-57.046
$S_{32}-C_2-C_2-S_{32}$	V_2	-25.759	-3.196
$S_R-C_2-C_2-S_{32}$	V_2	10.814	-13.975
$S_R-C_2-C_2-S_R$	V_2	-44.726	0.876
$S_R-C_R-C_R-S_R$	V_2	-19.943	-0.217
$C_2-S_{32}-C_3-H$	V_3	1.531	0.684
$C_2-S_{32}-C_3-C_3$	V_3	-2.586	-2.605
$C_3-S_{32}-C_2-C_2$	V_2	0.720	1.825
$C_3-S_{32}-C_2-S_R$	V_2	-0.020	0.170
$C_R-S_R-C_2-C_2$	V_2	2.764	-3.149
$C_R-S_R-C_2-S_{32}$	V_2	-0.774	-4.459
	V_3	1.845	0.000
$C_2-S_R-C_R-C_R$	V_1	6.756	12.840
	V_2	0.844	0.263
	V_3	-0.350	0.000
$C_2-S_R-C_R-S_R$	V_2	1.175	-1.393
	V_3	2.127	0.000

	Neutral	Cation
Inversion Constant(K_ω)		
$C_2-S_R-S_{32}-C_2$	5.738	4.917
$C_2-S_R-C_2-S_{32}$	85.778	155.854
$C_2-S_{32}-C_2-S_R$	6.745	1.651
$C_R-S_R-S_R-C_R$	10.713	16.128
$C_R-S_R-C_R-S_R$	53.616	50.178

Table 4. Calculated (HF)and experimental frequencies and Raman and infrared (IR) intensities for ET. The frequencies are in cm^{-1}, IR intensities are in KM/Mole, Raman intensities are in $Å^4$/AMU.

Sym.	Modes	HF	Intensity		Experiment		FF
			IR	Raman	IR	Raman	
A	C-H str.	3302	11.60	71.75	-	(2964)	2957.9
B	C-H str.	3302	3.28	51.36	2958 w(2958)	-	2957.9
A	C-H str.	3290	0.01	256.30	-	-	2915.0
B	C-H str.	3290	0.37	9.60	-	-	2915.0
A	C-H str.	3237	0.20	606.22	-	(2920)	2958.3
B	C-H str.	3237	79.71	4.30	2958 w(2922)	-	2958.3
A	C-H str.	3229	10.24	161.39	-	-	2909.8
B	C-H str.	3228	2.68	6.80	-	2916 w	2909.8
A	C=C str.	1815	0.57	354.11	-	1552 m(1551)	1546.9
B	C=C str.	1790	1.48	0.26	1505 w(1509)	1511 m	1519.5
A	C=C str.	1772	0.35	509.60	-	1494 s(1493)	1490.0
A	CH_2 bend	1608	3.02	10.70	-	(1408)	1424.3
B	CH_2 bend	1608	1.11	14.73	1420 w(1409)	-	1424.3
A	CH_2 bend	1594	11.27	9.51	-	1406 m(1422)	1401.4
B	CH_2 bend	1594	4.86	32.12	1409 vw(1422)	-	1401.4
A	CH_2 wag	1466	2.41	0.93	-	1285 vw(1283)	1295.0
B	CH_2 wag	1466	63.72	1.71	1282 m(1284)	-	1295.0

Sym.	Modes	HF	Intensity		Experiment		FF
			IR	Raman	IR	Raman	
A	CH_2 wag	1434	5.66	1.19	1259 w(1261)	-	1247.4
B	CH_2 wag	1434	0.90	0.57	-	1256 vw(1257)	1247.4
A	CH_2 twist	1321	0.27	15.70	-	1175 vw	1164.2
B	CH_2 twist	1321	0.06	2.33	1173 vw	-	1164.2
A	CH_2 twist	1260	2.48	0.29	1132 sh	1132 vw	1127.4
B	CH_2 twist	1260	2.44	14.41	1125w	1126vw	1127.4
A	Ring Def. (I.P.)[b]	1131	0.21	0.34	-	1016 vw(1000)	1029.5
B	Ring Def. (I.P.)	1128	7.06	0.02	(997)	-	1013.0
A	Ring Def. (I.P.)	1125	0.01	0.59	-	(1013)	1009.3
B	C-C str.	1093	0.03	0.61	996 w(992)	-	998.6
A	C-C str.	1093	0.01	7.15	987 w	-	998.6
A	CH_2 rock.	1033	1.64	7.62	-	-	948.1
B	CH_2 rock.	1033	22.58	5.39	938 vw	-	948.1
B	CH_2 wag	996	12.99	1.83	917 s(906)	-	915.5
A	CH_2 wag	990	5.72	0.04	-	919 vw(889)	915.5
B	Ring Def. (I.P.)	967	28.10	0.77	905 m(919)	-	900.0
A	Ring Def. (I.P.)	967	3.50	1.81	-	911 vw(918)	899.6
B	Ring Def. (I.P.)	951	2.29	0.28	890 m(890)	890 vw	854.1

Sym.	Modes	HF	Intensity		Experiment		FF
			IR	Raman	IR	Raman	
B*	Ring Def. (I.P.)	847	12.03	0.13	875 vw(687)	875 vw	758.6
B	Ring Def. (I.P.)	846	42.37	0.02	772 s(771)	-	761.6
A	Ring Def. (I.P.)	842	0.17	1.96	860 vw	-	824.4
A	CH_2 rock.	759	0.10	15.90	-	687 w	726.8
B	CH_2 rock.	759	2.47	1.86	687 w	-	724.9
A	CH_2 rock.	716	0.02	44.08	-	653 m(625)	629.9
B	CH_2 rock.	716	6.70	0.62	653 w(625)	-	628.9
B	Ring Def. (O.P.)[c]	623	4.54	11.88	-	-	724.9
B	Ring Def. (O.P.)	606	0.06	4.15	-	-	453.3
A	Ring Def. (O.P.)	605	0.05	0.92	-	-	449.6
A	Ring Def. (O.P.)	539	1.50	15.60	-	486 m(487)	502.3
B	Ring Def. (I.P.)	511	1.50	0.86	499 m(500)	-	481.3
A*	Ring Def. (I.P.)	510	0.03	1.73	-	625 w(654)	668.6
B*	Ring Def. (I.P.)	496	6.24	0.43	624 w(654)	-	667.8
A	Ring Def. (I.P.)	483	0.01	14.54	450 w	440 m(440)	446.0
B	Ring Def. (I.P.)	425	6.63	1.16	390 m(390)	-	389.3
B	Ring Def. (I.P.)	394	0.04	0.80	-	334 m(335)	361.6
A	Ring Def. (I.P.)	393	0.02	0.10	335 m(335)	-	373.4
A	Ring Def. (I.P.)	383	0.0.09	8.42	-	348 w(348)	347.3

Sym.	Modes	HF	Intensity		Experiment		FF
			IR	Raman	IR	Raman	
A	Ring Def. (O.P.)	356	1.02	4.00	-	308 w(309)	303.0
B	Ring Def. (O.P.)	327	3.16	0.17	278 m(277)	-	288.1
A	Ring Def. (O.P.)	315	0.04	2.72	-	-	361.9
B	Ring Def. (O.P.)	309	0.28	0.05	-	-	269.8
A	Ring Def. (O.P.)	300	0.04	0.20	-	-	261.4
B	Ring Def. (I.P.)	286	3.72	0.02	257 m(258)	260 w	264.9
A	Ring Def. (O.P.)	270	0.01	0.75	-	-	177.1
B*	Ring Def. (O.P.)	262	4.45	0.61	-	127 vw	62.2
A	Ring Def. (O.P.)	206	0.01	0.72	-	159 s(161)	183.5
A	Ring Def. (I.P.)	173	0.03	14.86	-	151 s(161)	153.6
A	Ring Def. (O.P.)	130	0.03	0.18	-	-	177.0
B	Ring Def. (O.P.)	129	0.00	0.28	96 m	-	127.0
B	Ring Def. (I.P.)	60	1.14	0.87	-	-	98.1
A	Ring Def. (O.P.)	53	0.16	0.19	-	-	53.1
B	Ring Def. (O.P.)	44	2.71	0.37	-	-	46.7
A	Ring Def. (O.P.)	43	7.24	0.26	30 w	-	45.2
B	Ring Def. (O.P.)	38	0.26	0.63	-	-	36.9
A	Ring Def. (O.P.)	20	2.21	1.28	-	-	15.7
RMS Error		134	-	-	0	0	32.1

[a]Relative intensities, vs: very strong, s: strong, m: medium, w: weak, vw: very weak, sh: shoulder, br: broad.

[b]In-plane ring deformation mode [c]Out-of-plane ring deformation mode

* Experimental assignment of this mode is not consistent with the quantum chemical calculation and not included in RMS error.

Table 5. Calculated and experimental frequencies and Raman and infrared (IR) intensities for ET^+. The frequencies are in cm^{-1}, IR intensities are in KM/Mole, Raman intensities are in $Å^4$/AMU.

Sym.	Modes	HF	Intensity		Experiment		FF
			IR	Raman	IR	Raman	
B_3	C-H str.	3316	1.41	90.73	2936 w	-	2935.9
B_2	C-H str.	3316	0.21	86.51	-	-	2935.9
A	C-H str.	3305	0.00	251.75	-	-	2916.5
B_1	C-H str.	3305	2.13	0.57	2914 vw	-	2916.5
A	C-H str.	3248	0.00	1086.34	-	-	2871.1
B_1	C-H str.	3248	24.15	1.76	-	2847 vw	2871.1
B_2	C-H str.	3242	0.29	13.57	2883 w	-	2857.5
B_3	C-H str.	3242	5.22	179.42	-	-	2857.5
A	C=C str.	1697	0.00	60707.55	-	1455 m	1496.0
B_1	C=C str.	1620	3060.40	1.32	1445 w	-	1457.7
A	CH_2 bend	1601	0.00	24.83	-	-	1422.2
B_1	CH_2 bend	1601	5.04	4.97	1422 sh	-	1422.2
B_3	CH_2 bend	1594	23.93	6.92	1411 s	-	1416.4
B_2	CH_2 bend	1594	4.55	56.09	-	-	1416.4
A	C=C str	1565	0.00	34573.66	-	1431 vs	1385.1
A	CH_2 wag	1469	0.00	279.93	-	1294 vw	1285.5
B_1	CH_2 wag	1467	209.74	1.47	1283 m	-	1285.3
B_3	CH_2 wag	1435	7.32	3.71	-	1274 vw	1263.6
B_2	CH_2 wag	1435	0.00	0.72	1277 sh	-	1263.6
A	CH_2 twist	1325	0.00	16.62	-	-	1173.5
B_1	CH_2 twist	1325	1.47	2.08	1180 w	-	1173.5

Sym.	Modes	HF	Intensity		Experiment		FF
			IR	Raman	IR	Raman	
B_3	CH_2 twist	1264	1.38	1.56	1125 sh	-	1135.0
B_2	CH_2 twist	1264	2.21	18.511	-	1120 w	1135.0
B_3	Ring Def. (I.P.)[b]	1171	0.25	623.99	-	1056 w	1059.4
B_2	Ring Def. (I.P.)	1141	16.86	0.06	1024 w	-	1026.3
B_3	Ring Def. (I.P.)	1138	0.10	5.88	-	-	1025.6
A	C-C str.	1093	0.00	31.22	-	976 mw	991.2
B_1	C-C str.	1093	0.30	0.61	1010 vw	-	991.2
A	CH_2 rock.	1029	0.00	247.37	-	931 vw	952.3
B_1	CH_2 rock.	1029	5.24	5.10	-	-	936.4
B_2	CH_2 wag	997	0.04	2.42	915 w	-	935.7
B_3	CH_2 wag	991	8.04	0.00	-	-	887.1
B_2	Ring Def. (I.P.)	969	4.06	74.29	900 w	-	895.7
A	Ring Def. (I.P.)	963	0.00	7905.13	-	905 w	885.0
B_1	Ring Def. (I.P.)	927	5.84	225.12	-	-	950.9
B_1	Ring Def. (I.P.)	881	5.86	956.10	812 w	-	826.0
B_2	Ring Def. (I.P.)	857	6.11	0.09	886 w,br	-	841.1
B_3	Ring Def. (I.P.)	853	0.29	3.72	-	-	839.3
B_3	CH_2 rock.	749	0.00	13.32	-	-	691.6
B_2	CH_2 rock.	749	4.23	2.77	640 vw	-	691.6

Sym.	Modes	HF	Intensity		Experiment		FF
			IR	Raman	IR	Raman	
A	CH_2 rock.	707	0.00	339.78	-	-	686.4
B_1	CH_2 rock.	706	36.60	0.04	672 vw	-	684.9
B_1	Ring Def. (O.P.)[c]	610	0.01	3.23	-	-	636.0
A	Ring Def. (O.P.)	607	0.00	14.03	-	-	636.0
B_2	Ring Def. (O.P.)	596	0.02	6.19	-	-	581.2
A	Ring Def. (I.P.)	570	0.00	5148.20	-	511 mw	512.9
B_3	Ring Def. (I.P.)	514	0.35	0.04	-	-	487.1
B_2	Ring Def. (I.P.)	512	2.91	1.11	-	-	476.5
B_1	Ring Def. (I.P.)	504	605.79	0.00	503 w	-	512.0
A	Ring Def. (I.P.)	492	0.00	2986.58	-	489 m	453.9
B_1	Ring Def. (I.P.)	438	3.85	0.05	406 w	-	397.6
B_2	Ring Def. (I.P.)	392	0.49	0.2	-	-	344.6
B_3	Ring Def. (I.P.)	387	0.06	4.84	-	355 vw	387.0
B_3	Ring Def. (I.P.)	371	0.00	93.14	335 w	-	349.4
B_3	Ring Def. (O.P.)	357	1.70	0.21	-	-	340.3
A	Ring Def. (I.P.)	348	0.00	4.39	-	320 w	335.2
B_1	Ring Def. (I.P.)	328	21.53	0.04	-	-	339.7
B_2	Ring Def. (O.P.)	309	0.52	3.25	265 w	-	272.7

Sym.	Modes	HF	Intensity		Experiment		FF
			IR	Raman	IR	Raman	
B_2	Ring Def. (I.P.)	295	4.79	0.01	-	-	335.2
B_3	Ring Def. (O.P.)	294	0.07	0.32	-	-	282.2
A	CH_2 wag	294	0.00	0.32	-	-	234.0
B_1	CH_2 wag	283	0.00	0.07	-	-	219.5
B_3	Ring Def. (I.P.)	187	0.012	3.46	-	-	179.8
A	Ring Def. (I.P.)	175	0.00	185.20	-	169 w	162.8
A	Ring Def. (O.P.)	120	0.00	6.81	-	-	83.6
B_1	Ring Def. (O.P.)	120	0.48	0.57	-	-	83.1
B_2	Ring Def. (O.P.)	86	0.07	16.63	-	-	70.3
B_2	Ring Def. (I.P.)	61	0.16	0.00	-	-	53.6
B_3	Ring Def. (O.P.)	49	8.93	0.29	-	-	46.1
B_2	Ring Def. (O.P.)	43	0.02	0.17	-	-	34.4
A	Ring Def. (O.P.)	36	0.00	0.00	-	-	19.8
B_3	Ring Def. (O.P.)	28	2.04	0.02	-	-	8.4
RMS Error		167	-	-	0	0	20.0

[a] Relative intensities, vs: very strong, s: strong, m: medium, w: weak, vw: very weak, sh: shoulder, br: broad.

[b] In-plane ring deformation mode.

[c] Out-of-plane ring deformation mode.